May 2017

Assessments of Concrete Internal Damage Caused By Freeze-Thaw Cycles and Mechanical Loading

Zeqian Li
University of Wisconsin-Milwaukee

ASSESSMENTS OF CONCRETE INTERNAL DAMAGE CAUSED BY FREEZE-THAW CYCLES AND MECHANICAL LOADING

by

Zeqian Li

A Thesis Submitted in

Partial Fulfillment of the

Requirements for the Degree of

Master of Science

in Engineering

at

The University of Wisconsin-Milwaukee

May 2017

ABSTRACT

ASSESSMENTS OF CONCRETE INTERNAL DAMAGE CAUSED BY FREEZE-THAW AND MECHINICAL LOADING

by

Zeqian Li

The University of Wisconsin-Milwaukee, 2017
Under the Supervision of Dr. Jian Zhao

Concrete in bridge decks in Northern States, such as Wisconsin, is subjected to both freeze-thaw cycles and mechanical stresses. Standard testing methods are available to evaluate the deterioration of concrete, including ASTM C215 (Dynamic Modulus test), ASTM C1202 (Rapid Chloride Ion Penetrability test), and ASTM WK37880 (ESR test) are available. In addition, ASTM C642 (water absorption test) helps quantification of permeable voids in concrete. These tests have been used to evaluate undamaged concrete or concrete samples after freeze-thaw cycles.

The concrete samples in this study have been subjected to compressive stresses ($0.4f_c'$) and freeze-thaw cycles (100 to 300 cycles) to better represent the concrete in Wisconsin bridges. It is believed that concrete can develop the microcracks under compressive stresses similar to freeze-thaw cycles. Therefore, the study focuses on the comparison of the standard testing methods on the evaluation of damaged concrete.

A total of 36 discs were tested for their chloride permeability in this study. Combined with the other tests conducted for the same samples by Mitchell (2016), it is concluded that: 1) the water absorption after immersion is closely related to the chloride permeability of concrete with internal damage; 2) the average surface resistivity has a strong relationship with chloride permeability of

concrete with damage; 3) the average surface resistivity has a closer relationship with water absorption after immersion of cylinders than with average water absorption of discs sliced from the cylinders; and 4) the dynamic modulus seems not efficient in evaluating concrete with internal damage in this study.

The permeability of concrete in bridge decks might not be conveniently represented by rapid chloride ion penetration tests; however, the internal damage caused by traffic loading and environmental attacks may be represented well the water absorption of field concrete samples. This line of research is expected to contribute to a durability design methodology that can be used to design bridges for local truck traffic targeting a variety of desired service lives.

Dedicated to:

my parents:

Li,Haiqing; Song, Xufeng

TABLE OF CONTENTS

LIST OF FIGURES

LIST OF TABLES

LIST OF ABBREVIATIONS

ACI	American Concrete Institute
CFIRE	National Center for Freight & Infrastructure Research & Education
COD	Crack Opening Displacement
ESEM	Environmental scanning electron microscopy
ESR	Electrical Surface Resistivity
FA	Fly Ash
F/T	Freeze Thaw
HSC	High Strength Concrete
ITZ	Interfacial Transition Zone
NWC	Normal Weight Concrete
PV	Percent Volume of Permeable Voids

R^2	Coefficient of Determination
RCIP	Rapid Chloride Ion Penetration
SCM	Scanning Electronic Microscopic
WisDOT	Wisconsin Department of Transportation
CQU	Chongqing University, Chongqing, China
ACP	Average Charge Passed
DM	Dynamic Modulus
ESR	Electrical Surface Resistivity
WA	Water Absorption after Immersion
ABA	Average Water Absorption after Immersion
WAC	Water Absorption of Cylinder

ACKNOWLEDGEMENTS

In recognition of your unwavering support, guidance, and outstanding character, I would like to extend my deepest gratitude to Dr. Jian Zhao, my thesis advisor at UWM.

I would like to thank the CQU-UWM graduate student exchange program, through which my graduate study and research at UWM can be possible. Specifically, I would like to thank Dr. Gang Liu, my thesis advisor at CQU, for your great patience and guidance. I would also like to thank Dr. Chuan Zhang at CQU and Dr. David Yu for the support and encouragement through the exchange program.

Thank you to John Condon and all the others at the UWM Machine Shop for donating materials and aiding in the fabrication of necessary testing equipment.

Special thanks to (arranged alphabetically by last name):

- Dr. Yin Lin for your guidance and encouragement;
- Hua Liu for your friendship and many hours of assistance;
- Dr. Konstantin Sobolev for allowing access to your lab space and equipment;
- Dr. Habib Tabatabai for allowing access to your lab space and equipment;
- Dr. Hani Titi for allowing access to your lab space and equipment; and All UWM staff, especially Betty Warras, Marina Lvanovna Kozhuhova, Asadollah Khoddam Mohammadi, Cui Fu, and for all of those not mentioned, thank you so much for your support, patience, and cooperation.

CHAPTER 1 INTRODUCTION

1.1 Concrete Bridge Deck

The deterioration of well-constructed concrete bridges is mainly caused by traffic loads, especially heavy trucks and various environmental attacks (AASHTO, 2008; Tabatabai et al., 2011). The environmental attacks include chloride penetration and subsequent corrosion of steel reinforcement; freeze-thaw (F/T) cycles on concrete in saturated or near-saturated conditions; and scaling of concrete exposed to deicing salts (Mirza, 2006). The concrete deck of some bridges in Northern states such as Wisconsin might be under severe environmental attack due to the extensive use of deicing salt. The chloride ions infiltrate the protective layer, leading to corrosion and the deterioration of concrete (Kostem, 1978).

Tabatabai et al. (2011) observed that a higher traffic volume can cause a higher deterioration rate on concrete bridge deck. Therefore, deterioration of deck concrete may be affected by the truck-induced stresses in concrete (Lin et al., 2012). Unlike the resulted tensile stresses in decks, these compressive stresses may cause internal microcracks, which increase the porosity and permeability of concrete (Elzafrancy and Soroushian, 2015; CEB, 1992). The microcracks near to a surface may lead to spalling and eventually the decomposition of concrete (Lin, et al., 2012).

The development of microcracks under compressive stresses was identified by Lin et al. (2012) as a likely source of bridge deck deterioration along with F/T cycles. The contribution of high compressive stress on microcracks development in concrete samples was found significant. The high local compressive stress on bridge decks may be caused by trucks weighed more than the legal limits.

The impact of these overweight trucks on bridge safety has been addressed in detail while their impact on deck deterioration has not been considered well. For example, 1.3 million out of 6 million trucks on Wisconsin highways were overweight according to a previous study using weight–in-motion truck records (Zhao and Tabatabai 2010). The permit fee structure for single-trip permits is simply $20 for vehicles weighting 0 through 90,000 pounds, or $84 plus $10 for each additional 10,000 pounds for overweight vehicles weighting 150,000 pounds or more (WisDOT, 2005, p.1). The effect of high local compressive stress induced by overweight vehicles on durability of concrete bridge deck cannot be overlooked, as illustrated in Figure1.1.

For concrete the bridge decks, heavy axle loads can significantly affect the stresses in both longitudinal and transverse directions (Lin, et al., 2012). Overweight trucks with high axle loads thus may cause high compressive stress (beyond $0.4f_c'$) in deck concrete. "Such stresses are high enough to cause internal microcracks in concrete, which increase the permeability of concrete, and accelerate the deck deterioration" (Lin, et al., 2012). Therefore, it is necessary to study the durability of concrete under freeze-thaw cycles and compressive stress.

There were lots of research studying on the effect of material selection, construction, environmental attacks such as F/T cycles on durability of concrete respectively (Arezoumandi 2015; Rhee et al., 2009; Shiotani et al., 2012; and Ishida, 2016). However, few studies focus on the damage to bridge deck induced by combined effect of compressive stresses and freeze-thaw cycles (Lin et al., 2012; Mitchell, 2016).

1.2 Measuring Concrete Deterioration

A variety of standard test methods exist for evaluating the concrete. The standard method ASTM C1202 (RCIP test) determines the electrical conductance of concrete to provide a rapid indication of its resistance to the penetration of chloride ions. Yang (2016) proposed that dynamic

modulus test is an efficient method to estimating the deterioration of concrete sample by freeze-thaw cycles. America Society for Testing and Materials proposed the ESR test ASTM WK37880 as an alternative to the Rapid Chloride Ion Penetrability test (RCIP test). Lin (2012) proposed that water absorption after immersion of the specimens subjected to combination of freeze-thaw cycles and compressive stresses has strong relationship with chloride ion penetrability. These methods have been used in previous studies, which focused on undamaged concrete samples. Meanwhile, concrete in bridge decks are likely damaged by mechanical stresses and/or F/T cycles.

Lin et al. (2012) observed a strong relationship between water absorption and the amount of charges passed samples, after being subjected to combined effects of mechanical loading and freeze-thaw cycles. In the tests by Lin et al. (2012), concrete cylinders (4× 8-inch) were subjected to compressive stresses and 300 F/T cycles. The rapid chloride ion penetrability (RCIP) tests were conducted per ASTM C1202. The water absorption of the concrete samples was measured using air-dried samples prior to the RCIP test. This relationship in Lin et al. (2012) can been seen in Figure 1.2.

Note that the water absorption measurement of air-dried concrete samples in the tests by Lin et al. (2012) may not represent all microcracks in the concrete samples. Hence, the measured water absorption may have a systematic error. The conclusion that water absorption of concrete samples correlates to the chloride permeability needs further validation. In addition, the relatively high comprehensive stresses (up to $0.8f_c'$) used in the tests may not be representative for deck concrete.

In the study by Mitchell (2016), specimens were subjected to lower compressive stresses and F/T cycles. Electricity surface resistivity test, the volume of permeable pore space, dynamic modulus test were used in study. The author observed that the volume of permeable pore space (%) in concrete has strong relationship with surface resistivity (kO/cm), but the relationship with

dynamic modulus is weak. The reason for ESR test generally accepted as an efficient method to estimate the penetration of concrete is strong relationship between result of ESR tests and result of the RCIP tests. Therefore, in this study, RCIP tests were conducted to the same samples from Mitchell (2016) in order to compare the different methods used to estimat the durability of damaged concrete samples.

1.3 Research Objectives:

This study continues the research by Mitchell (2016) to evaluate standard testing methods for durability of concrete damaged by combined mechanical stresses and F/T cycles. Combined with the standard tests conducted by Mitchell (2016), this study is to examine the relationships between the measured water absorption and other parameters such as the dynamic modulus and the surface resistivity of concrete cylinders, and electrical charges passed through discs sliced from the cylinders. Note that the cylinders used in this study are same as those tested in Mitchell (2016) facilitate the comparison. The objectives of this study are to:

1. Conduct rapid chloride ion penetration tests of the samples,
2. Examine relationship between measured water absorption and other measurements designed to evaluate the durability of concrete.
3. Understand the deterioration mechanism of concrete damaged by the combined compressive stresses and F/T cycles.
4. Develop relationships between testing methods for estimating the deterioration of concrete subjected to compressive stress and freeze-thaw cycles base on the water absorption.

1.4 Organization of Thesis

This thesis is organized as follows: A review of existing experimental tests is provided in Chapter 2. The experimental program is described in Chapter 3, and the program focused on the

measurement of the chloride permeability and water absorption of concrete samples. The measured chloride permeability and water absorption are compared with other measurements by Mitchell (2016) in Chapter 4. In addition to a summary and main conclusions, a series of subjects are proposed for future study in Chapter 5. Finally, the raw data and images of the concrete samples are included in the appendix.

Figure 1.1: Overweight vehicle causing visible deflection in bridge (Lin et al., 2012)

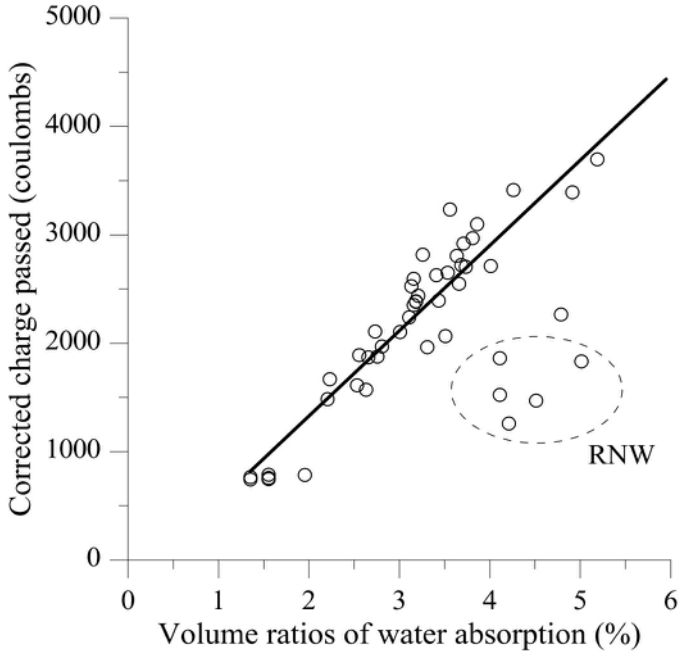

Figure 1.2: Charge passed through samples with water absorption (Lin et al., 2012)

CHAPTER 2 LITERATURE REVIEW

2.1 Impact of Overweight Vehicles (With Heavy Axle Loads) On Bridge Deck Deterioration by Lin et al., (2012)

2.1.1 Introduction

The traffic loads and environmental attacks such as severe cold, extreme hot can cause damage to concrete. Some studies focused on traffic loads effects. Some studies focused on environmental attacks. Lin et al. (2012) attempted to quantify the impact of overweight vehicles, along with freeze-thaw cycles on the bridge decks. The authors conducted analyses of a steel girder bridge with a concrete bridge deck to estimate the compressive stresses in the deck concrete. The impact of tensile stresses has been studied extensively in literature, hence only compressive stresses induced by overweight truck loads were considered. A range of compressive stresses were applied to eight groups of three 8in. cylinders cast using commercial air-entrain concrete. The stresses were 40 though 80 percent of the measured compressive strength, measured according to ASTM C39. "The cylinders were exposed to 300 freeze-thaw cycles following a procedure similar to that described in ASTM C666" (Lin et al., 2012, vii). Rapid Chloride Ion Penetration (ASTM C1202) tests were conducted to the discs extracted from the cylinders to evaluate the damage to concrete caused by the combined mechanical stresses and freeze-thaw cycles.

2.1.2 Experimental Program

In this study, Wisconsin Department of Transportation(WisDOT) specified the mixture of the air-entrained concrete, the standard mixture, Grade A-FA, was used (Lin et al., 2012, p. 25). The amount of fly ash by weight of total cementitious material is 30 percent and the water-cementitious material ratio (w/cm) is 0.4. An air entraining admixture is air 260 from Chryso (Lin et al., 2012,

p. 25). A slump test (ASTM C143), an air content measurement (ASTM C231) and other ASTM standard was followed in measuring properties of fresh concrete. The range for typical air-entrained concrete is 5 to 8 percent (ASTM C260-10a, 2010), and the measured slump was 6 in. After 28 days curing, the average compressive strength is 3.9 ksi. It increased significantly to 5.6 ksi experienced 120 days curing, which reflects the typical behavior of concrete with fly ash (Lin et al. 2012, p. 34).

Eight groups of three cylinders were used in the test. The specimens were divided into three categories which are RNW specimens, RW specimens and RD specimens. One group of eight cylinders which were named as RNW specimens was kept in air after 28 days of curing in saturated lime water. Another group of three cylinders was kept in water. Another group of three cylinders was kept in water after 28 days curing, considering that hydration process may continue for the fully saturated cylinders that were subjected to freeze-thaw cycles. Other five groups of cylinders were subjected to 300 freeze-thaw cycles which were named as RD specimens, except for one of six groups were not subjected any load because this group was defined as a reference, other five groups of cylinders were subjected to five levels of compressive load (Lin et al.,2012, p. 25). The compressive loads ranged from "40 through 80 percent of the measured ultimate compressive load" (Lin et al.,2012, p. 25).

Note that the applied compressive 80 percent of the measured ultimate compressive load may be higher than daily truck traffic. However, this study focused on overweight vehicles which may be able to generate 80 percent of the measured ultimate compressive strength in concrete decks. The repeated truck loading was not considered in this study.

2.1.3 Rapid Chloride Ion Penetration (RCIP) Test

To evaluate the internal damage by the mechanical stresses and F/T cycles. RCIP test was introduced to this study. The RCIP is for measuring chloride permeability of concrete which is a key symbol of durability. Besides that, test time of RCIP is shorter when compared to other tests such as salt ponding tests (ASTM C1543) and chloride diffusion tests (ASTM C1556) (Lin et al., 2012, p. 27).

Two samples with a thickness of 2-inch were extracted from the middle part of each cylinder. Every group has six samples. Totally 48 samples were tested including RW and RNW cylinders (Lin et al., 2012, p. 27). The conclusion is "chloride permeability of the concrete samples increased significantly with an increase in the applied compressive loads" (Lin et al., 2012, vii). The highest increase in average passing charge can be seen by comparing D60 and RD samples, passing charge in a D80 specimen almost doubled that through RNW specimens.

2.1.4 Microcracks

There are no major cracks existed in the samples. However, the micrographs of the samples revealed that more microcracks existed in concrete subjected to combined actions. The images of concrete specimens under meso- or micro- scale indicated that the microcracks are likely responsible for 25 percent and 186 percent increase when RD samples are compared to RNW samples and RW samples in chloride permeability. According to Lin et al. (2012), "The picture of a D40 samples showed that some cracks had connected into a passageway for chloride ions", "These passageways were further opened and interconnected during the freeze-thaw cycles due to an increase in hydraulic pressure." The formation and expansion of ice crystals within the void space of the concrete was responsible for the increase in hydraulic pressure. As a result, 10 percent increase in the average value of charge passed of D40 compared with RD samples was observed.

2.1.5 Water Absorption

The author also measured water absorption for the samples before they were used in the RCIP tests. In general, water absorption of test samples increased with an increase in the applied load. The water absorption of these samples was found closely related to the charge passed in RCIP tests Figure1-1. The water absorption was proportional to the amount of charge passed in RCIP tests.

The average charge passed of RNW specimens which is dried in air at 120 is not corresponding to water absorption of them. This may because microcracks in RNW specimens did not form passageways for water and chloride ions in these specimens. The microcracks and air voids in concrete can be accessed by outside water and aggressive chemical indicated by the strong relationship between the measured absorption and the chloride permeability. Therefore, the study proposed that water absorption could be used as a viable alternative to determining the durability of concrete, especially for concrete samples obtained from the field to evaluate the bridge deck conditions.

2.1.6 Summary

By comparing the data from RCIP test and absorption, a strong relationship between water absorption and chloride permeability was identified, both may have close relationship with the propagation of microcracks. However, the method of water absorption applied in Lin et al. (2012) is not standard test. Thereby another study in which all tests are standard tests is necessary to explore the relationship between water absorption and chloride permeability. In this study, the water absorption of all specimens was measured by ASTM C642 and charge passed though the specimens measured by ASTM C1202.

2.2 Durability of Mechanically Loaded, Freeze Thawed Concrete Determined by Water Absorption; by Mitchell (2016)

2.2.1 Introduction

The deterioration of concrete of the bridge deck requires expensive repaired before the designed service life of bridge can come to term. Large number of bridges are afflicted by early deterioration of bridge deck. Lin et al (2012) proposed that overweight trucks can develop microcracks networks in concrete deck which subjected to F/T cycles. Through finite element analyses, Lin et al. (2012) determined that the local compressive stress caused by simulated overweight trucks increased to as much as $0.4f_c'$. Previous studies have focused on several deleterious mechanisms on the durability, however, very few evaluate the damage to bridge deck caused by the combined effects of compressive stresses and F/T damage.

Dynamic modulus (ASTM C215), RCIP test (ASTM C1202), ESR test have been deemed efficient in estimating the deterioration of concrete. However, testing of field specimen would be very difficult due to complication arising from bridge deck that perfectly matches dimensions which is strictly limited by test standard, and the samples can not contain reinforcement as this would alter the results of the test. Lin et al. (2012) proposed that water absorption has a strong relationship with passing charge from RCIP test in the concrete samples subjected combination of F/T cycles and compressive stress. Therefore, the ASTM C642: Density, Absorption, and Voids in Hardened Concrete, might be used to determine the deterioration of concrete.

2.2.2 Experimental Program

The concrete samples mixed with Wisconsin Department of Transportation Type A-FA mixture. The water-cementitious material ratio was 0.4, and the amount of fly ash by weight of total cementitious materials was 30 percent. The maximum size of coarse aggregate was 3/4 inch.

The target concrete compressive strengths for the normal strength concrete was 4000 psi. Some specimens in this study were subjected to combination of F/T cycles and compressive stresses.

The 2-inch tall concrete were separated into groups of nine and were labeled with a "D" denoting disc samples. These samples were labeled alphabetically ranging from B-H, and then numerically 1-9 (e.g. D-1F). These concrete samples were tested for water absorption and volume of permeable voids according to ASTM C642.

The concrete cylinders retained their original designations which intermittently ranged from C06 through C-42. These samples were tested for dynamic modulus (ASTM C215), water absorption (ASTM C642), and electric resistivity. After these tests, using a water-cooled diamond saw, the cylinders were cut down to 2-inch tall discs. These discs then were tested for water absorption according to ASTM C642.

2.2.3 Dynamic Modulus

The cylinders were tested by dynamic modulus using the contact driven forced resonance method outlined in the ASTM C215. The mass, length and cross sectional area wre measured for all of the concrete cylindrical specimens. The specimen was subjected to vibrations at varying frequencies ranging from 1K to 10k frequency. The frequency at which the needle on the meter indicator reached its peak value was recorded as the fundamental transverse frequency of specimen.

The average peak frequency of C-28 and C-40 is higher than 2345Hz, the two samples were considered outliers. Other samples had average peak frequency with significantly high standard deviations. The comparison between the consolidated data for dynamic and ratio of volume of permeable voids is extremely weak.

2.2.4 Permeable Voids

The water absorption of samples was evaluated per ASTM C642. There are four kinds of states for samples in this study. First, oven-dried state: the concrete samples were oven-dried at temperature of 110 °C for 24hours. Second, saturated after immersion state: the samples sat submerged in the water for a period of 48 hours. Third, saturated after boiling state: samples were boiled for five hours and cooled by natural heat loss for not less than 14 hours to a final temperature of 20°C to 25 °C. Last, immersed apparent state: the mass of concrete samples immersed in water determined. When every state is end, record the mass of samples. Calculating the mass from these state, water absorption (after immersion) and ratio of permeable of voids can be got.

2.2.5 Electric Resistivity

ESR of the concrete samples was evaluated using a Giate Surf testing apparatus of a measuring device and a samples chamber. Each sample was tested three time in different direction to determine the electrical surface resistance.

Mitchell observed that ESR and PV have an inversely proportional relationship. The relationship between ESR and dynamic modulus is weak.

2.2.6 Conclusion

A relationship between the dynamic modulus and ESR; and dynamic modulus and PV could not be determined. The linear regression and general equations were generated from absorption test. Excluding the two outliers, a very strong relationship, with R^2 equal to 63.5%, was identified between PV and ESR.

2.3 The effect of Damage on Mass Transport in Cement-Based Materials; by Ghasemzadehsomarin et al. (2016)

This study focused on the difference between different methods estimating mass transport on the damaged mortar caused by freeze-thaw cycles. These methods include: water sorptivity (ASTM C1585), rapid chloride ion penetrability test (ASTM C1202), electrical surface resistivity, water permeability, and air permeability.

The specimens are from 4×8 inch mortar cylinder, and ordinary Portland cement Type I and river sand with fineness modulus of 2.65 were used. The mortar mixture had a water-to-ratio (w/c) of 0.43 and mortar was made according to ASTM C192-07. A total 25 freeze-thaw cycles were used and cylinders were demolded and cut into appropriate geometries because different standard for size of samples in these tests. Different cycles represent different degree of damage. There are totally 5 degrees for damage. The samples in every test include five different degrees. Totally 4 samples each degree for the RCIP test, 3 samples each degree for electrical resistivity, 3 samples each degree for air permeability and 4 samples each degree for water permeability.

The results of rapid chloride penetration test show that the current increased with the time when the highest current is lower than 480mA, as shown is Figure 2.2. However, current reaches a plateau at a high degree of damage. The passing charge plateau of may have been caused by the fact that the chloride concentration reduces in the NaCl solution cell in the tests with high observed passing charges. But for the low degree of damage, for which the current was lower than 480mA, the current increased with time.

In resistivity test, resistivity decrease with high rate of damage due to the freeze-thaw cycles in concrete. With further increase of damage the electrical resistivity decreases with a lower rates

as shown in Figure 2.3. It indicates that electrical resistivity might only sensitive to low damage levels.

In this study, the author also tried to use the concept of percolation to describe the effect of microcracks on water sorptivity, electrical resistivity, and saturated hydraulic conductivity (permeability) in cement concrete. The dangling ends merge and from more loops, resulting in expansion of the microcracks networks that through the specimens, for sorptivity test, the dangling ends facilitate access to the capillary pores that are far from the sorptivity surface of sample.

Cement paste is the most conductive phase in concrete and the pore solution is the main contributor to the electrical conductivity of the cement paste. “Due to the contribution of the cement paste to electrical conductivity, the contribution of the microcracks to electrical conductivity is less pronounced as compared to the contribution of the cracks to saturated hydraulic conductivity.”

The authors concluded that the hydraulic conductivity cannot represent the microcracks with dangling ends in the concrete. However, the hydraulic conductivity of a crack increase linearly with an increase in these microcracks.

2.4 An Evaluation of Performance-Based Alternatives to the Durability Provisions of the ACI 318 Building Code; by Obla et al. (2015)

There is a trend of developing performance-based specification for durability of concrete which is specified with prescriptive specifications. The existence and use of reliable test methods and specification criteria that can measure the durability of concrete mixtures and provide the expected service life is a challenge to develop performance-based specifications. This study focused on proposed performance criteria for concrete to ensure the durability of concrete.

The RCIP test is the best way to estimating the chloride penetrability of concrete. A good correlation between RCIP test and conductivity was observed. The conductivity might be used as an alternative to the RCIP test as shown in Figure 2.4. The electrical conductivity of concrete samples was measured per ASTM C1760. In the figure, 28-acc day and 56 days represent specimens were accelerated cured for 28 days and standard cured for 56 days respectively. The strong relationship between conductivity and RCIP test indicates that electrical resistivity closely related to charge pass through specimens.

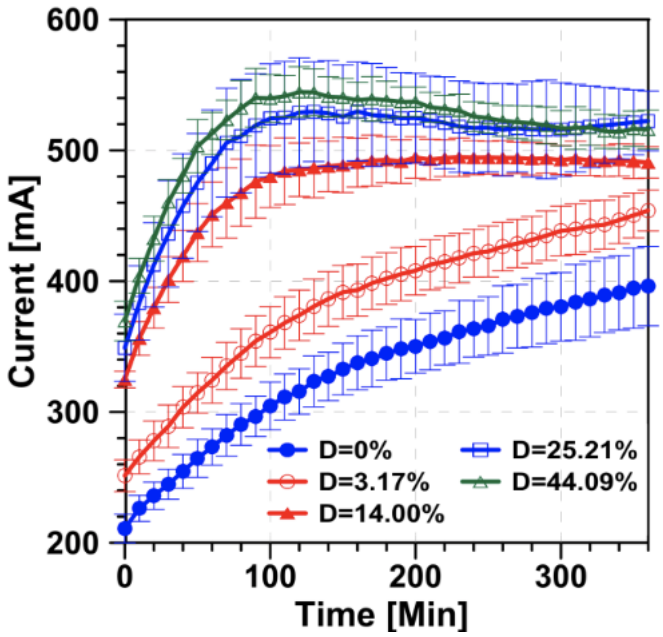

Figure 2.1: Passing current vs. time for specimens with different degrees of damage.

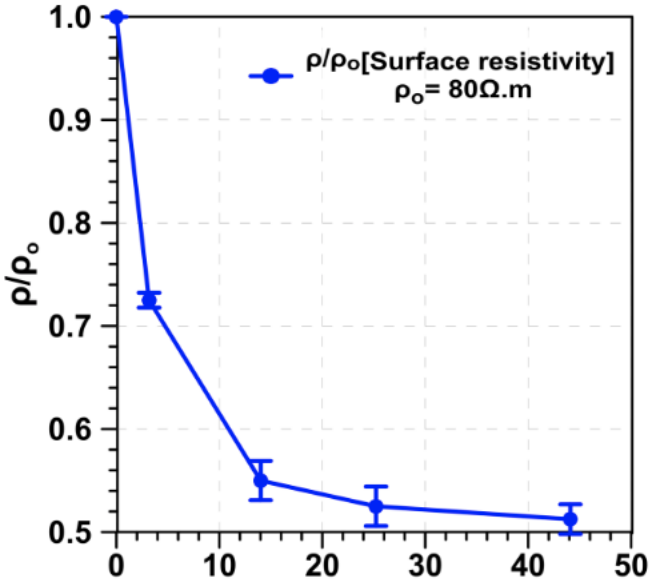

Figure 2.2: The surface resistivity of specimens with different degrees of damage.

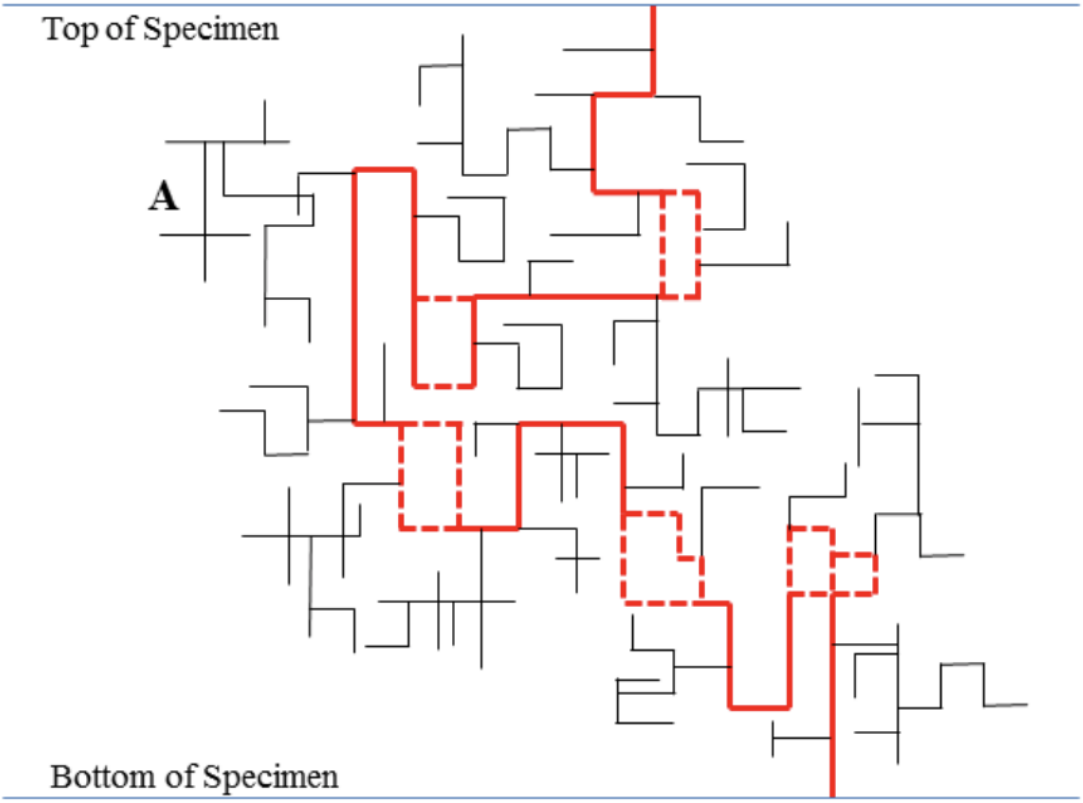

Figure 2.3: The schematic of a possible microcracks network in concrete specimens (Ghasezahsomarin, et al., 2016)

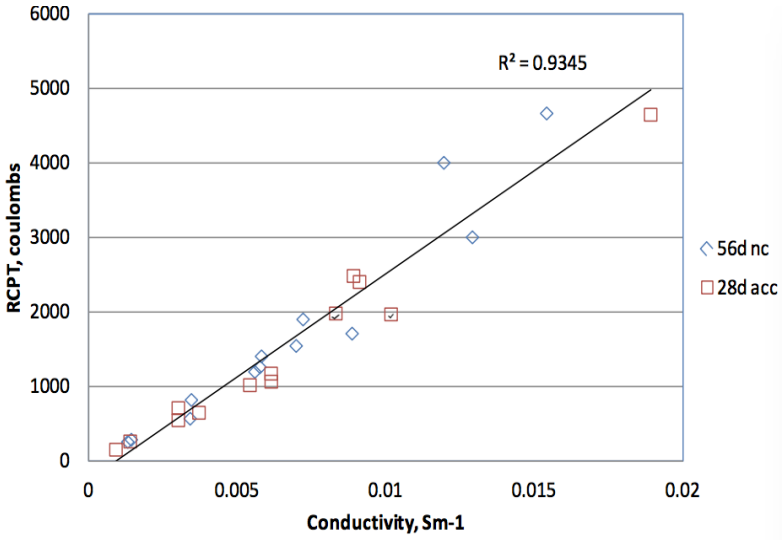

Figure 2.4: The relationship between charge passed and the electrical conductivity of concrete specimens (Obla, et al., 2015).

Chapter 3 EXPERIMENTAL PROGRAM

3.1 Introduction

Many ASTM standard tests exist for evaluating concrete. ASTM C215 describes a standard test method for fundamental transverse, longitudinal, and torsional resonant frequencies of concrete specimens. Yang et al. (2005) showed the dynamic moduli measured ASTM C215 can be used to evaluate the internal damage of concrete after freeze-thaw cycles. ASTM C1202 describes a standard test method for electrical indication of concrete's ability to resist chloride ion penetration. This test has been used to evaluate chloride permeability of undamaged concrete or concrete samples after freeze-thaw cycles. ASTM C642 describes a standard test method for density, absorption, and voids in hardened concrete. The tests by Lin et al. (2012) have shown that water absorption of concrete samples can be used to measure the permeable microcracks and voids in concrete. ASTM WK37880 describes a new test method for measuring the surface resistivity of hardened concrete using the Wenner four-electrode method. The America Association of State Highway and Transportation Officials has adapted surface resistivity test (AASHTO TP 95) as a method to provide rapid indication of concrete resistance to chloride ion penetration.

The focus of this study is on the chloride permeability of concrete in bridge desks, which can be subjected to high compressive stresses and F/T cycles among other environmental attacks. Most of these existing methods are developed for the samples from undamaged concrete or concrete after freeze-thaw cycles. It is therefore necessary to evaluate the applicability of these methods to concrete damaged by combined mechanical stresses and freeze-thaw cycles. These standard tests were conducted on the same set of concrete samples. Damage in some specimens caused by freeze-thaw cycles, in other specimens caused by combination of freeze-thaw cycles and mechanical

loading. The results of the standard tests are compared in this study. Part of the test results were obtained by Mitchell (2016) while this study focused on the water absorption and chloride permeability of the same concrete samples.

3.2 Specimens

The specimens are from a previous study by Mitchell (2016). The dimension of the concrete cylinder is 4x8inch, some of which were subjected to compressive stresses of varying percentage of f_c' along with vary numbers of F/T cycles. The compressive stress was about $0.4f_c'$ and the cylinder samples were subjected to 100 to 300 F/T cycles. There was a shaft in the research focus, that is the original research goal was to quantify the impact of combined mechanical stresses and freeze-thaw cycles on the chloride permeability of concrete while the research goal of this study and that by Mitchell (2016) was to investigate the applicability of four standard test methods to evaluate chloride permeability of concrete with internal damage.

3.2.1 Origin of specimens

Ready mixed concrete with Wisconsin Department of Transportation Type A-FA mixture was used as shown in Table 3.1. The mixture design of the concrete is shown in. The water – cementitious material ratio was 0.4, and the amount of fly ash by weight of total cementitious materials was 30 percent. The maximum size of coarse aggregate was specified as 3/4 inch. The specified target concrete compressive strengths for the normal strength concrete was 4000 psi. The concrete used was from the same batch for a separate study by Lin et al. (2012). From the test report, the measured air content of fresh concrete was 6.4 percent and the measured slump was 4 inch. Compression tests of hardened concrete cylinders were conducted following ASTM C39. The rate of loading was kept at 250 lb/s to 630 lb/s in accordance with ASTM C39. The hardened concrete had a compressive strength of 5800 psi at 28 days, and the compressive strength went up

6900 psi at about 84 days, as listed in Table 3.2. The concrete cylinders were stored in room condition after 28 days; hence it is envisioned that the concrete compressive strength was close to 6090 psi when the cylinders were loaded and used in this study.

A total of eighteen 4 inch cylinders were included in the original study by Lin (2016) to study the effects of compressive stresses and freeze-thaw cycles on penetrability of concrete. The eighteen cylinders, shown in Figure 3.1, were divided into three groups of six cylinder. The three groups of cylinders were subjected to 100, 200, and 300 freeze-thaw cycles respectively. Within each group of six cylinders, half of them were subjected to a compressive stress equal to 40 percent of measured concrete compressive strength equal to 40 percent of measured concrete compression strength. This study was to extend the study by Lin et al. (2012).

The study was continued by Mitchell (2016). The specimens were deemed no longer suitable for the original purpose. Hence, the cylinders were mixed up such that the four standard testing methods can be compared for their capability of evaluating concrete damaged by compressive stresses and/or freeze-thaw cycles. Some comparisons have been reported in Mitchell (2016) while this report focuses on the comparisons between chloride permeability per ASTM C1202 and other parameters.

3.2.2 Summary of Tests by Mitchell (2016)

Mitchell (2016) measured the dynamic modulus, surface resistivity of a total of 14 cylinders. Mitchell (2016) also partly measured the ratio of water absorption after immersion and ratio of volume of permeable pore space (voids) of the cylinders.

3.2.3 The specimens used in this study

Two-inch discs were sliced from the cylinders used in the tests by Mitchell (2016). The specimens were divided to two groups, and show in Table 3.3. The specimens in the first group

are named xx 1 or 2. For example, in the name of this disc sample 11-1, the first number represents the cylinder number created by Lin (2016) and the second number represents the number of the disc from the same cylinder. The ratio of water absorption for this group of specimens were measured for both the cylinders and the discs sliced from the cylinders. The second group:1F 4F 5F 8F 1D 3D 7D 2H 7H 9H, because they had been sliced from cylinder before the study begun. Therefore, ESR test and dynamic modulus test cannot be measured in these samples.

3.3 Rapid Chloride Ion Penetration (RCIP) Tests

The impact of internal damage was evaluated by measuring chloride permeability of concrete samples in this study. All procedures of the RCIP tests were performed according to ASTM C1202.

3.3.1 Specimen preparation

The discs are sliced from cylinders using a diamond saw, as shown in Figure 3.3. The thickness of all specimens is in range from 48.26mm to 51.05 mm as listed in the Table 3.3. The specimen variation is also within the allowed variation by ASTM C1202. No correction is needed for the measured charges passing through the discs in consideration of disc thickness.

The surface of samples was stained with epoxy residue during the specimen preparation. As shown is the Figure 3.5, there is epoxy residues on the surface of samples. In this case, Chloride ions cannot pass though the specimens. Hence the surface of the samples surface was milled to remove the epoxy residue. A AMERICA TURNMASTER 1525 Engine Lathes with diamond drill was used for cutting epoxy off the surface of samples, as shown in Figure 3.6. It is deemed that the milling process also removed the carbonation on the disc surfaces.

3.3.2 Specimen conditioning

The specimens were kept in a desiccator which was sealed for three hours, the inside pressure is below 50mm Hg (6650Pa). After this step, sufficient de-aerated water was added into the desiccator and the specimens were submerged in de-aerated water for one additional hour as shown in the Figure 3.7. During the 4-hours conditioning process, the insider pressure of desiccator was kept below 50mm Hg (6650Pa). After that, the specimens were under standard atmospheric pressure and submerged in de-aerated water for additional 18 hours as shown in the Figure 3.8.

3.3.3 RCIP tests Type equation here.

After a total 22 hours, a PROOVE'it© System by Germann Instruments was used to conduct the RCIP tests (Figure 3.9). Before that, the sodium chloride solution (3.0 % by mass in distilled water) and the sodium hydroxide solution (0.3 N in distilled water) were prepared. The sodium chloride solution is from Fisher Scientific and the sodium hydroxide solution is from RICCA.

Specimens were removed from immersion, and two rubber rings were applied at the two ends of the disc before the specimen was inserted into a test cell. The side of cell, connected to the negative terminal of the power supply, was filled with 3.0% NaCl solutions, while the other side of cell, connected to the positive terminal of power supply, was filled with 0.3 N NaOH solution. After that, electrodes were connected, and a voltage of 600.1V was applied. The electrical current and the specimen temperature were obtained using an apparatus as shown in Figure 3.9. Finally, the charges passed through the specimens were acquired by PROOVE'it© Germann Instruments and displayed the data on the PC screen by PROOVE'it© software.

The specimens used in this study were subjected to compressive stresses and/or freeze-thaw cycles. This has caused dilation of the concrete cylinders; hence the disc diameter is slightly different from that of the original cylinder. The actual disc diameters are listed in Table 3.3. The

measured total charges passed must be adjusted for the disc diameter. The adjustment is made by multiplying the value (charge) by the ratio of the cross-sectional areas of the standard and the actual specimens. That is:

$$Q_s = Q_x \times (\frac{95}{x})^2, \quad (3.1)$$

where:

Q_s = charge passed (coulombs) through a 95-mm diameter specimen,

Q_x = charge passed (coulombs) through x (mm) diameter specimen, and

X = diameter (mm) of the nonstandard specimens

The equations (3.1) were used to correct the final charge passed in this study.

3.4 Summary

A variety of standard test methods exist for evaluating the concrete. The standard method ASTM C1202 determines the electrical conductance of concrete to provide a rapid indication of its resistance to the penetration of chloride ions. Yang et al. (2016) proposed that dynamic modulus test is an efficient method to estimating the deterioration of concrete sample by freeze-thaw cycles. America Association of State Highway and Transportation Officials adopts the ESR test as an alternative to the Rapid Chloride Ion Penetrability test (RCIP test). Lin et al. (2012) proposed that water absorption after immersion of the specimens subjected to combination of freeze-thaw cycles and compressive stresses has strong relationship with chloride ion penetrability.

The focus of this study is to compare the results of four testing methods applied to a group of concrete samples that have been subjected compressive stresses and/or freeze-thaw cycles. The RCIP test (ASTM C1202) estimates the durability through the number of coulombs through the specimens. The cracks which through the sample filled with water are the path for the chloride

ions to penetrate the concrete. In other words, only the cracks that through the samples can be represented by results of the RCIP tests.

All test results are included in Appendix A along with the images of samples. The detailed comparison of the test results is shown in Chapter 4.

Table 3.1: Mixture of WisDOT Type A-FA Concrete

Materials	Mixture Designation (lbs/yard^3)*
Cement	395
Coarse Aggregate	2002
Fine Aggregates (35%)	1075
Design Water	27gals
Maximum Water	32gals
Silica Fume	0
Fly Ash	170

Note: Water/(cement+fly ash)=0.4.

Table 3.2: Compressive Tests of Cylinders (48 in.)

Concrete	Test 1	Test 2	Test 3	Test 4
28 days	5650	5930	5790	5790
84 days	6410	7150	7170	6910

Table 3.3: Parameters of specimens: AT: average thickness; AD: average diameter.

No.	AT (mm)	Max. Thickness (mm)	Min. Thickness (mm)	AD (mm)	Max. diameter (mm)	Man. diameter (mm)
11-1	50.28	50.38	50.18	101.78	102.20	101.35
11-2	49.16	49.24	49.07	102.55	103.35	101.75
14-1	50.88	49.71	49.61	101.97	102.51	101.4.3
14-2	49.66	50.91	50.84	102.84	103.80	101.88
15-1	50.91	50.99	50.88	102.34	103.69	101.00
15-2	48.36	48.41	48.30	102.87	104.62	101.11
16-1	49.37	49.38	49.36	102.09	102.70	101.48
16-2	50.64	50.77	50.50	102.62	103.50	101.73
17-1	50.68	50.79	50.56	102.07	102.54	101.59
17-2	50.66	50.77	50.55	102.69	103.33	102.04
21-2	50.52	50.67	50.37	102.77	103.91	101.63
22-2	50.85	50.96	50.74	102.86	104.70	101.02
28-1	49.31	49.35	49.27	102.54	103.55	101.53
28-2	49.18	49.19	49.17	102.77	103.53	102.01
29-1	51.18	50.23	50.13	102.24	102.69	101.79
29-2	49.04	49.07	49.01	102.21	102.50	101.91
30-1	48.26	48.37	48.19	102.18	102.60	101.75
30-2	51.05	51.15	50.95	103.16	104.00	102.31
34-1	49.41	49.44	49.38	102.67	103.60	101.73
34-2	50.85	50.92	50.77	102.34	103.19	101.60
35-1	49.72	49.86	49.59	102.22	102.73	101.71
35-2	50.58	50.60	50.57	102.40	102.69	101.78
40-1	48.12	48.23	48.00	102.43	102.91	101.94
40-2	50.07	50.10	50.04	102.43	102.84	102.02
42-1	49.65	49.66	49.63	102.15	101.54	102.76
42-2	50.24	50.25	50.22	102.30	103.25	101.35
1F	49.61	49.65	49.57	102.25	103.05	101.45
4F	49.95	49.96	49.94	102.14	102.61	101.06
5F	49.92	49.93	49.91	102.00	102.70	101.30
2	48.93	48.95	48.90	102.27	102.39	102.14
1D	49.98	50.01	49.96	102.55	103.40	101.69
3D	48.76	48.77	48.75	102.51	102.91	102.11
7D	50.77	50.88	50.66	102.61	103.27	101.95
2H	49.35	49.44	49.26	102.85	103.43	102.26
7H	50.73	50.81	50.65	102.13	102.83	101.43
9H	50.60	50.60	50.59	102.71	103.01	102.40

Figure 3.1: The cylinders were subjected to freeze-thaw cycles or combination of freeze-thaw cycles and compressive stress.

Figure 3.2: The samples for RCIP tests are from middle of cylinders.

(a)Specimens before coating

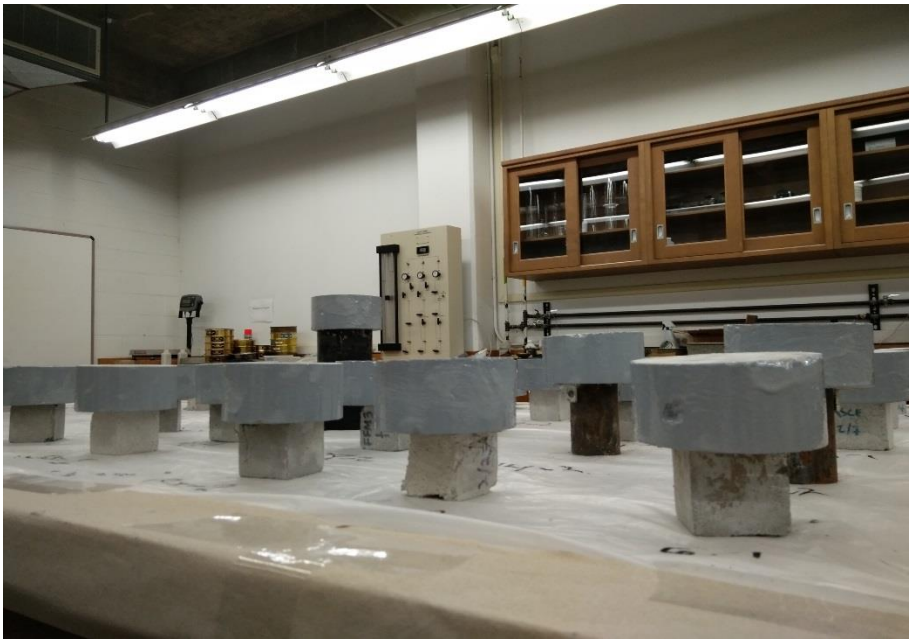

(b)Specimens after coating

Figure 3.3: Specimens were coated in the lab

(a)Surface of sample with some paint

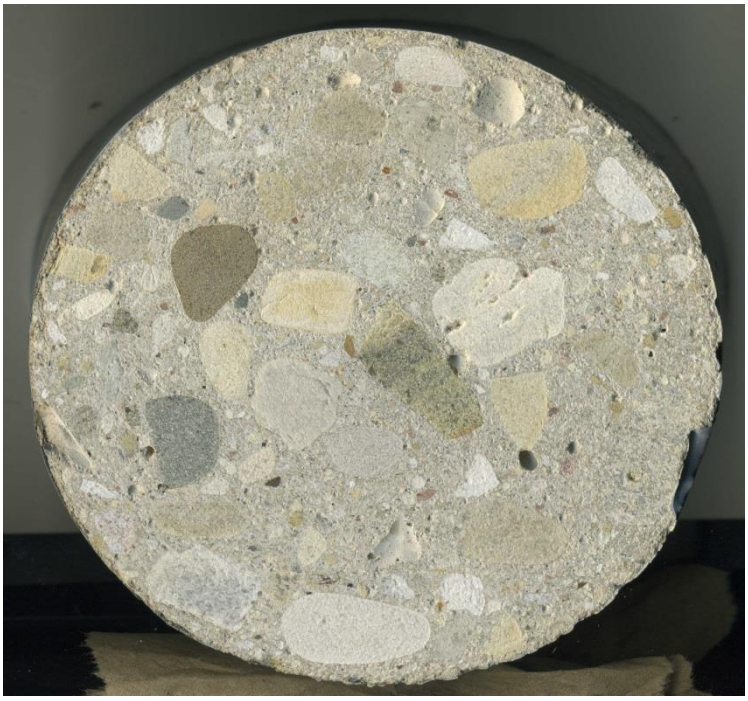

(b)Surface of sample after cutting

Figure 3.4: Sample surface treatment

Figure 3.5: Milling sample surfaces using AMERICA TURNMASTER 1525 Engine Lathe

Figure 3.6: Concrete samples covered by de-aerated water in a vacuum desiccator.

Figure 3.7: test specimens immersed in de-aerated water under atmospheric pressure.

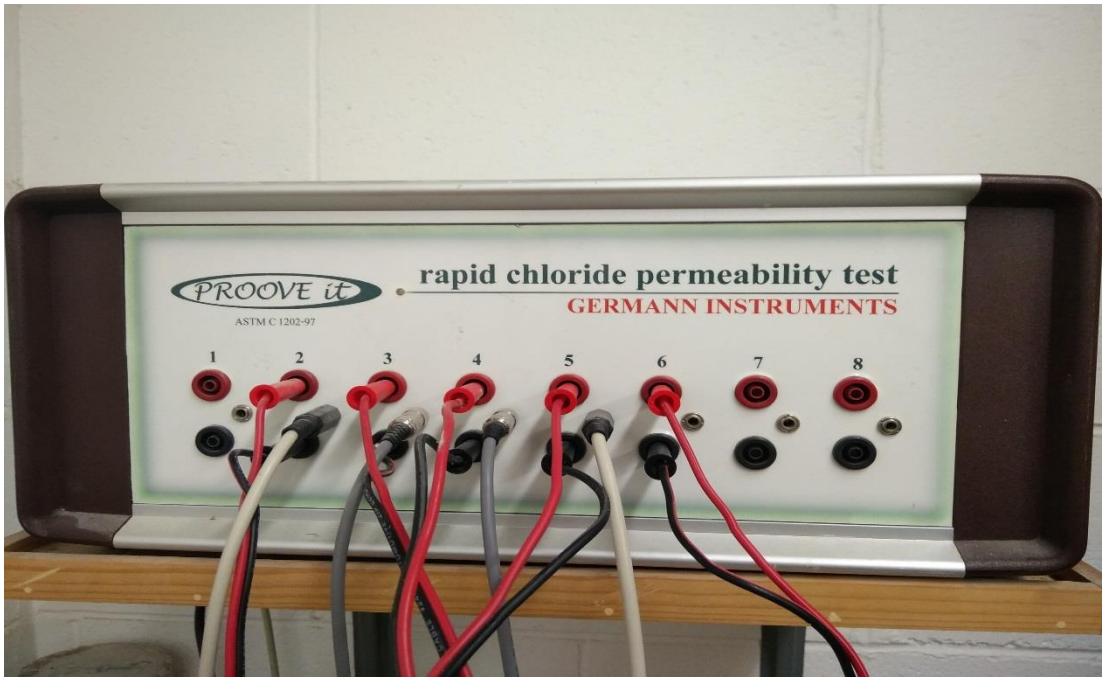

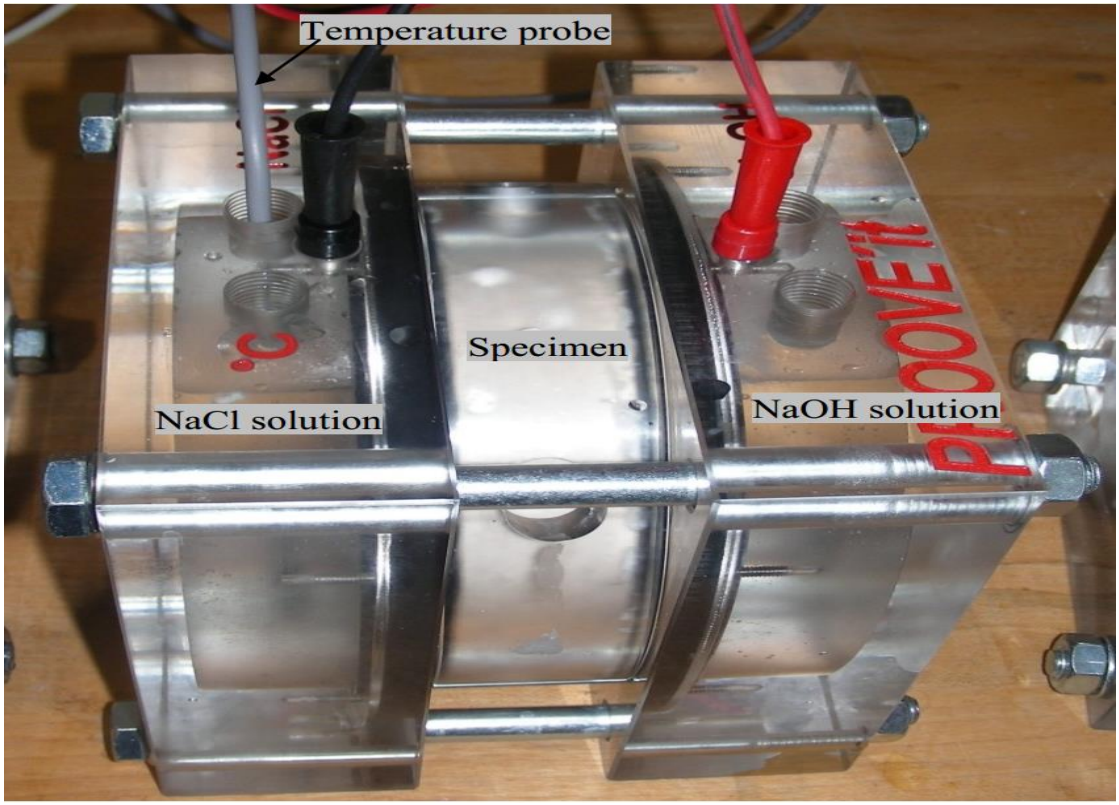

Figure 3.8: APROOVE'it System by Germann Instruments used in RCIP tests

Figure 3.9: The EPSON scanner used for scanning the specimens.

Chapter 4 DATA ANALYSIS

The results of the RCIP tests (ASTM C1202), ESR test (ASTM WK37880), dynamic modulus test (ASTM C215) and water absorption tests (ASTM C642) are shown in Table 4.1. These measurements are briefly described below, and the relationship of these measurements are discussed in this chapter.

4.1 Chloride Penetrability (ACP)

The recorded original data, including the temperature of the solution and measured current through each specimen is shown in Appendix A. The maximum specimen temperature is 51°C. According to ASTM C1202, these temperatures is lower than the allowed elevation; hence the results of charge passed are acceptable.

The cross-section dimensions of the specimens changed after the mechanical loading and freeze-thaw cycles, as shown by the measured disc diameters in Table 3.3. This may have been due to the internal permanent damage, such as permanent microcracks developed in the samples. The final charge passed through the discs was corrected based on the Equation (3.1).

After 24 hours conditioning, two sides of specimens which immersed in 0.3% NaCl solution or 0.3 N NaOH solution were under 60 volts for 6 hours. During this process, the amounts of chloride ions passed through specimens was used to indicating the penetrability of concrete samples. In general, these eight samples have high chloride permeability:14-2, 22-2, 28-2,30-1,34-1,35-1, 35-2, 40-1; the Sample 8F is low; others are moderate, according to the Table 4.2. The highest charge passed through the Sample 34-1, the lowest charge through sample 8F.

It is noted that discs from a same cylinder showed different chloride permeability. Specifically, the largest deviation between discs is about 11%, as shown in Table 4.1. It is interesting to note

that usually the disc cut from the bottom of a cylinder allowed less charges than the discs above. This may have been due to the different levels of compaction. For example, Figure 4.2 shows a cylinder: the concrete at the bottom shows less surface cracks than that the top; 2). the thickness of specimens: from the Table 3.3, it is obviously that the thickness of every specimen is different from other others, ASTM C1202 does not provide any equations to correcting it, variation in thickness may affect the results: 3). the temperature: higher temperature might facilitate chloride ion through the specimen, and the temperature is higher in specimens which have higher penetrability. The penetrability of specimens indicated by charge passed could higher than it should be.

4.2 Electrical Surface Resistivity (ESR)

The measured Electrical Surface Resistivity for 12 cylinders is shown in Table 4.1. These measurements are obtained from the previous study by Mitchell (2016).

4.3 Water Absorption after Immersion (WA)

The measured Permeable Voids and Water Absorption (after immersion) in Concrete for 12 cylinders is shown in Table 4.1. These measurements are obtained from the previous study by Mitchell. Before the discs are used for rapid chloride ion penetration tests, the water absorption (after immersion) and permeable voids of these discs are measured.

It is envisioned that the measured permeable voids from cylinder specimens represents well microcracks on the surface of the concrete specimens. PV is the ratio of volume of permeable pore space and volume of the concrete. Water Absorption (after immersion), on the other hand, is the ratio of mass of water in sample after immersion and mass of oven-dried sample. Note that the water absorption measured in the study can be different from that obtained by Lin et al. (2012) using air-dried specimens.

The relationship between permeable voids and water absorption (after immersion) of discs in this study is shown in Figure 4.3. These two measurements in general agree with each other.

4.4 Dynamic Modulus (DM)

The measured dynamic modulus for only 12 cylinders is shown in Table 4.1. These measurements are obtained from the previous study by Mitchell. The dynamic modulus of specimens was measured according to ASTM C215. The tests were not conducted for the rest cylinders because their surfaces developed cracks and spalling such that the sensors were not able to reliably attach.

4.5 Comparison of ESR and ACP

Figure 4.4 shows the relationship between the average surface resistivity and average charges passed. ESR are only available for the 12 cylinders; hence the average charges passed two discs sliced from the cylinders are used in Figure 4.4. In general, the passing charge decreases with an increase in the surface resistivity. The specimens were saturated with water before the ESR tests (Mitchell (2016)). The water through surface cracks and pore networks provides smaller electrical resistance than concrete; hence, specimens with more cracks leads to higher chloride penetrability, but lower electrical resistivity. A linear regression, describes the general observation,

$$ACP = -2.1544ESR + 5836.6, \quad (4.1)$$

where *ACP* is the average charge passed in coulombs, and *ESR* is the cylinder surface resistivity in kΩ/cm. The frequency of ratio of charge from regression equation to value from test is shown in Figure 4.5.

The data obtained in this study and that by Mitchell (2016) is comparable to the data in the literature. Two power functions have been proposed in the literature based on average surface resistivity and average charge passed: one by American Association of State Highway and

Transportation Officials (AASHTO) and another buy Louisiana Transportation Research Center (LTRC) respectively as shown in the Figure 4.6. The data in this study fall in between these two models. Note that the models by AASHTO and LTRC are for concrete samples that do not contain internal damage induced by mechanical loading and freeze-thaw cycles as those in this study. A separate curve fitting is conducted as shown in the Figure 4.7. The power function seems to better describe the observed behavior,

$$ACP = 13962ESR^{-0.585}, \quad (4.2)$$

where *ACP* is the average charge passed in coulombs, and *ESR* is the cylinder surface resistivity in kΩ/cm. The frequency of ratio of charge from power function to value from test is shown in the Figure 4.8.

4.6 Comparison of WA and ACP

Lin et al. (2012) proposed that water absorption has a strong relationship with chloride penetrability. The conclusion seems questionable because 1) the stresses applied to the concrete is much higher than that experienced by bridge deck concrete; and 2) the water absorption was measured at air-dried conditions, as discussed in Chapter 2. In this study, the concrete cylinders are subjected to a compressive stress up to $0.4f_c'$, and the water absorption are measured for oven-dried specimens.

The water absorption and charges passed for each disc specimen is shown in the Figure 4.9. In general, the passing charge increases with an increase in the measured permeable voids. A closer look at the data shows that the water absorption of Sample 3D is high, while the charge passed through the sample relatively low: only about half of charge passed through the Sample 34-1 (4712 coulombs), which has roughly the same permeable voids. The surface image of the sample (Figure A.03), indicates that an aggregate with a diameter about 2 inch occupied roughly 20 percent of the

section of this sample. As a result, chloride ion may have not been able to pass through the aggregate, leading to a low chloride ion penetrability.

The relationship of Water Absorption (after immersion) and RCIP is replotted in Figure 4.10 with the sample 3D removed. A linear regression function can be used to describe the general observation:

$$CP = 0.0004WA + 3.3527, \quad (4.3)$$

where *CP* is the charge passed through a disc sample in coulombs and *WA* is the water absorption after immersion in percentage. The frequency of ratio of charge from regression equation and value from test is shown in the Figure 4.11.

Again, a power function was established between charge passed and water absorption, as shown in the Figure 4.12 to better describe the observation,

$$CP = 93.165WA^{2.347}, \quad (4.4)$$

where *CP* is the charge passed through a disc sample in coulombs and *WA* is the water absorption after immersion in percentage. The frequency of ratio of charge from power function to value from test is shown in Figure 4.13. Note that data is limited as water absorption after immersion is between 4 to 6 percent. The proposed relationship needs additional data to be applicable to the practice for concrete for the field.

The chloride ion penetration of concrete specimens mainly relies on microcracks networks in a concrete sample. The higher penetrability of specimens indicates more cracks in concrete, the cracks facilitate water penetrate in the specimens. This is a possible reason for the closely relationship between water absorption and charge passed.

A schematic cross section of the concrete sample is shown in the Figure 4.14. The standards (ASTM C1202) for the RCIP test requires that the size of samples: 2×4 inch, and lateral surface

was epoxy avoiding chloride ion penetrate through the lateral surface. Due to that, four parts of concrete as shown in the Figure 1-1 are possible taken as specimens which are measured by ASTM C1202 estimating the chloride ion penetrability. It is obviously that the red paths which indeed through concrete cannot be represented by the RCIP tests. However, the water can penetrate in concrete specimens through the red path, and leading to increase in water absorption.

4.7 Comparison of ACP and WA of Cylinder

The regression equation:

$$WAC = 0.0005ACP + 2.0087, \quad (4.5)$$

where *WAC* is water absorption (after immersion) of cylinder in percentage and *ACP* is average charge passed through a disc in coulombs; is based on the relationship between water absorption of cylinder and average charge passed as shown in the Figure 4.15. The relationship is weaker than that between charge passed through disc and water absorption of disc. It is probably because the disc tested in water absorption was only one of middle part of cylinder. The middle part might not represent entire cylinder.

4.8 Comparison of DM and ACP

Dynamic modulus was viewed as an index of concrete internal damage in a study by Mitchell (2016) and Yang et al. (2005). The damage to concrete in this study is caused by combined mechanical stresses (up to $0.4f_c'$) and freeze-thaw cycles. In the Figure 4.16, we can see that dynamic modulus was not related to average dynamic modulus for this group of tests. According to the ASTM C215, dynamic modulus should decrease as charge increase. The dynamic modulus of sample C16 is 3039 MPa, only higher than samples C34, but the average charge passed through C16 is 3152 coulombs the lowest in the specimens. The penetrability of C40 is high and 4109 coulombs passed during the six-hour test, according to the ASTM C215 the dynamic modulus

should lower than C16, in fact the dynamic modulus is 16730 MPa the highest among these specimens. This indicates that dynamic modulus is not an efficient method for the concrete samples in this study.

4.9 Comparison of Average WA and ESR

The water absorption (after immersion) of disc and water absorption (after immersion) of cylinder were tested by Mitchell et al. (2016) and me. Average water absorption (after immersion) is average water absorption of discs. The height of cylinder is 8-inch and the diameter is 4-inch. All disc samples were subjected to RCIP test. The disc samples:11-1,11-2;14-1,14-2;15-1,15-2;16-1,16-2;17-1,17-2;21-2;22-2;28-1,28-2;29-1,29-2;30-1,30-2;34-1,34-2;35-1,35-2;40-1,40-2;42-1,42 are from middle part of cylinder C11; C14; C15; C16; C17; C21; C22; C28; C29; C30; C34; C35; C40; C42 respectively. The water absorption of disc samples and the water absorption of cylinders all measured by ASTM C642. The data of average water absorption of disc is shown in the Table 4.3.

The regression equation based on average water absorption and average surface resistivity as shown in the Figure 4.17 is

$$ESR = -1.4031ABA + 16.621, \quad (4.6)$$

where *ESR* is average surface resistivity in kΩ/cm and *ABA* is average water absorption (after immersion) in percentage. The average water absorption of samples (11-1,11-2) is 4.852%, the average surface resistivity is 13.2 kΩ/cm the highest one. According to the regression equation the average surface resistivity should be 9.3764 kΩ/cm. One possible reason for the weak relationship is data of average water absorption was from test measuring in disc, however samples subjected to the ESR test were from cylinders. The discs are middle part of cylinders cannot represent entire cylinder.

4.10 Comparison of ESR and WAC

Considering this difference, the relationship between average surface resistivity and water absorption of cylinder is shown in the Figure 4.18. The regression equation is

$$ESR = -1.918WAC + 16.797, \quad (4.7)$$

where *ESR* is average surface resistivity in kΩ/cm and *WAC* is water absorption (after immersion) of cylinder in percentage. The frequency of ratio of water absorption of cylinder and value from test is shown in Figure 4.19.

The dynamic modulus is deemed a method for estimating internal damage of concrete. The relationships between dynamic modulus and average water absorption of disc, water absorption of cylinder is shown in the Figure 4.20 and the Figure 4.21 respectively. From the Figure 4.9, we know water absorption of disc has directly proportional relationship with penetrability of samples. Considering expected inverse relationship between charge passed through the specimens and dynamic modulus, average water absorption of disc may also inverse relates to dynamic modulus. However, as shown in the Figure 4.20, the relationship is very weak. Similar with average water absorption, cylinder water absorption also has very weak relationship with dynamic modulus.

The ratio of the surface and volume of the disc samples is 2, and the ratio for the cylinder samples is 1.25. It means water penetrates disc samples is easier than cylinder disc. This is one possible reason for the weak relationship between average water absorption of disc and water absorption of cylinders as shown in the Figure 4.22. Another possible reason proposed before is concrete in bottom denser than in top.

4.11 Summary

The comparisons in this study are summarized in Table 4.3. The table lists the coefficient of determination for each regression analysis. The conclusion based on these comparisons are shown in Chapter 5.

Table 4.1: Results of the test on concrete samples.

No.	Charge Passed (Coulombs)	Corrected Charge (Coulombs)	Water Absorption* (cylinder; %)	Water Absorption* (disc; %)	ESR* (kΩ/cm)	Dynamic Modulus* (kPa)
11-1	3955	3446	3.185	5.181	13.2	5.024E+06
11-2	3747	3216		4.523		
14-1	4565	3962	3.338	5.128	7.7	3.170E+06
14-2	5313	4534		5.128		
15-1	3612	3112	3.752	4.639	11.1	9.244E+06
15-2	4336	3698		5.291		
16-1	3664	3173	3.470	4.687	11.3	3.039E+06
16-2	3654	3131		4.615		
17-1	4126	3574	4.183	4.663	9.4	9.169E+06
17-2	3745	3205		4.592		
21-2	4140	3538	4.042	4.663	10.4	6.093E+06
22-2	5180	4419	4.183	4.615	7.9	6.042E+06
28-1	4659	3999	3.756	4.737	8.5	1.626E+07
28-2	4931	4214		5.263		
29-1	3984	3440	3.886	4.592	8.4	9.153E+06
29-2	4321	3733		4.639		
30-1	4911	4245	4.314	4.813	8.6	4.111E+06
30-2	4097	3474		4.615		
34-1	5503	4712	4.199	4.865	8	2.065E+06
34-2	4206	3624		4.639		
35-1	5059	4370	4.058	5.263	8.4	6.674E+06
35-2	5047	4344		4.592		
40-1	5436	4676	3.866	4.737	9.7	1.673E+07
40-2	4119	3543		4.569		
42-1	3717	3215	2.682	4.103	10.8	1.208E+07
42-2	3935	3393		4.569		
1F	3102	2678		4.124		
4F	2749	2378		4.145		
5F	2743	2379		4.124		
8F	2141	1847		4.188		
1D	3445	2956		4.737		
3D	2966	2547		5.946		
7D	2361	2024		4.028		
2H	2781	2373		4.103		
7H	2861	2475		4.016		
9H	2862	2448		4.103		

*Result from Mitchell et al. (2016)

Table 4.2: Chloride Ion Penetrability Based on Charge Passed

Charge Passed (coulombs)	Chloride Ion Penetrability
>4000	High
2000-3000	Moderate
1000-2000	Low
100-1000	Very Low
<100	Negligible

Table 4.3: Water absorption of cylinder and average water absorption of disc

Cylinder No.	Water Absorption of Cylinder (%)	Disc No.	Water absorption of Disc (%)	Average Water Absorption of Disc (%)
C11	3.185	11-1	5.181	4.852
		11-2	4.523	
C14	3.338	14-1	5.128	5.128
		14-2	5.128	
C15	3.752	15-1	4.639	4.965
		15-2	5.291	
C16	3.470	16-1	4.687	4.615
		16-2	4.615	
C17	4.183	17-1	4.663	4.628
		17-2	4.592	
C21	4.042	21-2	4.663	4.663
C22	4.183	22-2	4.615	4.615
C28	3.756	28-1	4.737	5.000
		28-2	5.263	
C29	3.886	29-1	4.592	4.616
		29-2	4.639	
C30	4.314	30-1	4.813	4.714
		30-2	4.615	
C34	4.199	34-1	4.865	4.752
		34-2	4.639	
C35	4.058	35-1	5.263	4.928
		35-2	4.592	
C40	3.866	40-1	4.737	4.653
		40-2	4.569	
C42	2.682	42-1	4.103	4.336
		42-2	4.569	

Table 4.4: Coefficients of determination

Name	Average charges Passed: ACP (coulombs)	Water Absorption: WA (%)	Electrical Surface Resistivity: ESR (kΩ/cm)	Dynamic Modulus: DM (GPa)
ACP	1.000	0.6515	0.6262	0.0004
WA	Figure 4.12	1.000	0.1402	0.0216
ESR	Figure 4.4	Figure 4.17	1.000	
DM	Figure 4.16	Figure 4.20		1.000

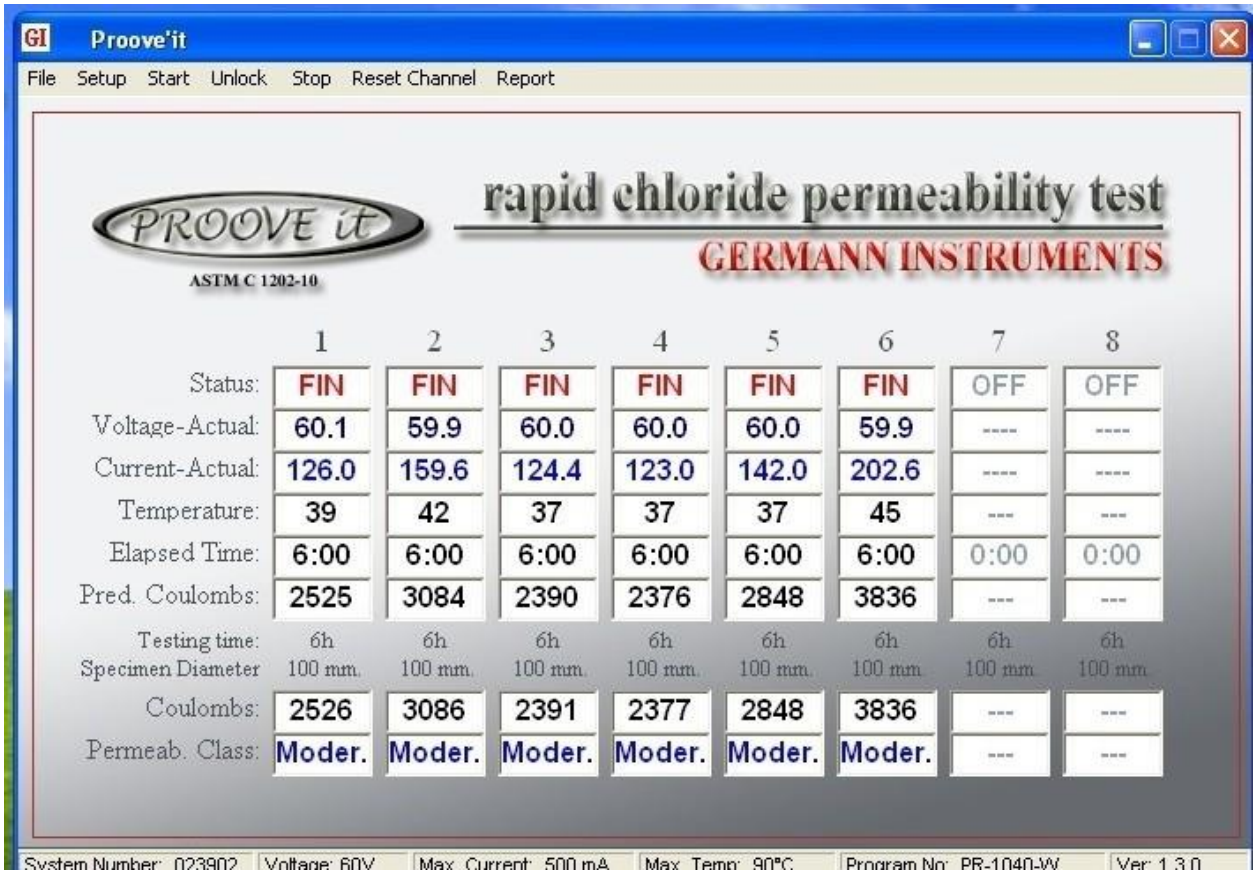

Figure 4.1: PROOVE'it© software in PC screen to run the test and acquire the data

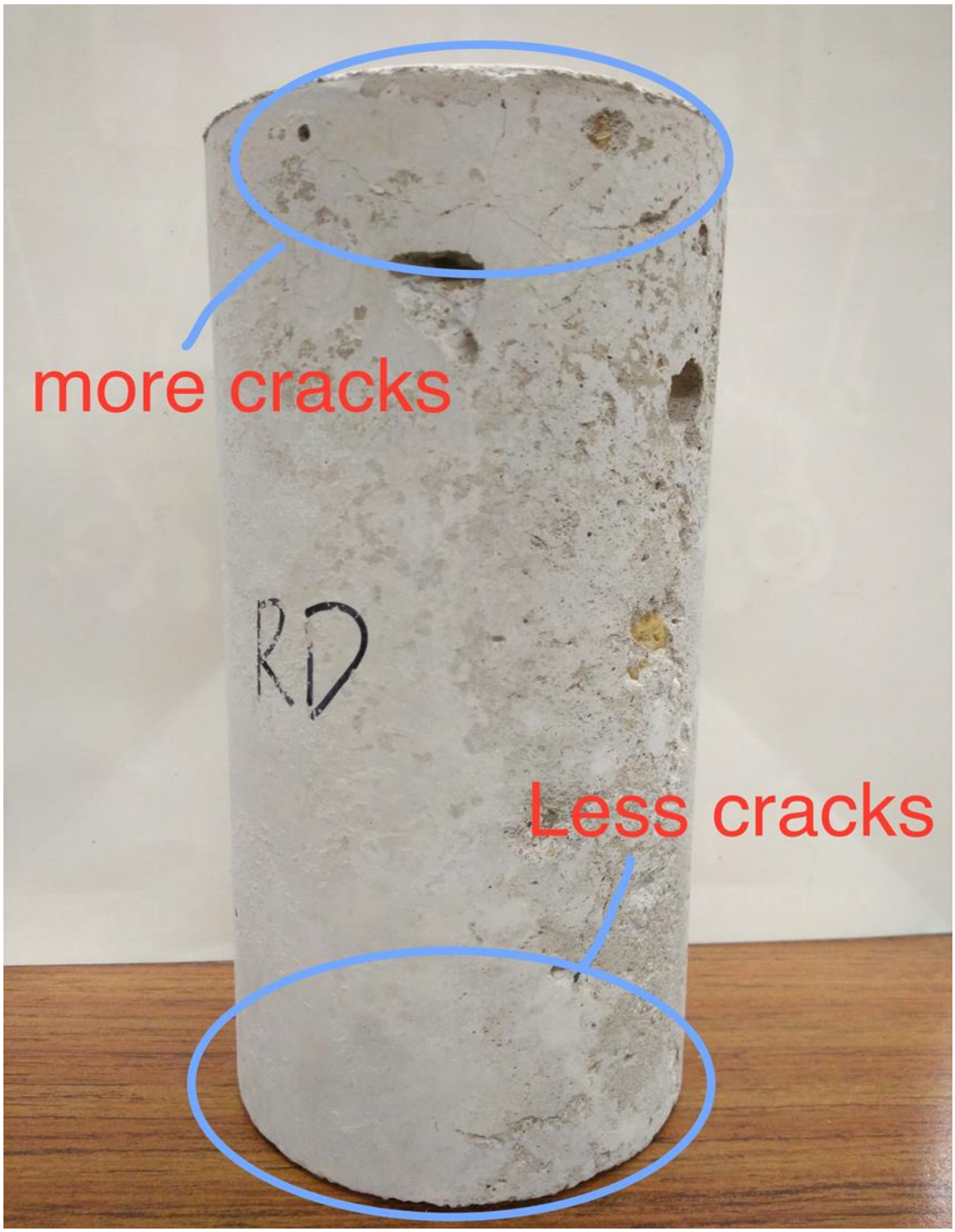

Figure 4.2: A concrete cylinder.

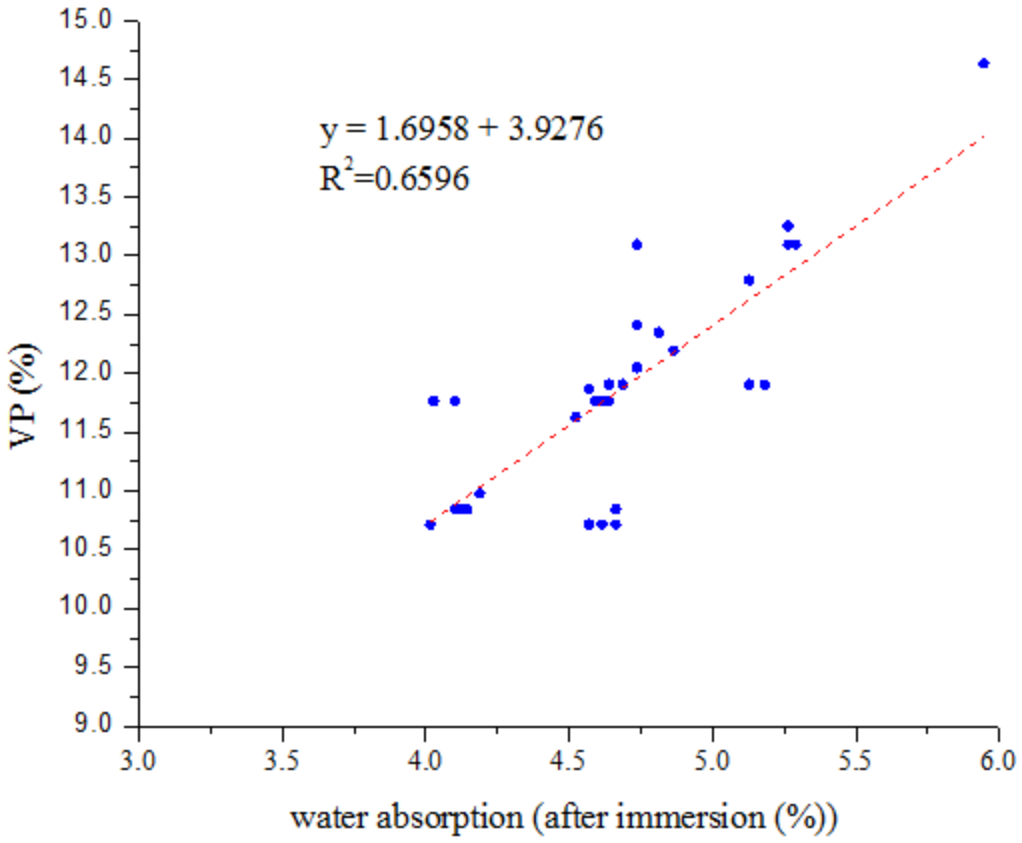

Figure 4.3: Relationship between VP and water absorption (after immersion (%))

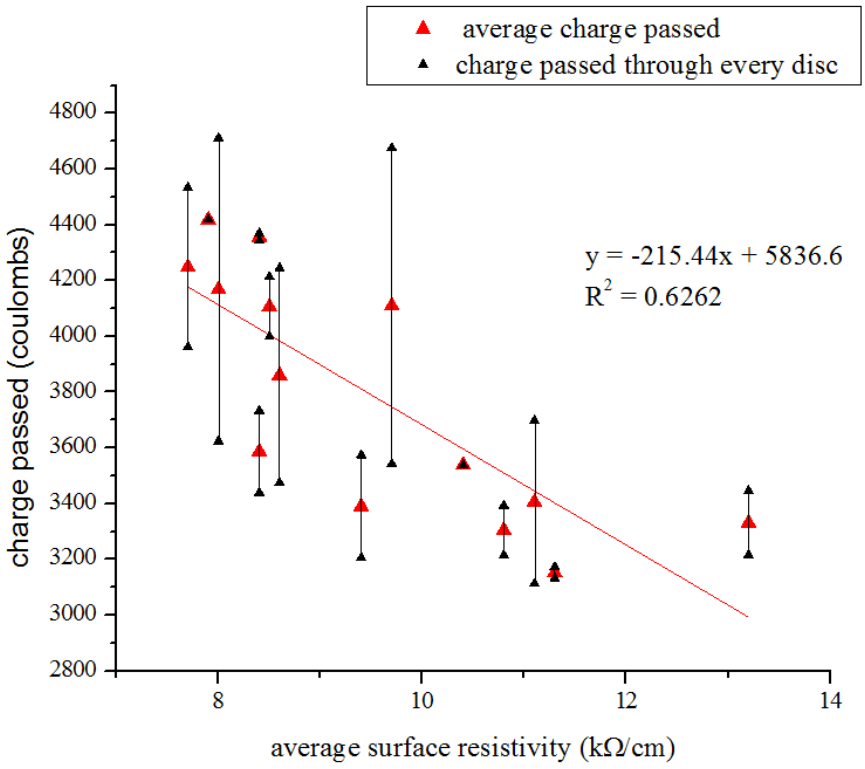

Figure 4.4: Relationship between average charge passed and average surface resistivity.

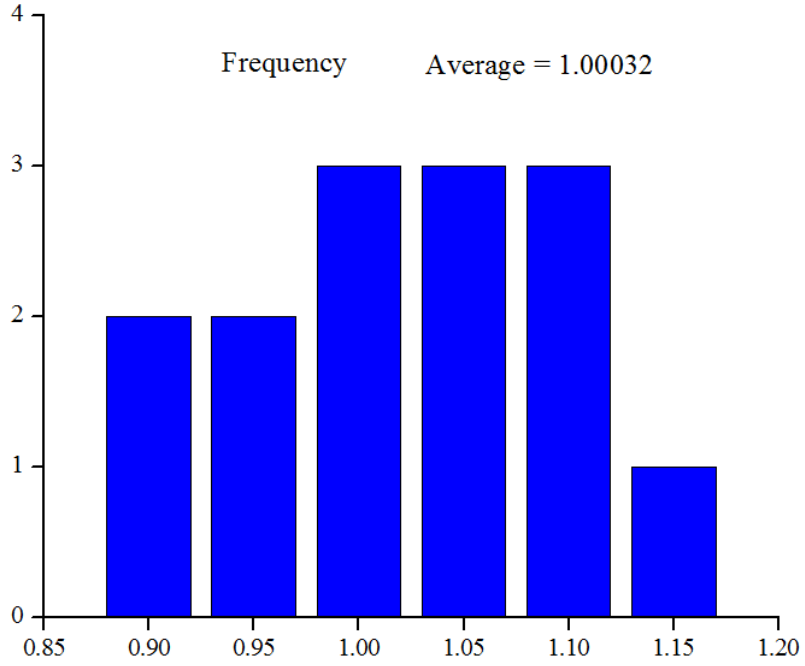

Figure 4.5: The frequency of ratio of average charge passed from regression equation and average surface resistivity.

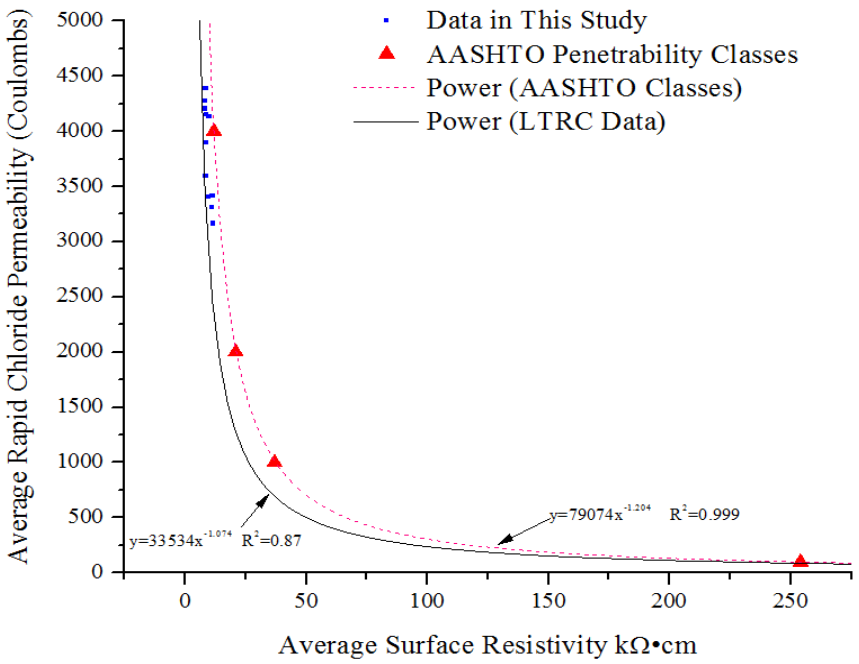

Figure 4.6: Power function between charge passed through the sample and average surface resistivity (Rupnow and Icenogle 2011).

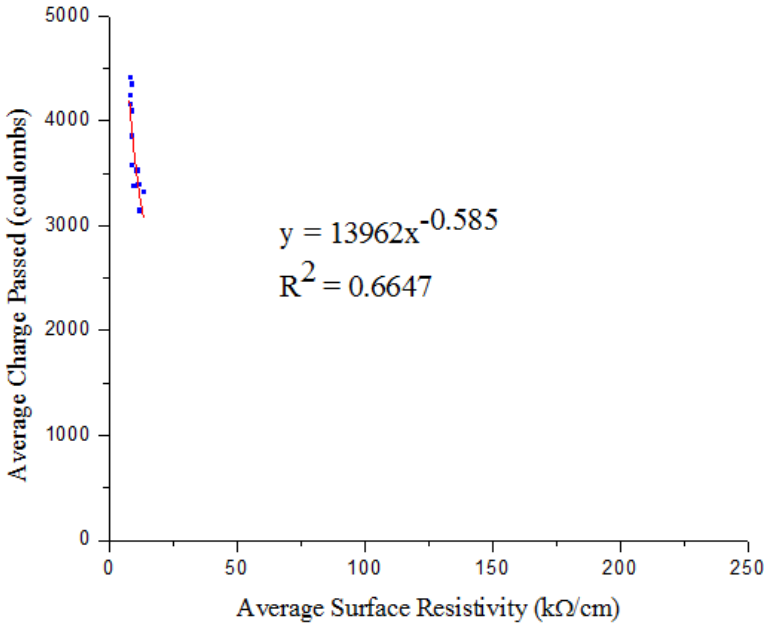

Figure 4.7: Power function based on relationship between average charge passed and average surface resistivity.

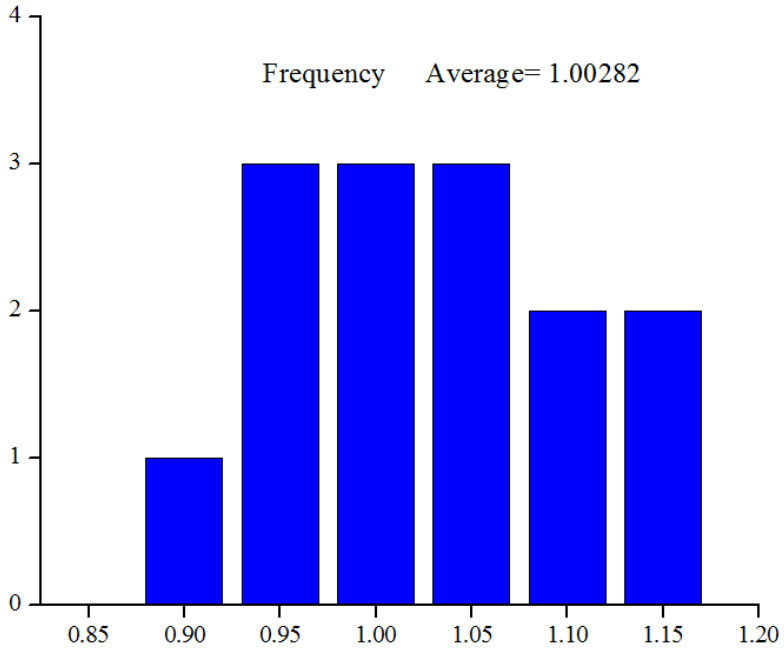

Figure 4.8 : The frequency of ratio of average charge passed from power function and average surface resistivity from test.

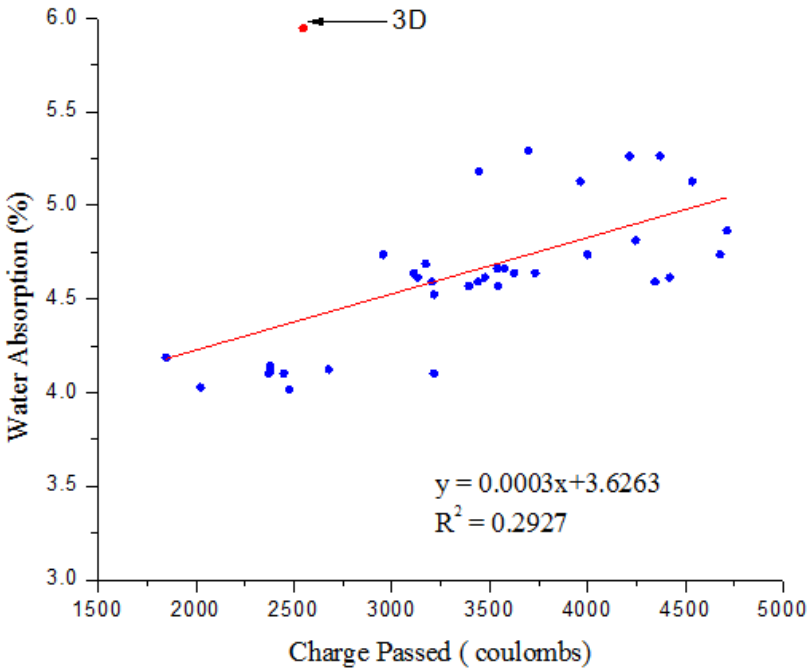

Figure 4.9: Relationship between water absorption and charge passed.

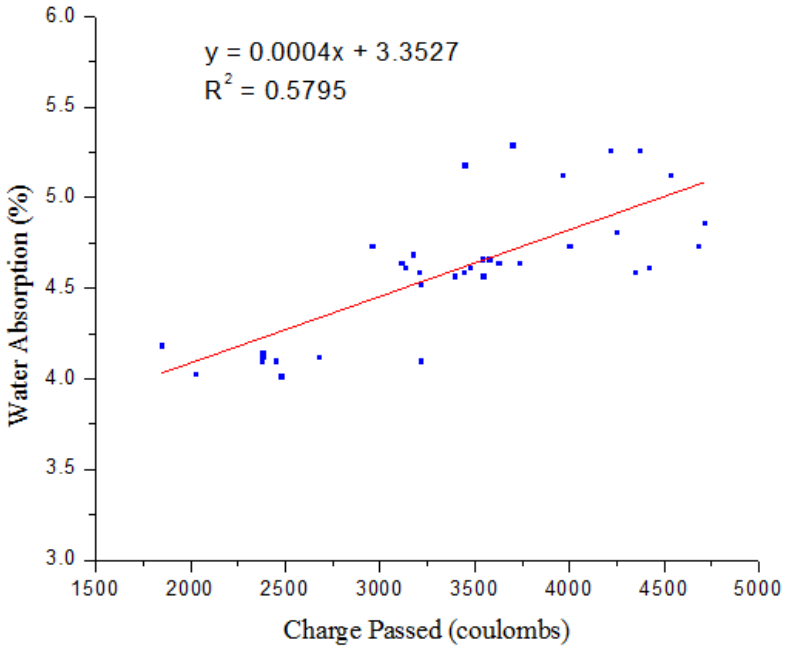

Figure 4.10: The regression equation based on the relationship between water absorption and charge passed.

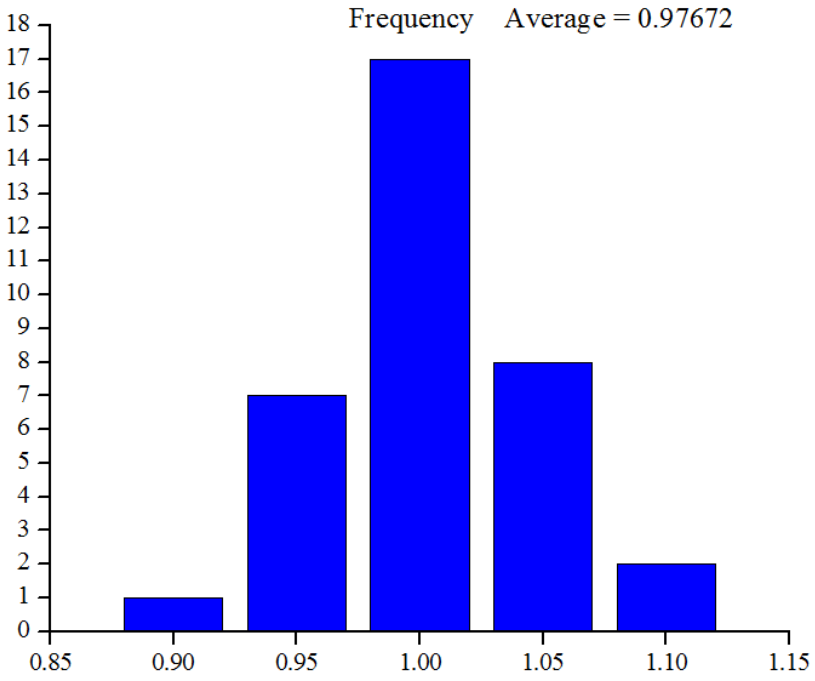

Figure 4.11: : The frequency of ratio of charge from regression equation and value from test.

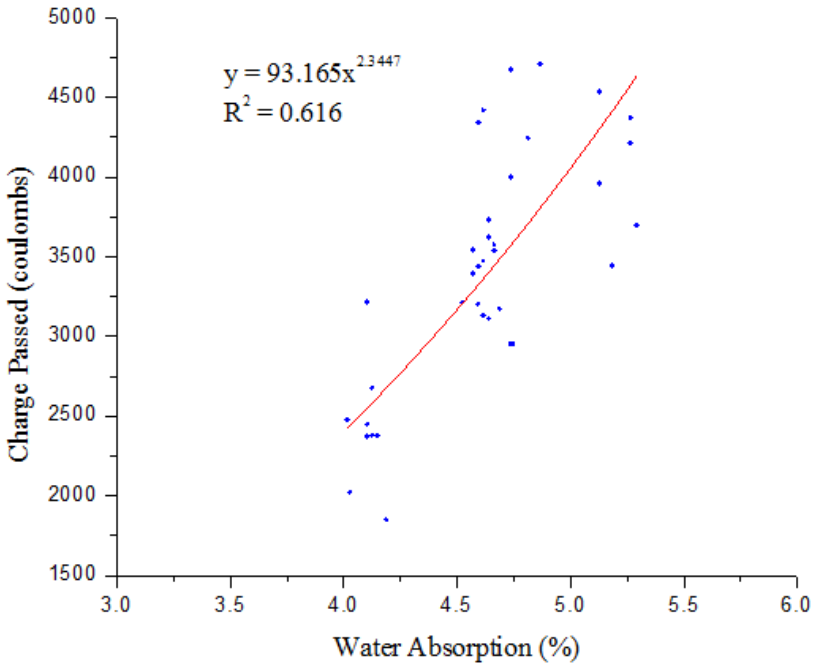

Figure 4.12: Power function based on the relationship between charge passed and water absorption.

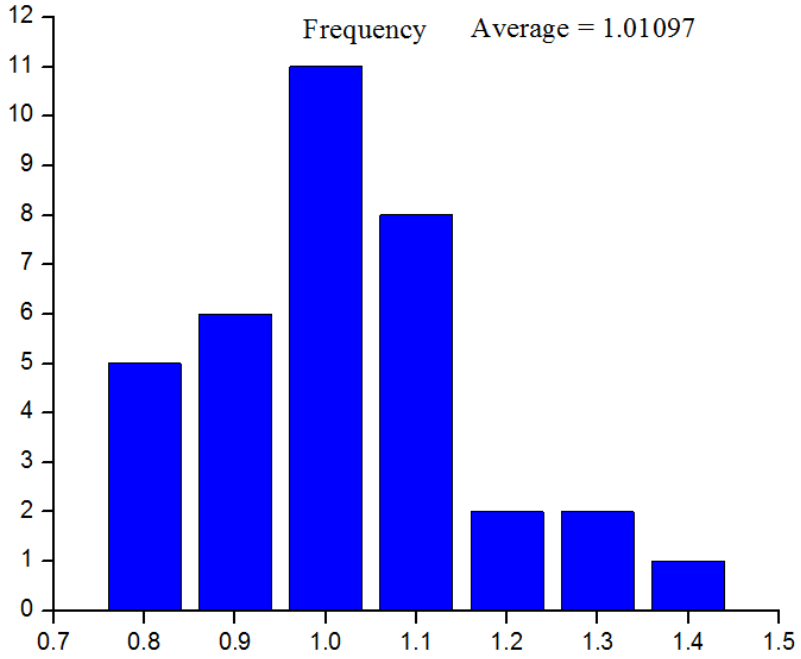

Figure 4.13: Rate of variation in charge passed from power function based on the relationship between water absorption and charge passed.

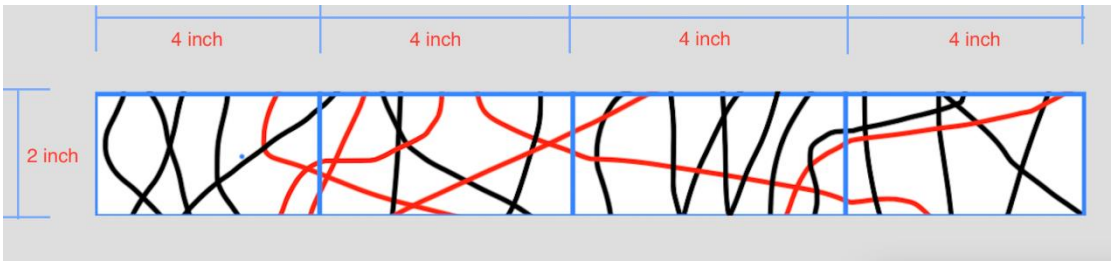

Figure 4.14: The cross-section from concrete in the field.

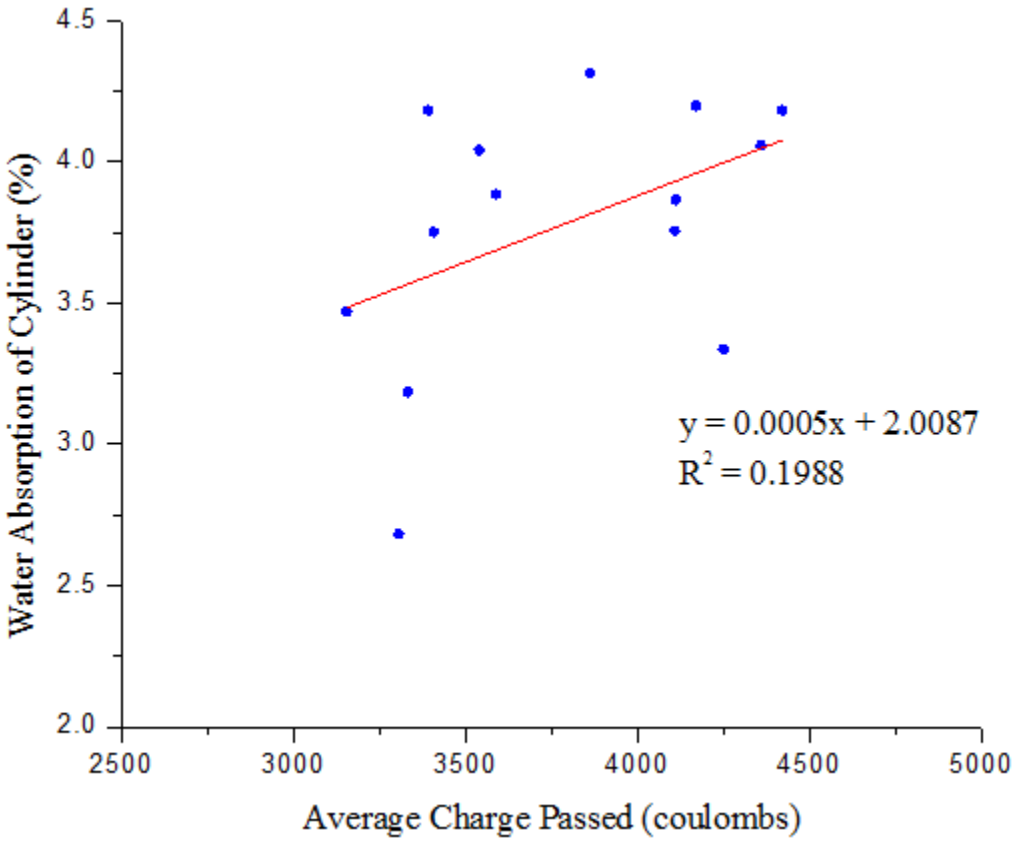

Figure 4.15: The relationship between water absorption of cylinder after immersion and average charge passed.

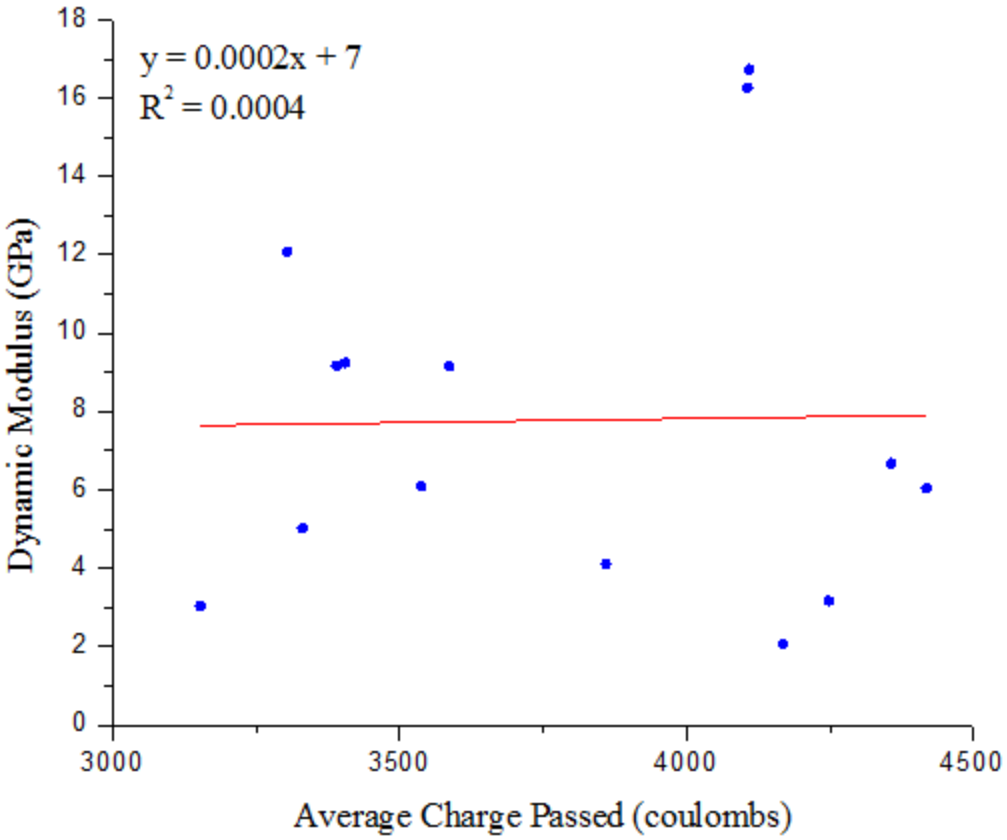

Figure 4.16: The relationship between dynamic modulus and average charge passed.

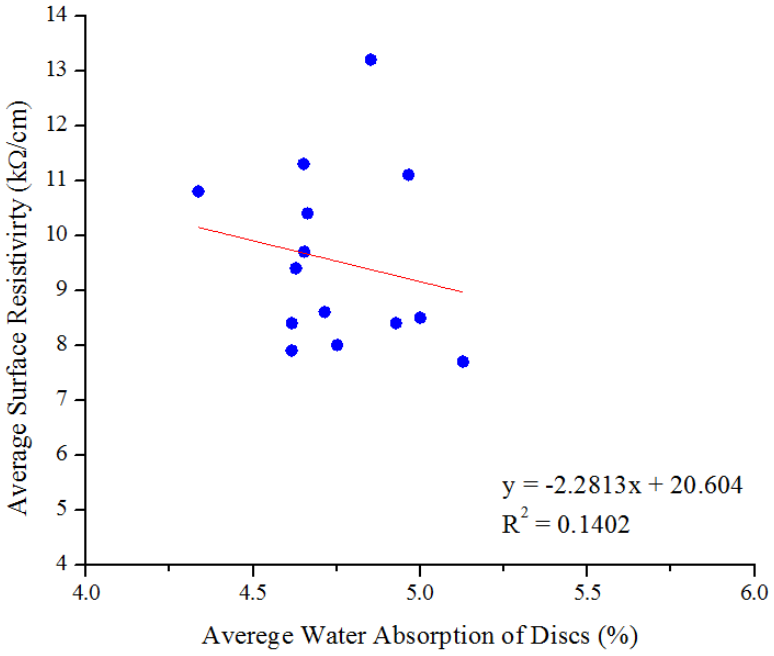

Figure 4.17: The relationship between average surface resistivity and average water absorption of disc after immersion.

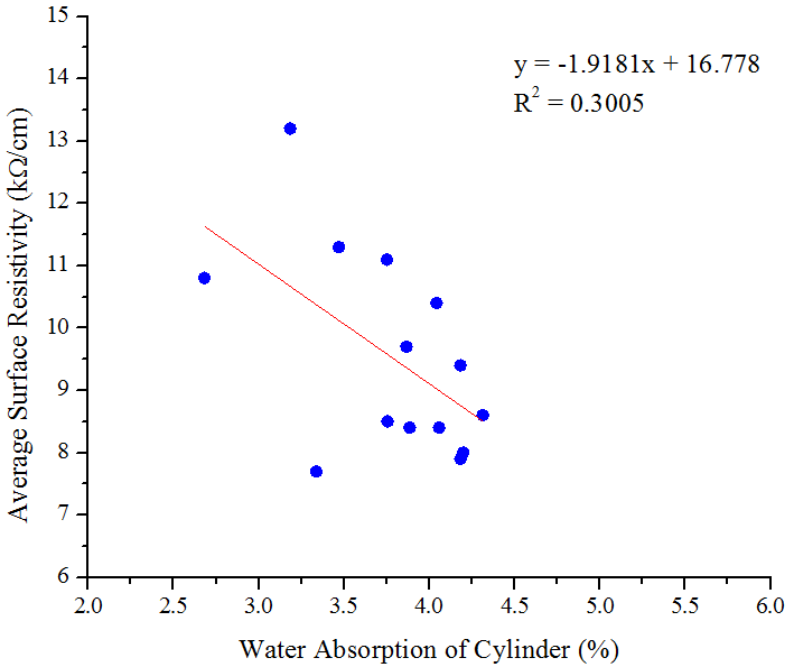

Figure 4.18: The relationship between average surface resistivity and water absorption of cylinder.

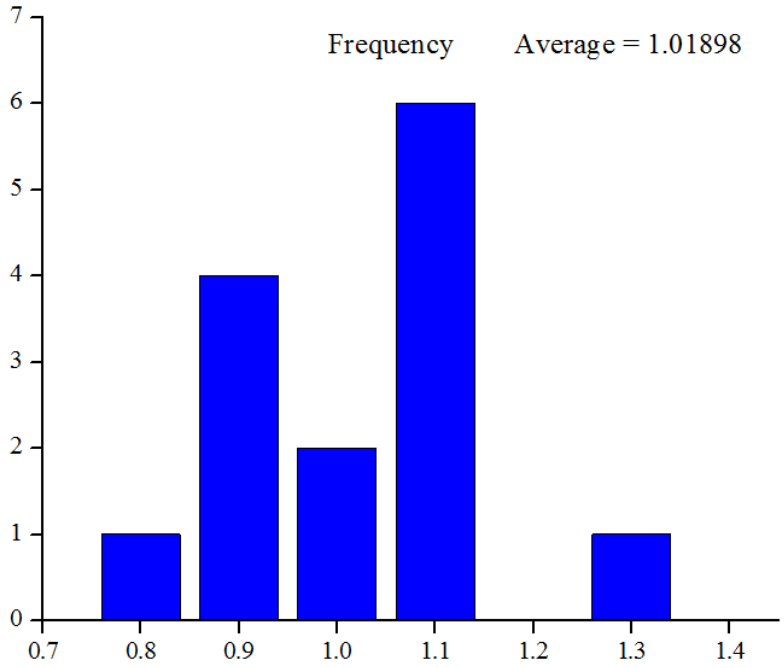

Figure 4.19: The frequency of ratio of water absorption of cylinder and value from test.

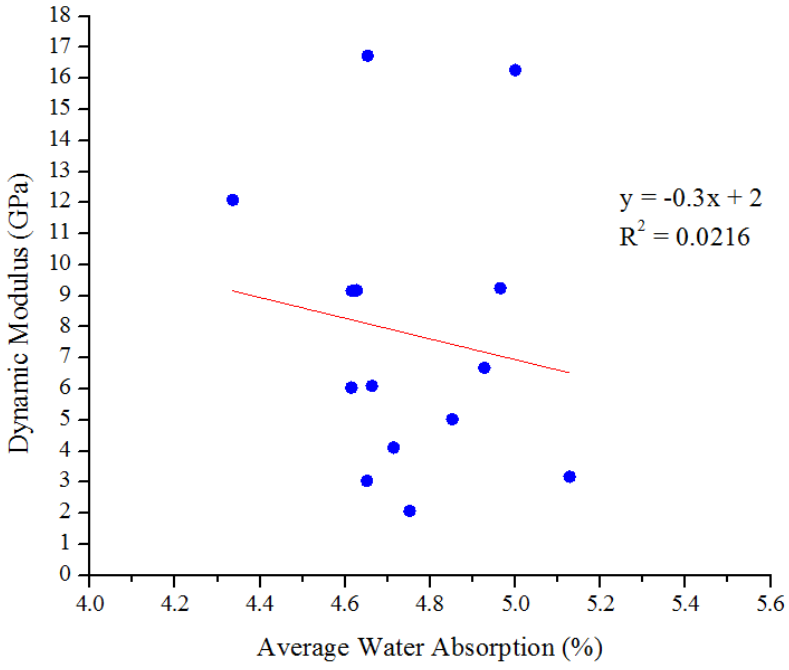

Figure 4.20: The relationship between dynamic modulus and average water absorption of disc.

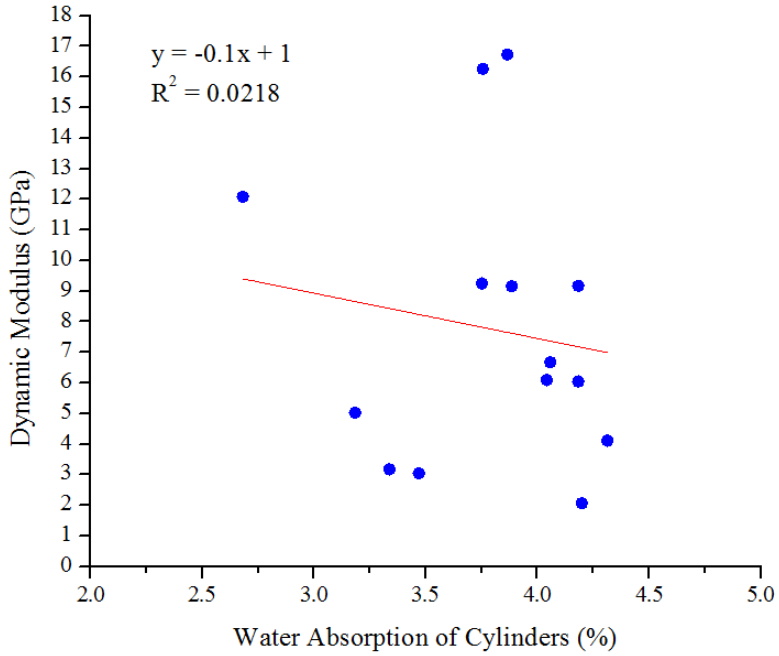

Figure 4.21: The relationship between dynamic modulus and water absorption of cylinder.

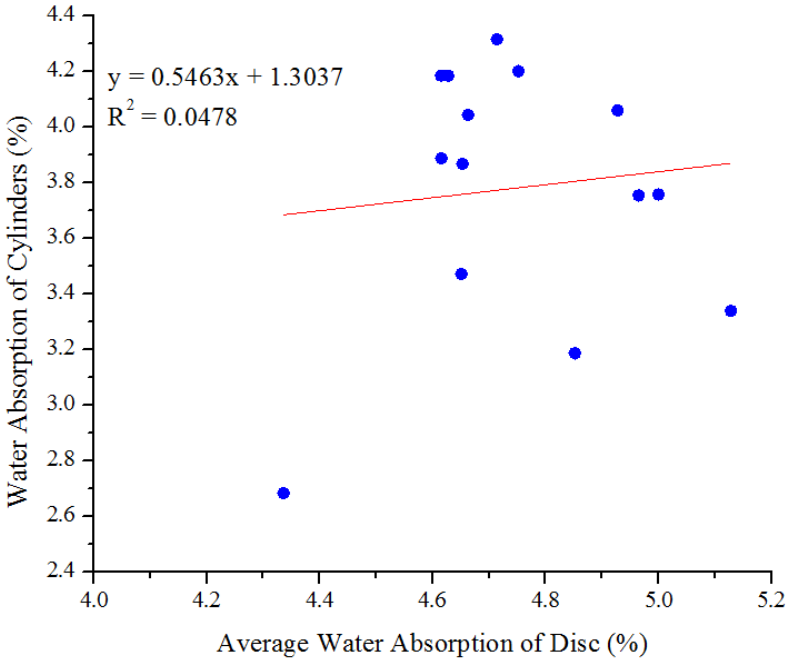

Figure 4.22: The relationship between water absorption of cylinder and average water absorption of disc.

Chapter 5 Summary and Conclusion

5.1 Summary

Several standard methods are available to measure the deterioration of concrete, including ASTM C215 (Dynamic Modulus test), ASTM C1202 (Rapid Chloride Ion Penetrability test), and ASTM WK37880 (Electrical Surface Resistivity). In addition, ASTM C642 (water absorption test) helps quantification of permeability voids in concrete. These tests have been used to evaluate undamaged concrete or concrete samples after freeze-thaw cycles.

Concrete in bridge decks in Northern States, such as Wisconsin, is subjected to both freeze-thaw cycles and mechanical stresses. In this study, concrete samples are subjected to compressive stresses (about 40 percent of the measured concrete compressive strength) and F/T cycles (100 to 300cycles) to better represent the concrete in Wisconsin bridges. It is believed that concrete can develop the microcracks under compressive stresses similar to freeze-thaw cycles. Therefore, this study focuses on the comparison of the standard testing methods on the evaluation of damaged concrete.

A total of 36 discs were tested for their chloride permeability. Combined with the electricity surface resistivity, water absorption (ASTM C642) and dynamic modulus (ASTM C215) measured in previous study, this study provides comparison of these measurements in evaluating the durability of concrete samples that may have been damaged by compressive stresses and/or freeze-thaw cycles.

5.2 Conclusion

Based on the 36 tests conducted in this study, the following conclusions can be made,

1. the water absorption (after immersion) of concrete discs is closely related to the charges passed through the samples in the rapid chloride ion penetration test. The relationship can be well described using a linear function.
2. the electrical surface resistivity is inversely proportional to the measured water absorption. In this case the water absorption measured using cylinder specimens must be used instead of discs sliced from the cylinders. This may have been due to the fact that both the electrical surface resistivity and the cylinder water absorption are closely related to the microcracks and permeable voids near the cylinder surface while the disc water absorption is more closely related to the microcracks and permeable voids away from the surfaces.
3. the relationship between the electrical surface resistivity the cylinders and charges passing through the discs is not strong, again this may have been due to the fact that the electrical surface resistivity is closely relate to the microcracks and permeable voids near to the microcracks and permeable voids away from the surfaces.
4. the measured dynamic modulus has large variation. This may be caused by the damaged concrete cylinders used in the tests. The measured surface resistivity for the cylinders in this study (after being subjected to compressive stresses and /or freeze-thaw cycles) seems not related to the measured passing charge, nor water absorption measured using cylinder and discs.

5.3 Further research

The goal of this line of studies is to quantify the impact of overweight vehicles on the durability of concrete bridge decks in Northern States. The tests by Lin et al. (2012) using concrete cylinders indicated that high compressive stresses (up to 0.8f'c) in concrete can cause deterioration to durable concrete designed to resist freeze-thaw actions. The tests by Mitchell (2016) and in this

study indicates that concrete durability can be negatively affected moderate compressive stresses ($0.4f_c'$) and freeze-thaw cycles. A variety of testing methods can be used to evaluate the permeability of concrete, and water absorption can be a suitable index for concrete permeability.

Meanwhile, the present study is limited because the tests have been conducted only for concrete cylinders in laboratories, which may be different from the concrete in a bridge deck. The following studies are suggested to continue this line of research:

1. further test of the relationship between water absorption and chloride permeability is necessary for establishing water absorption as another method to estimating deterioration of concrete
2. the test should be conducted on concrete taken from the field or from assimilated bridge deck. In this case, the bridge decks can be subjected to stresses from both super-heavy vehicle loads and/or trucks within legal limits. The impact of repeated loading can also be included.
3. more rigorous deck stress analyses should be conducted to establish the relationship between heavy trucks and the compressive stresses in decks that may impact the permeability of deck concrete.

This line of research is expected to contribute to a durability design methodology that can be used to design bridges for local truck traffic targeting a variety of desired service lives.

REFERENCES

1. AASHTO.2010. AASHTO LRFD Bridge Design Specifications, 5rd Edition, American Association of State Highway and Transportation Officials, Washington, DC, 1450 pp.
2. Arezoumandi, M. 2015. Feasibility of crack freeze reinforced concrete bridge deck from materials composition perspective: a state of the art review. Frontiers of Structural and Civil Engineering, 9(1), 91-103. doi: 10.1007/s11709-015-0274-1
3. ASTM C215. Standard Test Method for Fundamental Transverse, Longitudinal, and Torsional Resonant Frequencies of Concrete. (ASTM C215).
4. ASTM C642 Standard Test for Density, Absorption, and Voids in Hardened Concrete. (ASTM C642).
5. ASTM C1202 Standard Test Method for Electrical Indication of Concrete's Ability to Resist Chloride Ion Penetration. (ASTM C1202).
6. CEB.1992. Durability concrete structures: CEB design guide, Bulletin d' information No. 182, Switzerland: Comite Euro-International du Beton.
7. Elzafraney, M., and Soroushian, P. 2005. Quantitative Micro-structural Investigation of Deteriorated Reinforced Concrete Bridge Deck. Journal of Materials in Civil Engineering; 17(2): 150-167.
8. Ghasezadehsomarin, F., 2015. The Effect of Damage on Mass Transport in Cement Transport in Cement-based Materials. Raleigh, North Carolina
9. Ishida. 2016. Ecological Durability Design for RC Bridge Deck in Cold Regions, 1–9. Retrieved from https://www.researchgate.net/publication.

10. Kostem, CN. 1978. Overloading of Highway Bridges - Initiation of Deck Damage. Transportation Research Record 664 1978: 212-220.
11. Lin, Z. 2012. Impact of Overweight Vehicles: with Heavy Axle Loads on Bridge Deck Deterioration. CFIRE 04-06 Final report. Milwaukee, WI.
12. Lin,Z. 2016. Personal Communication.
13. Mirza, ED. 2006. Concrete: Microstructure, Properties, and materials (Third Edition)
14. Mitchell, BD. 2016. Durability of mechanically Loaded, Freeze-Thaw Concrete Determined by Water Absorption. MS Thesis, University of Wisconsin, Milwaukee, WI.
15. Shiotani, T. 2012. Damage Evaluation for Concrete Bridge Deck by Means of Stress Wave Techniques. Journal of Bridge Engineering. 17(6), 847–856. doi:10.1061/(ASCE)BE.1943-5592.0000373
16. Obla, K., Lobo, C., and Kim, H. 2015. An Evaluation of Performance-Based Alternatives to the Durability Provision of the ACI 318 Building Code. ACI 329R-14.
17. Tabatabai, H., Tabatabai M., and Lee CW. 2011. Reliability of Bridge Decks in Wisconsin. Journal of Bridge Engineering. 16(1): 53-62.

Zhao, J., Tabatabai, H. 2010. (in print, online accessible) Evaluation of a permit vehicle model using weigh-in-motion truck records. Journal of Bridge Engineering. 17(2): 389-392

Appendix: Images and Passing Current/Temperature Vs. Time

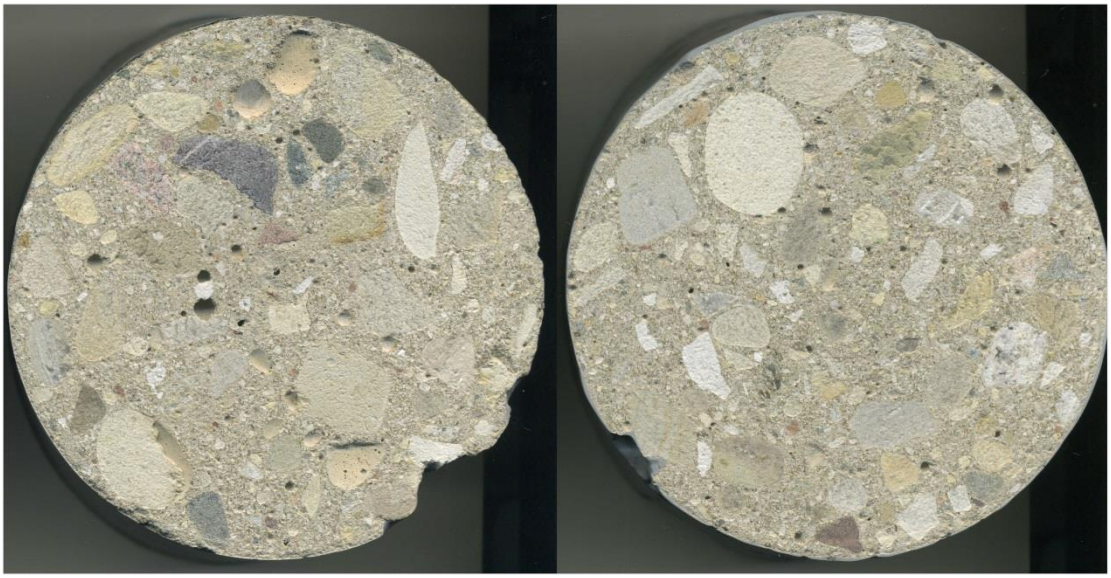

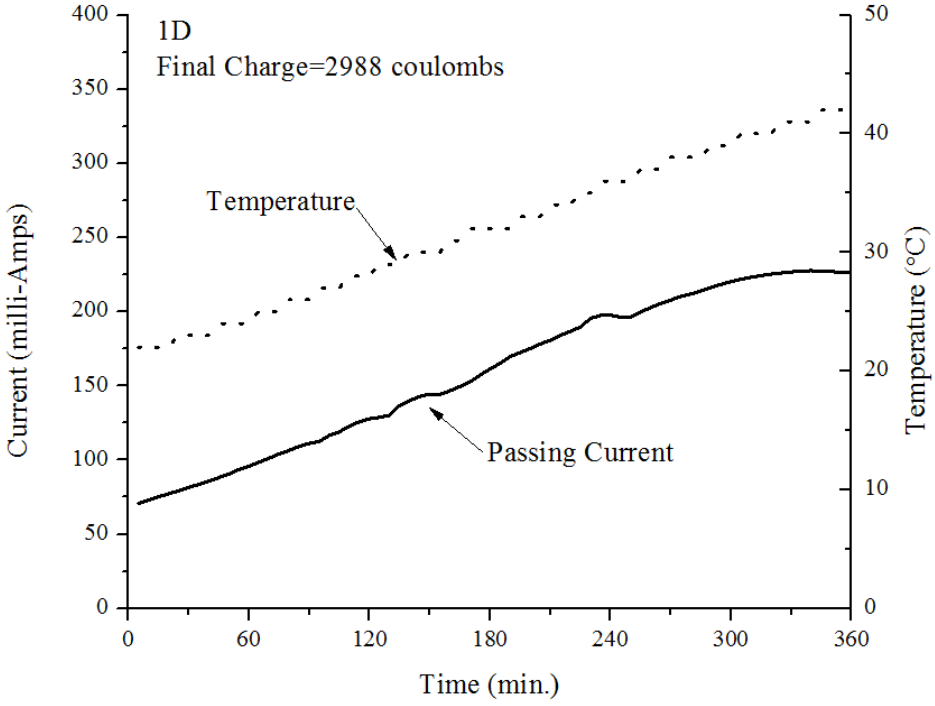

Figure A.1: The. picture and graph of passing current/temperature vs. time for sample 1D

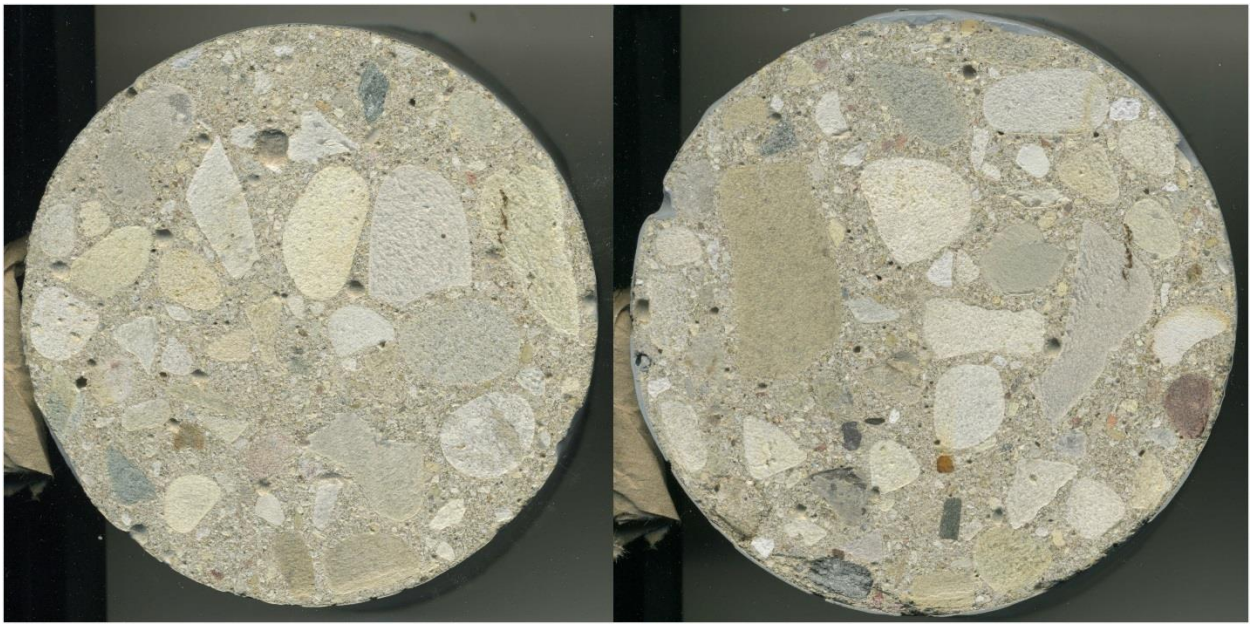

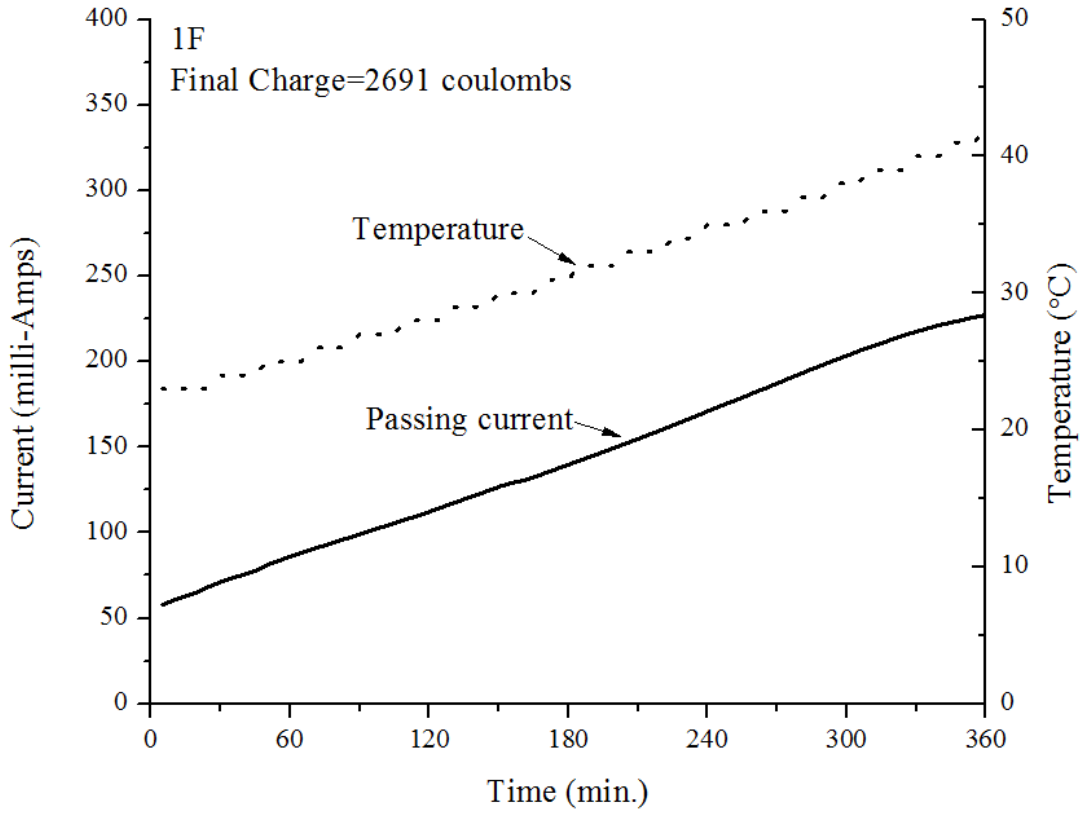

Figure A.2: The picture and graph of passing current/temperature vs. time for sample 1F.

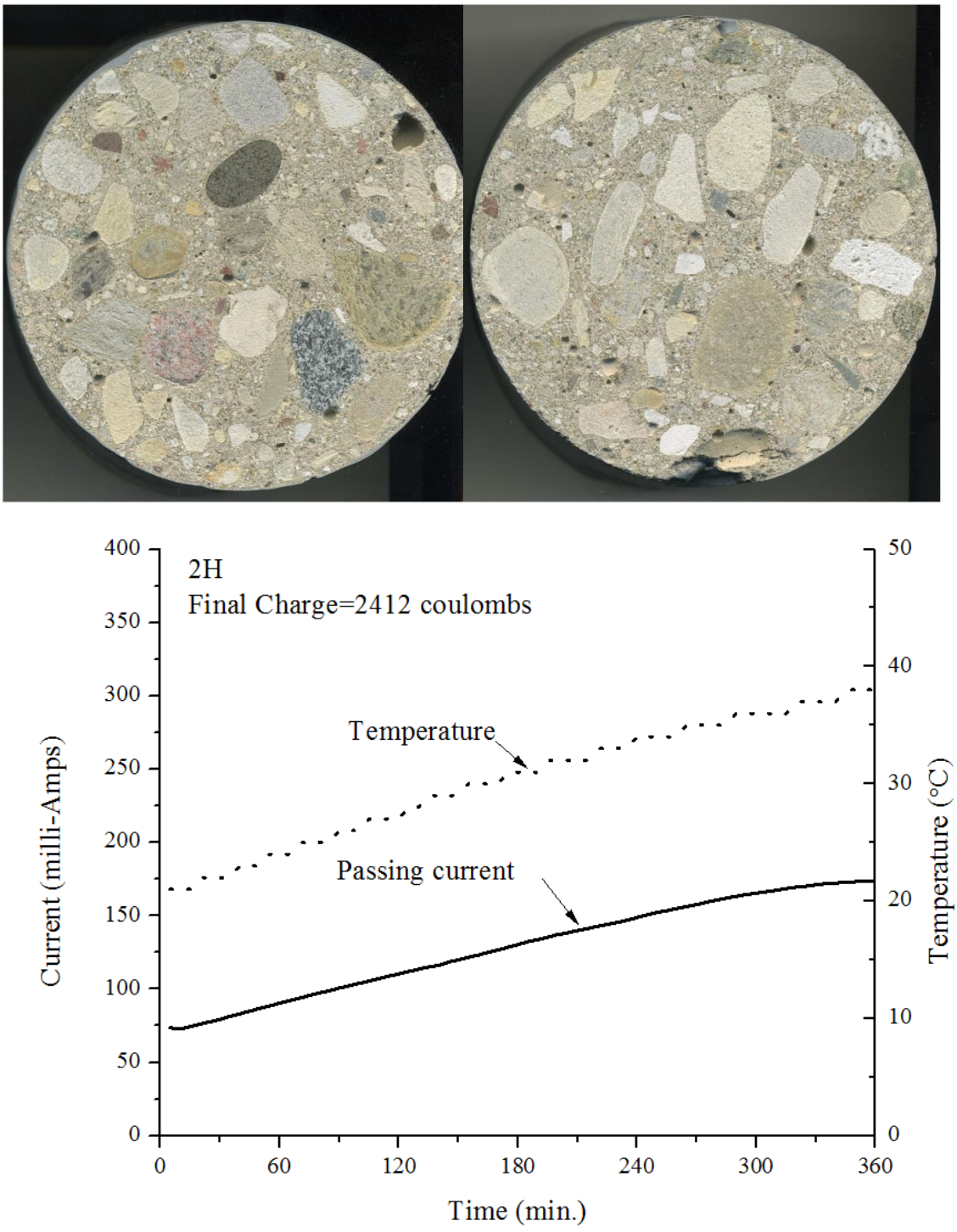

Figure A.3: The picture and graph of passing current/temperature vs. time for sample 2H.

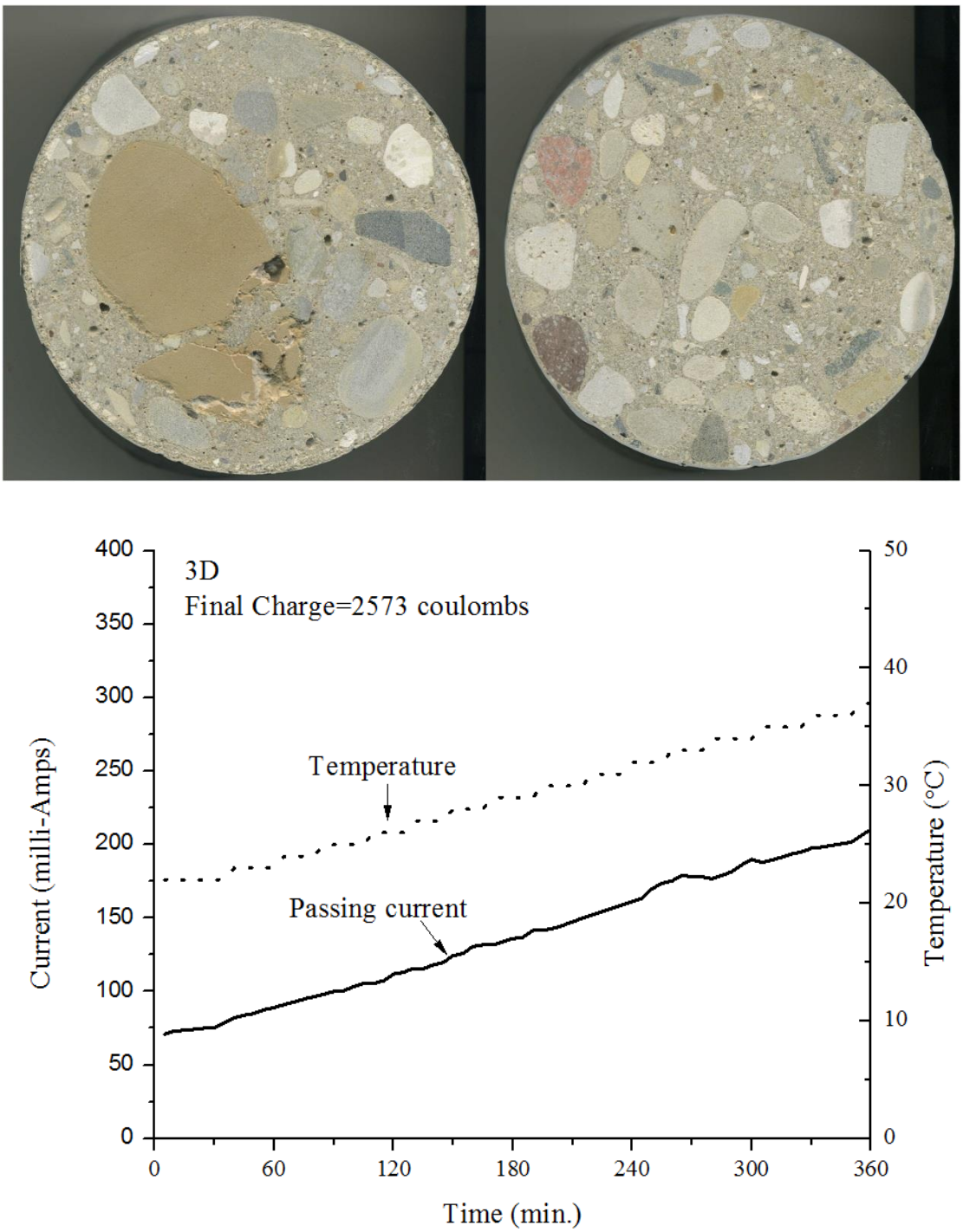

Figure A.4: The picture and graph of passing current/temperature vs. time for sample 3D.

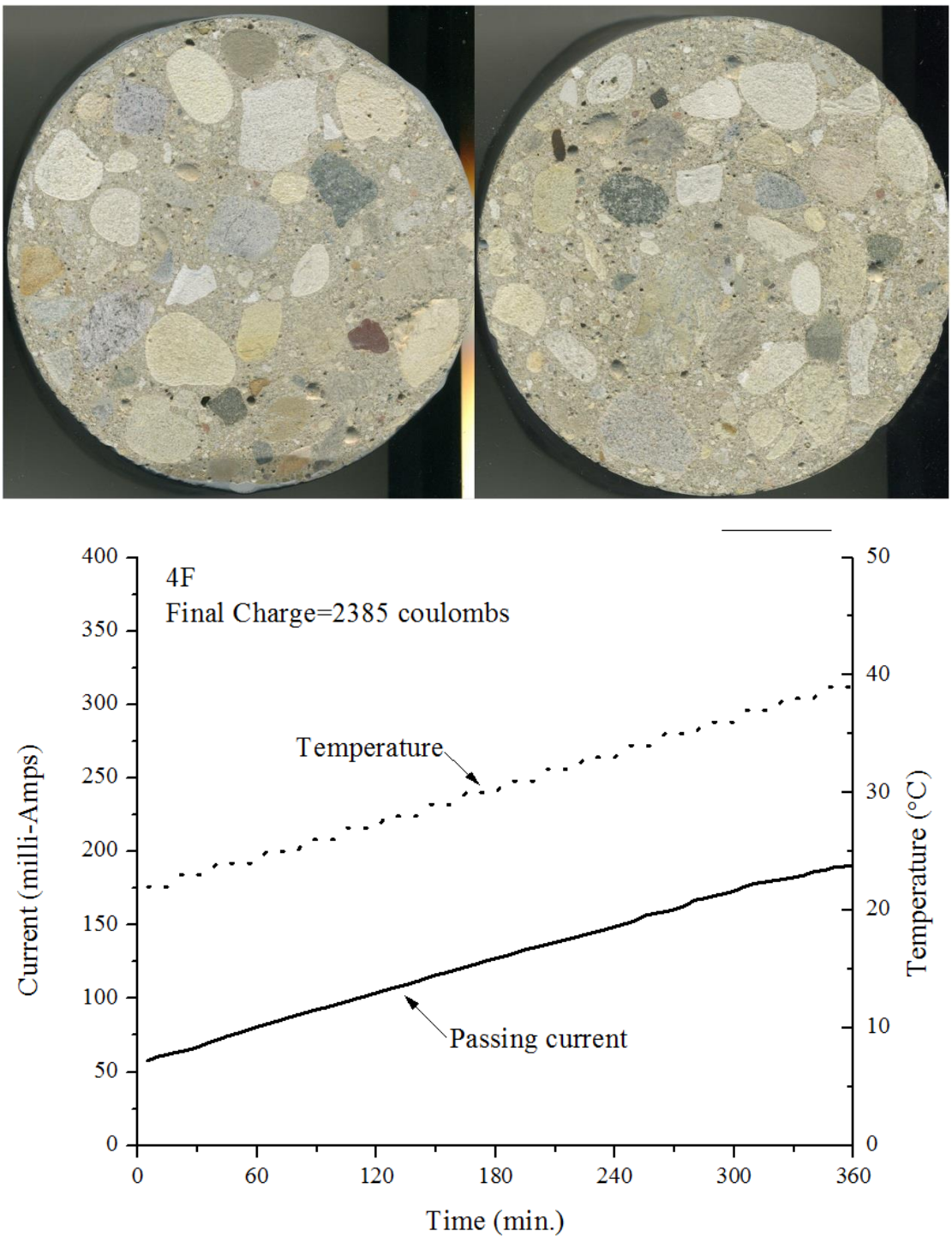

Figure A.5: The picture and graph of passing current/temperature vs. time for sample 4F.

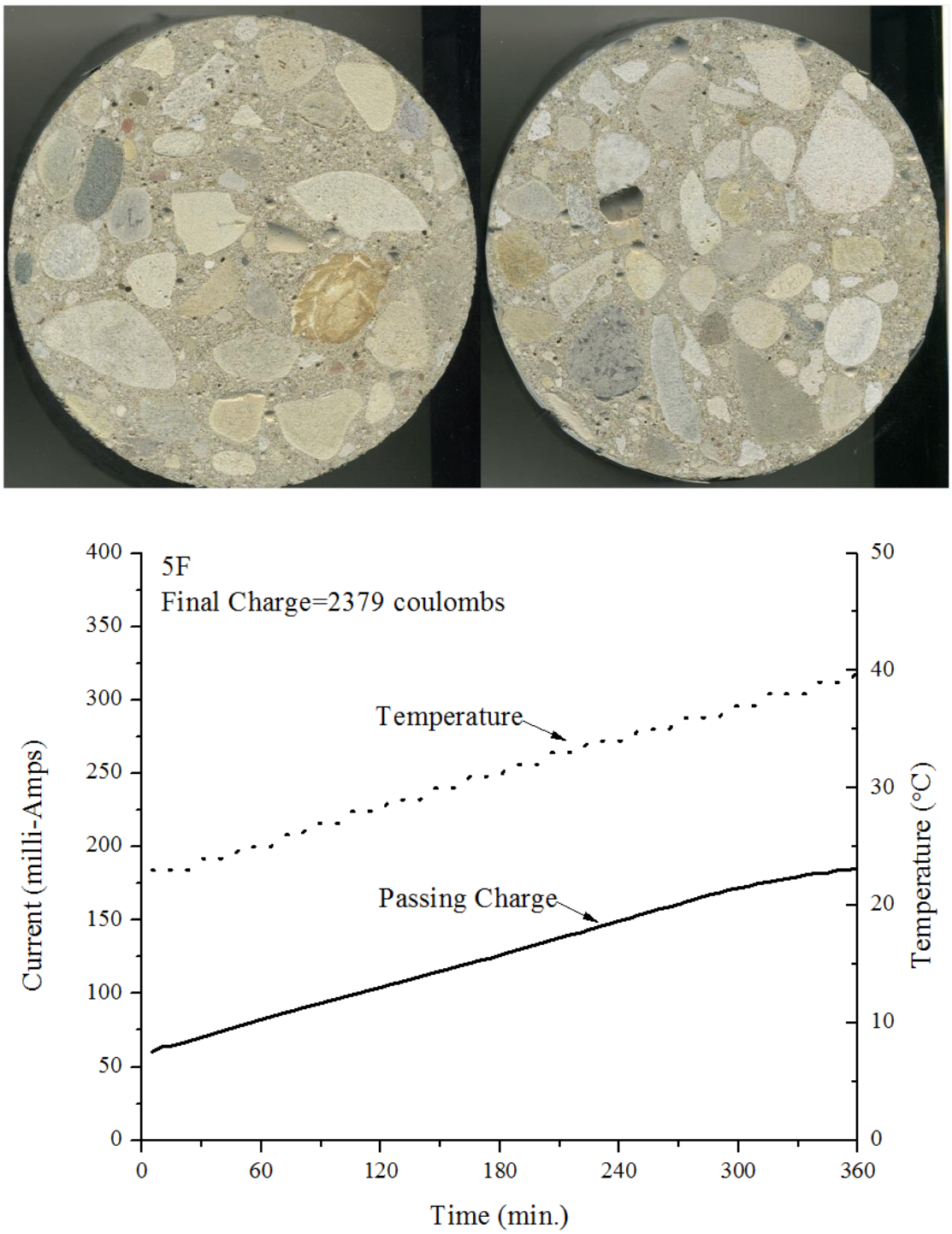

Figure A.6: The picture and graph of passing current/temperature vs. time for sample 5F.

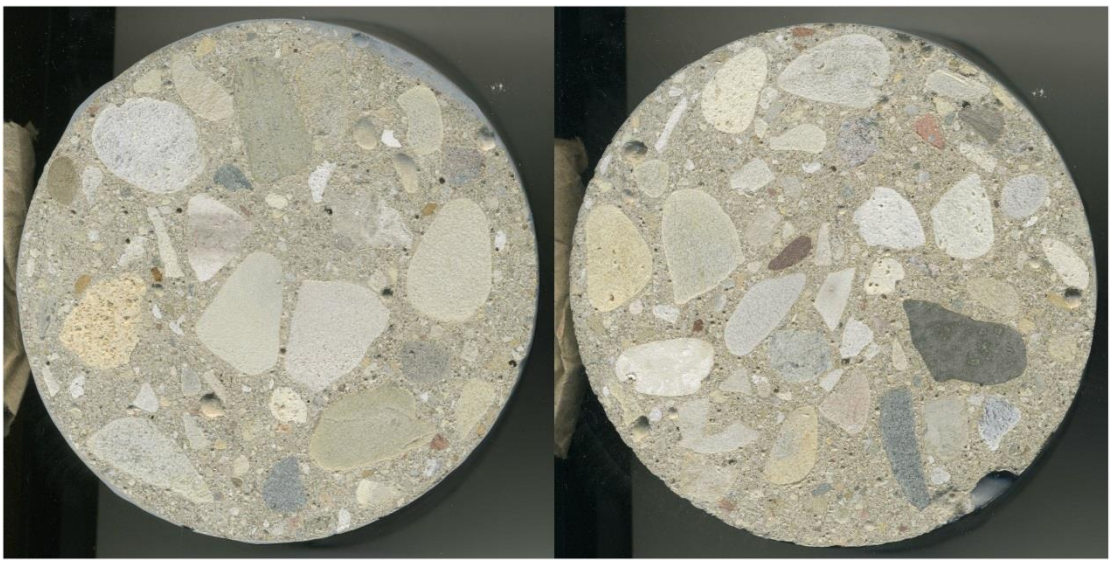

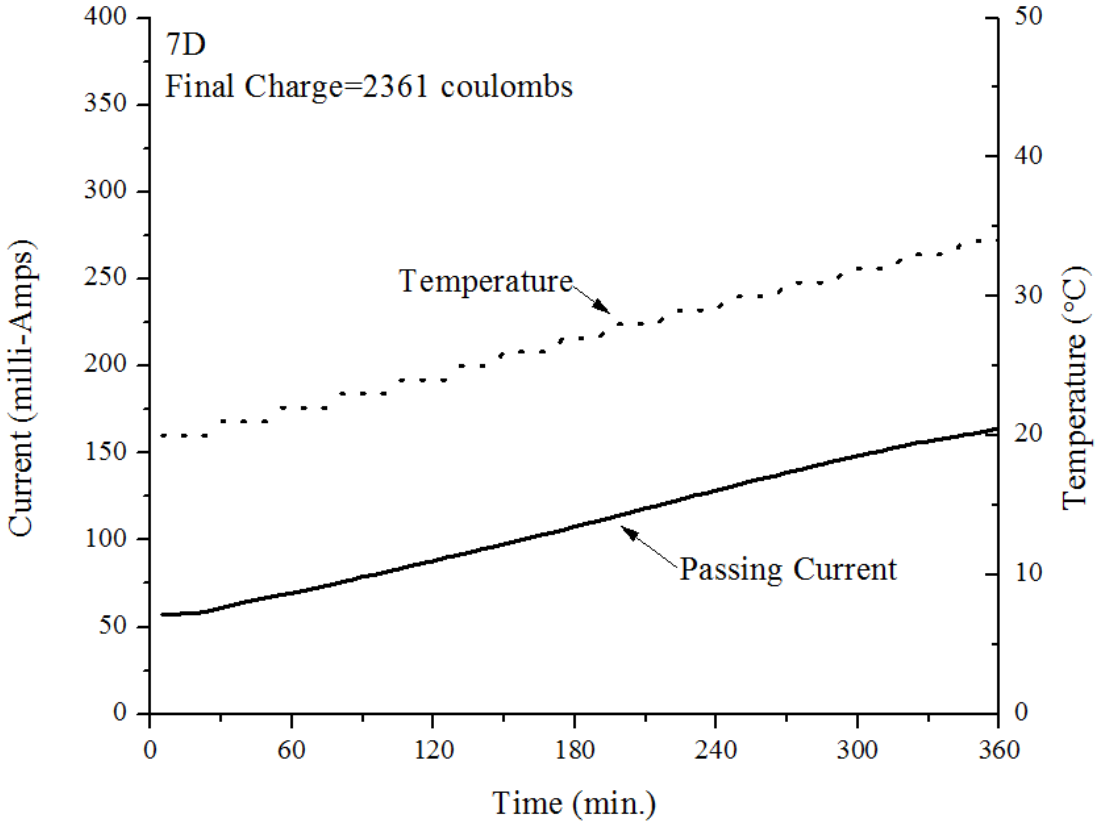

Figure A.7: The picture and graph of passing current/temperature vs. time for sample7D.

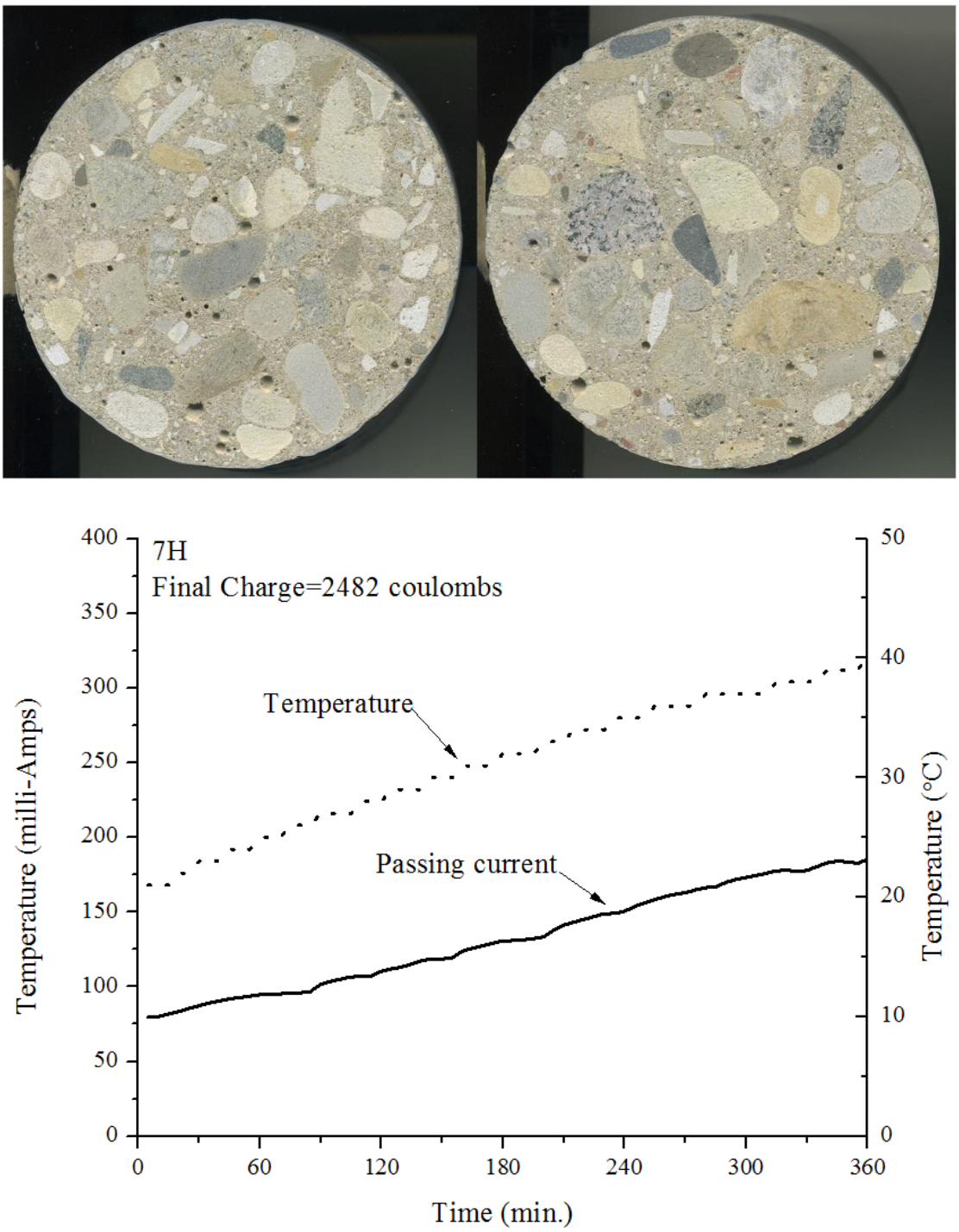

Figure A.8: The picture and graph of passing current/temperature vs. time for sample 7H.

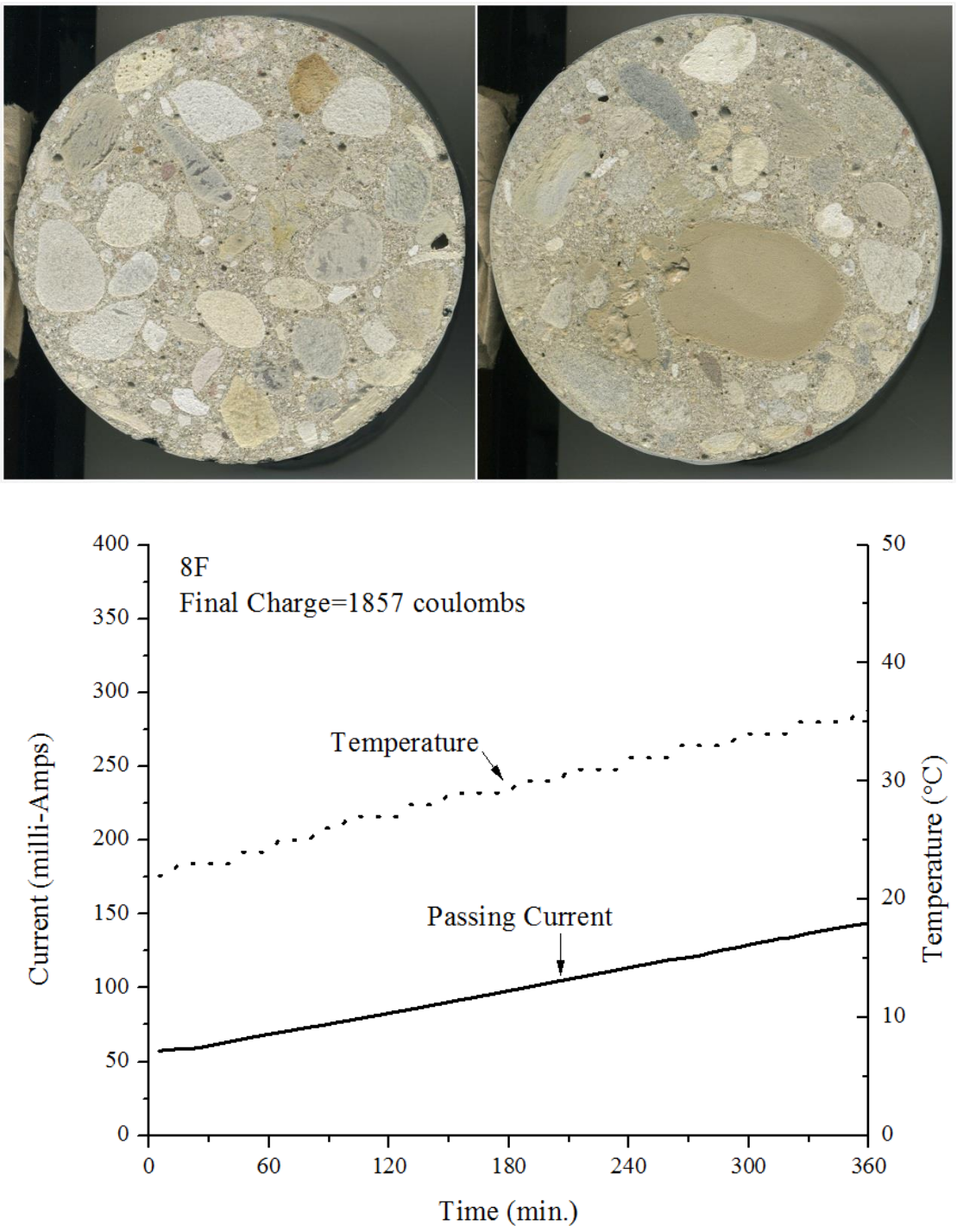

Figure A.9: The picture and graph of passing current/temperature vs. time for sample 8F.

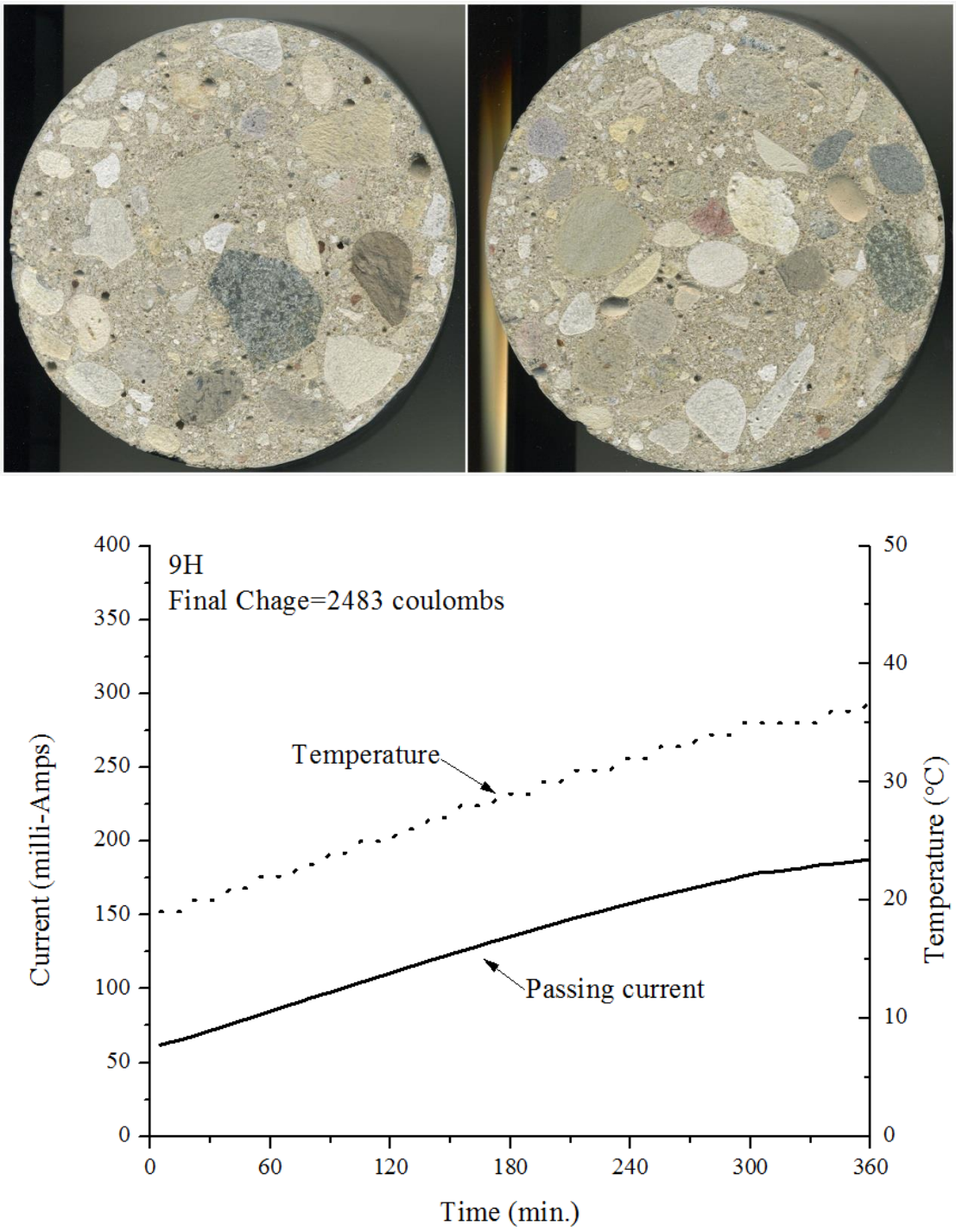

Figure A.10: The picture and graph of passing current/temperature vs. time for sample 9H.

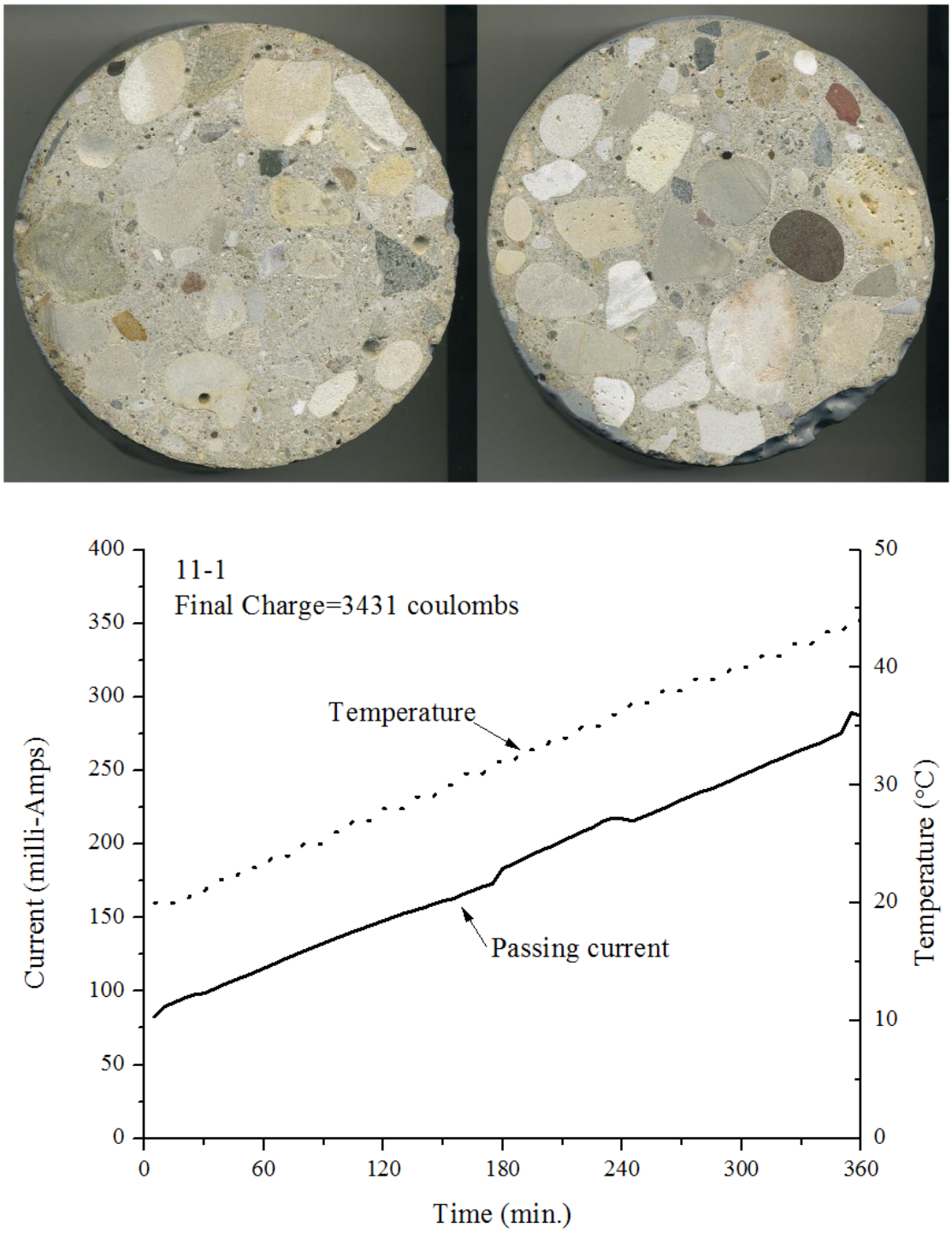

Figure A.11: The picture and graph of passing current/temperature vs. time for sample 11-1.

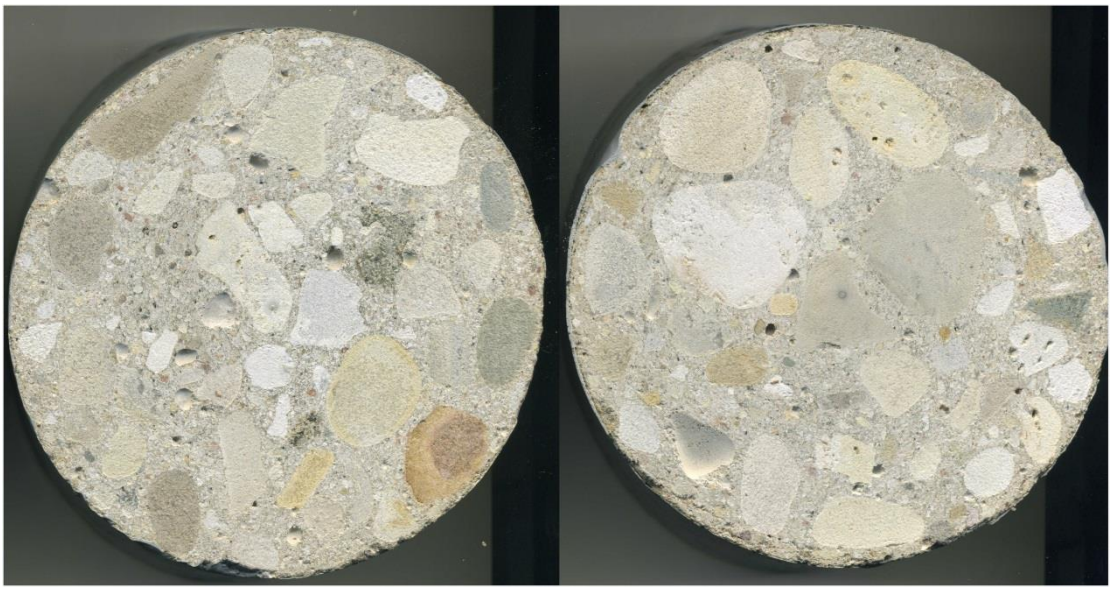

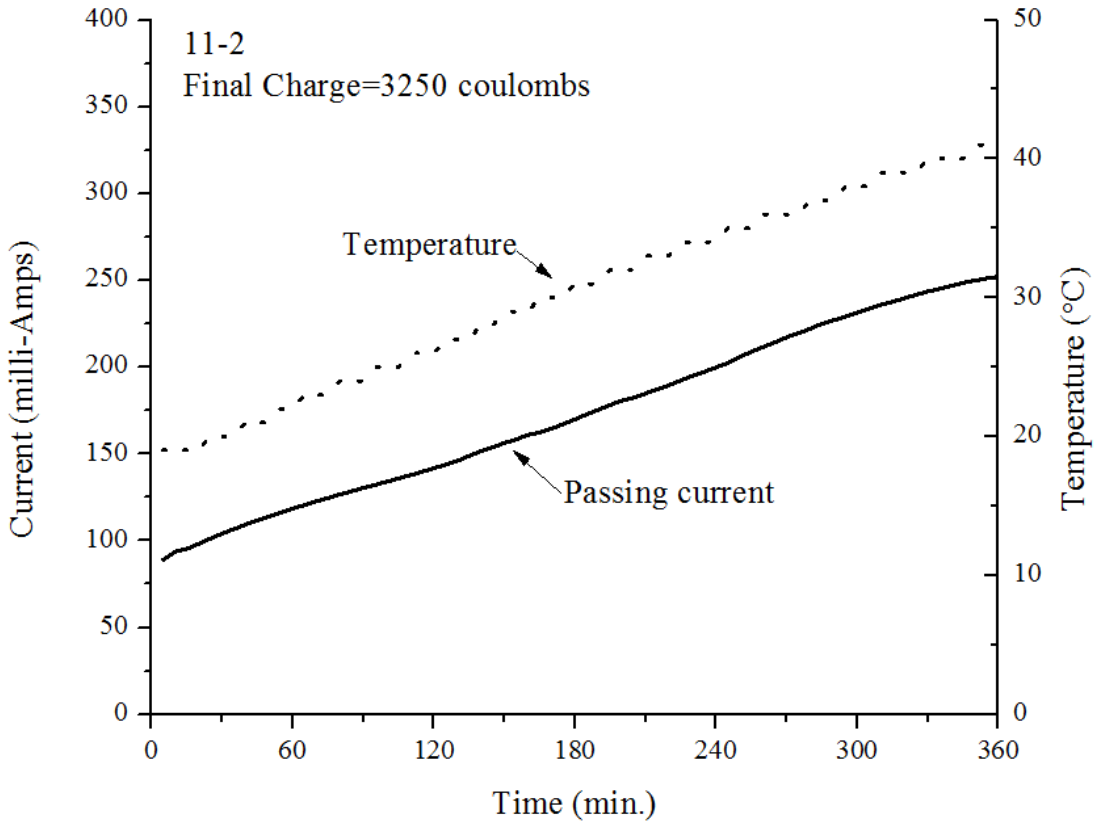

Figure A.12: The picture and graph of passing current/temperature vs. time for sample 11-2.

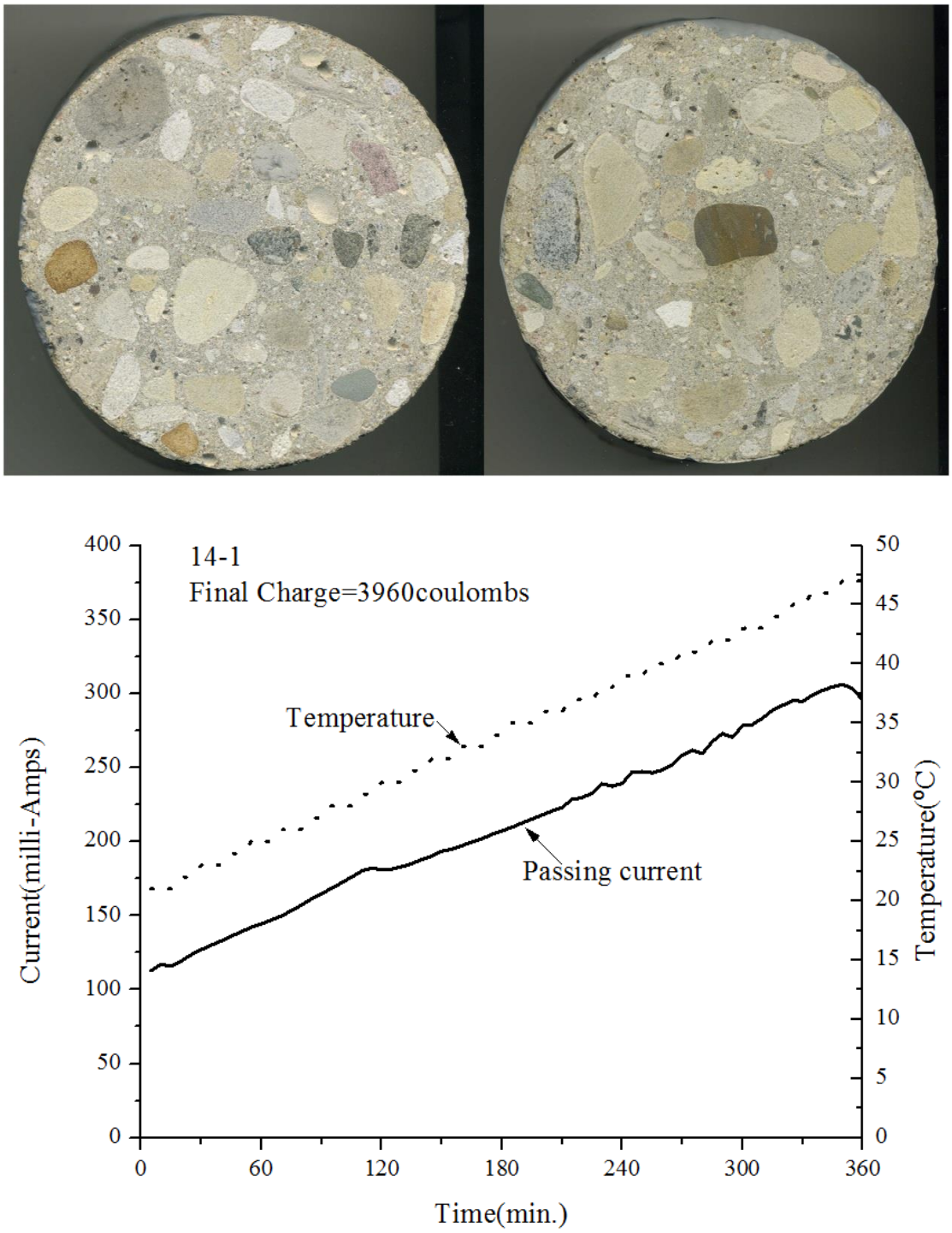

Figure A.13: The picture and graph of passing current/temperature vs. time for sample 14-1.

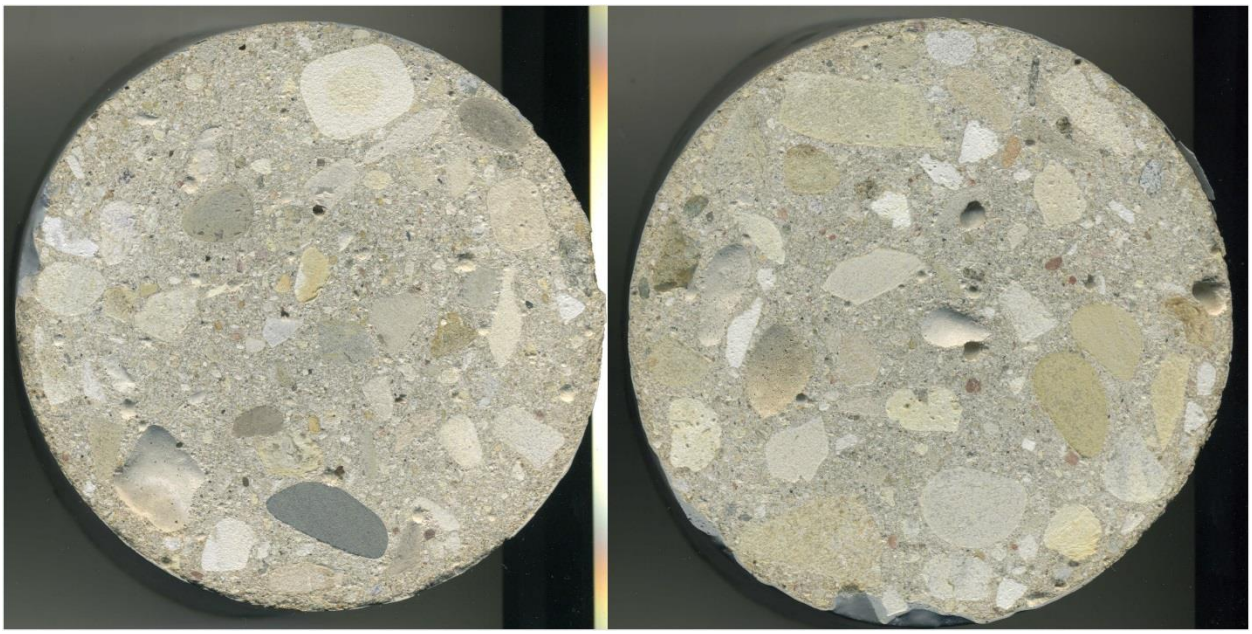

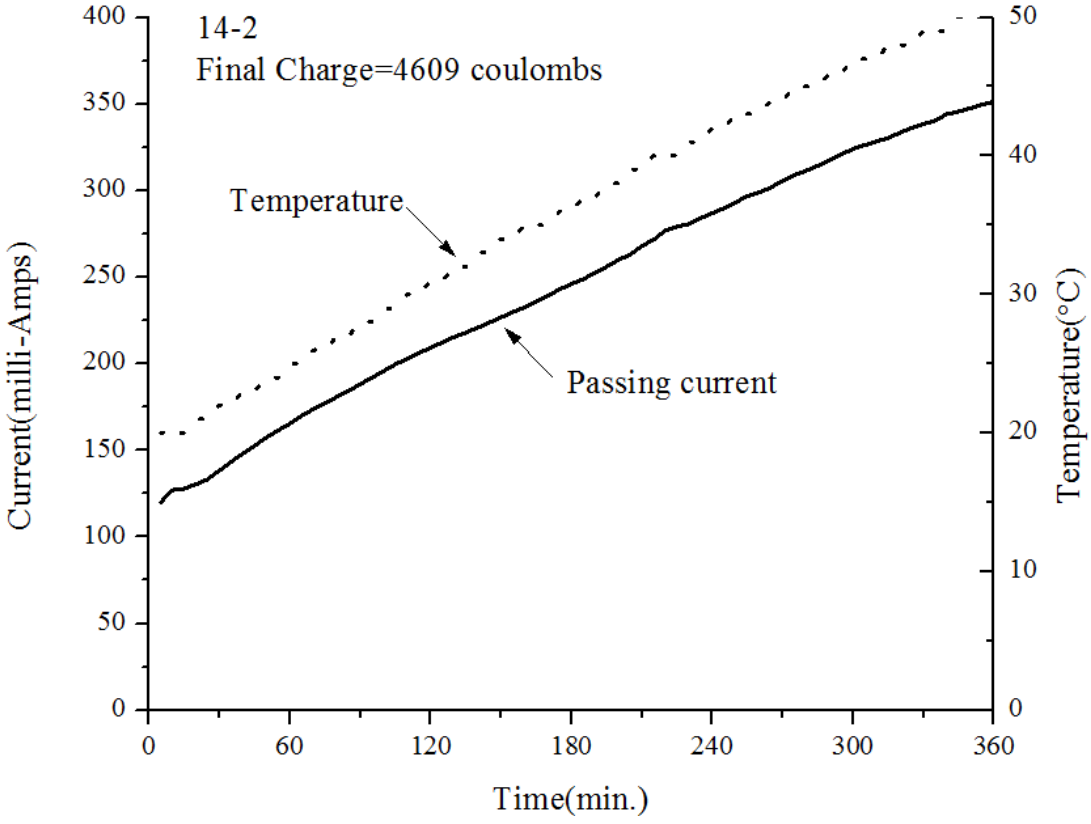

Figure A.14: The picture and graph of passing current/temperature vs. time for sample 14-2.

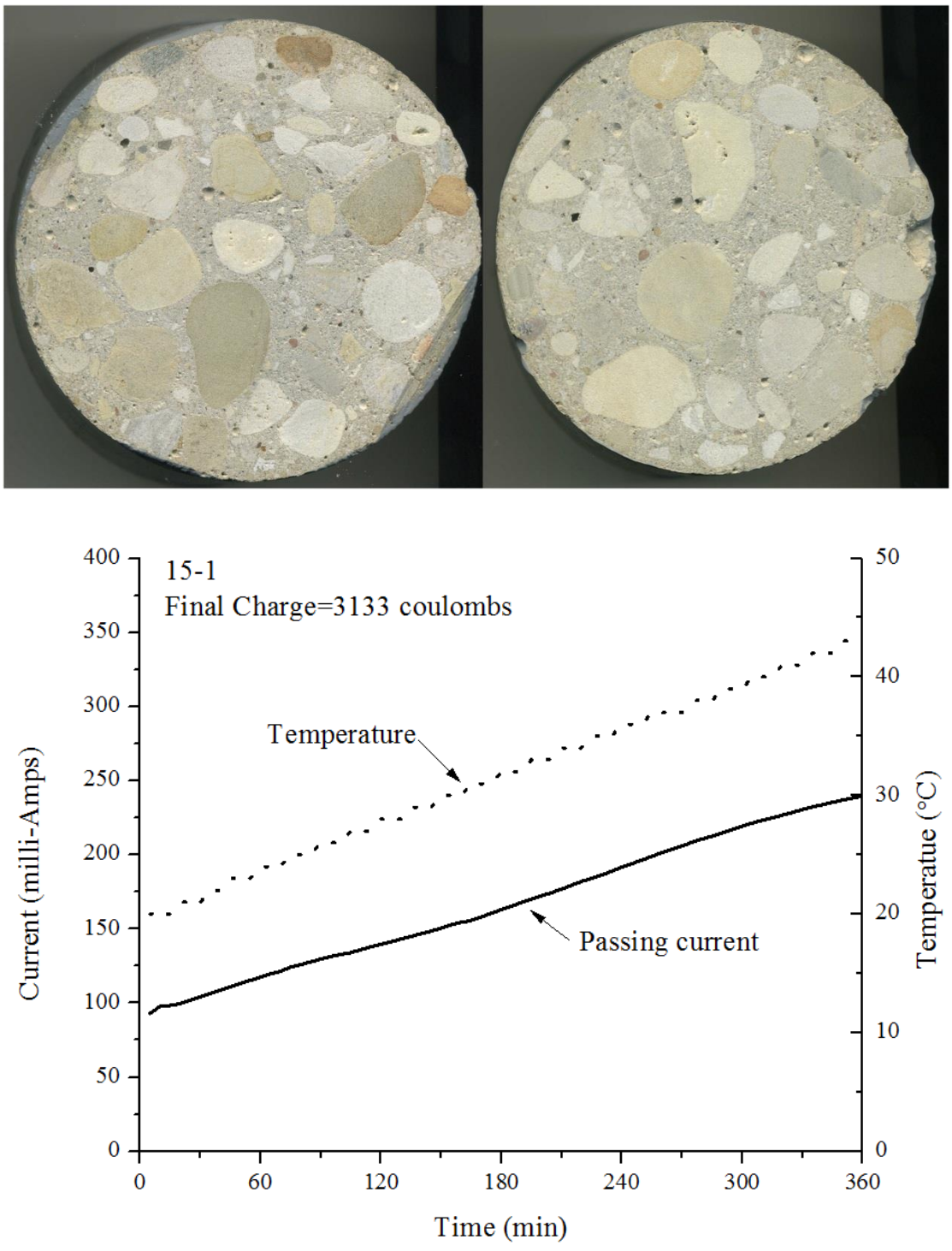

Figure A.15: The picture and graph of passing current/temperature vs. time for sample15-1.

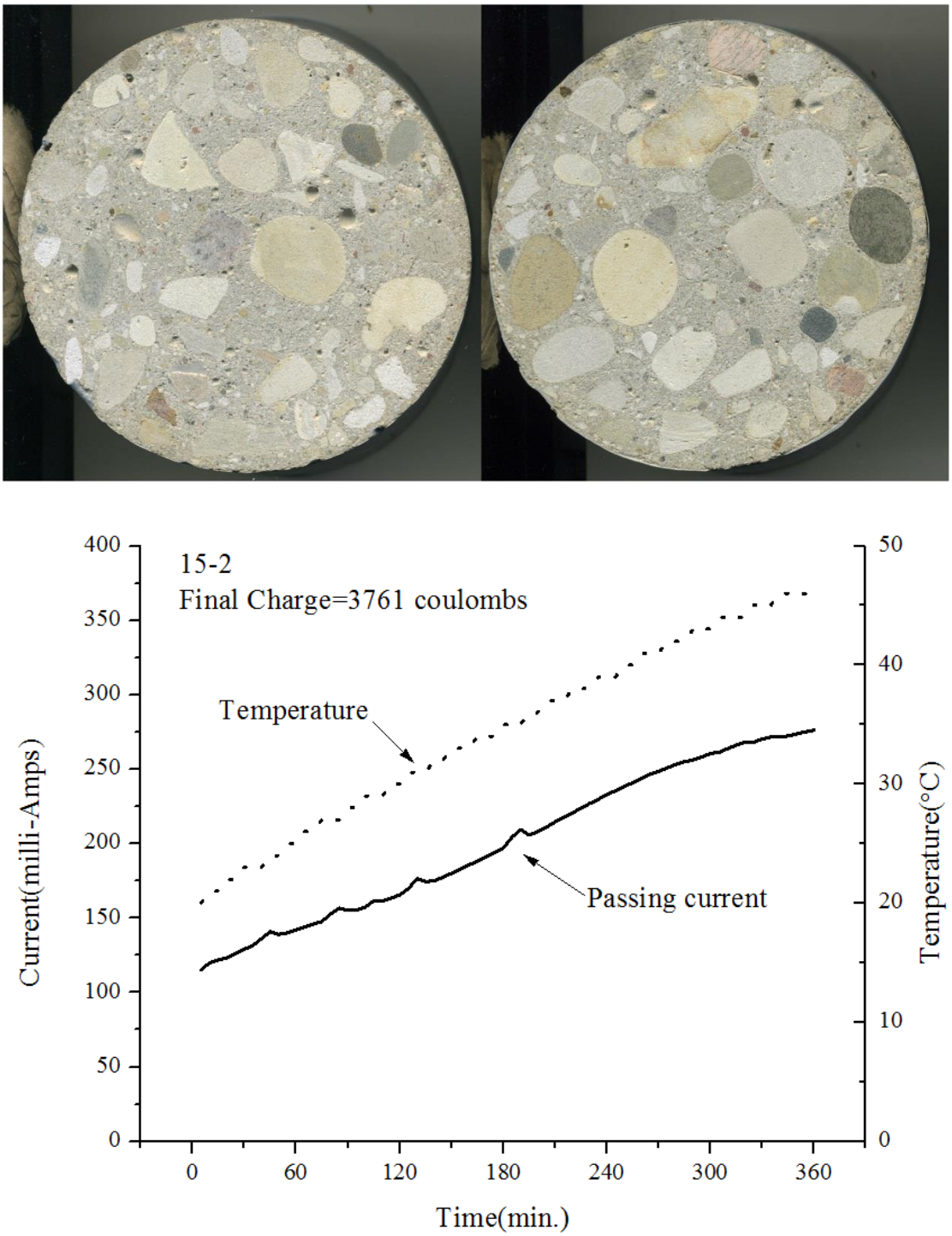

Figure A.16: The picture and graph of passing current/temperature vs. time for sample15-2.

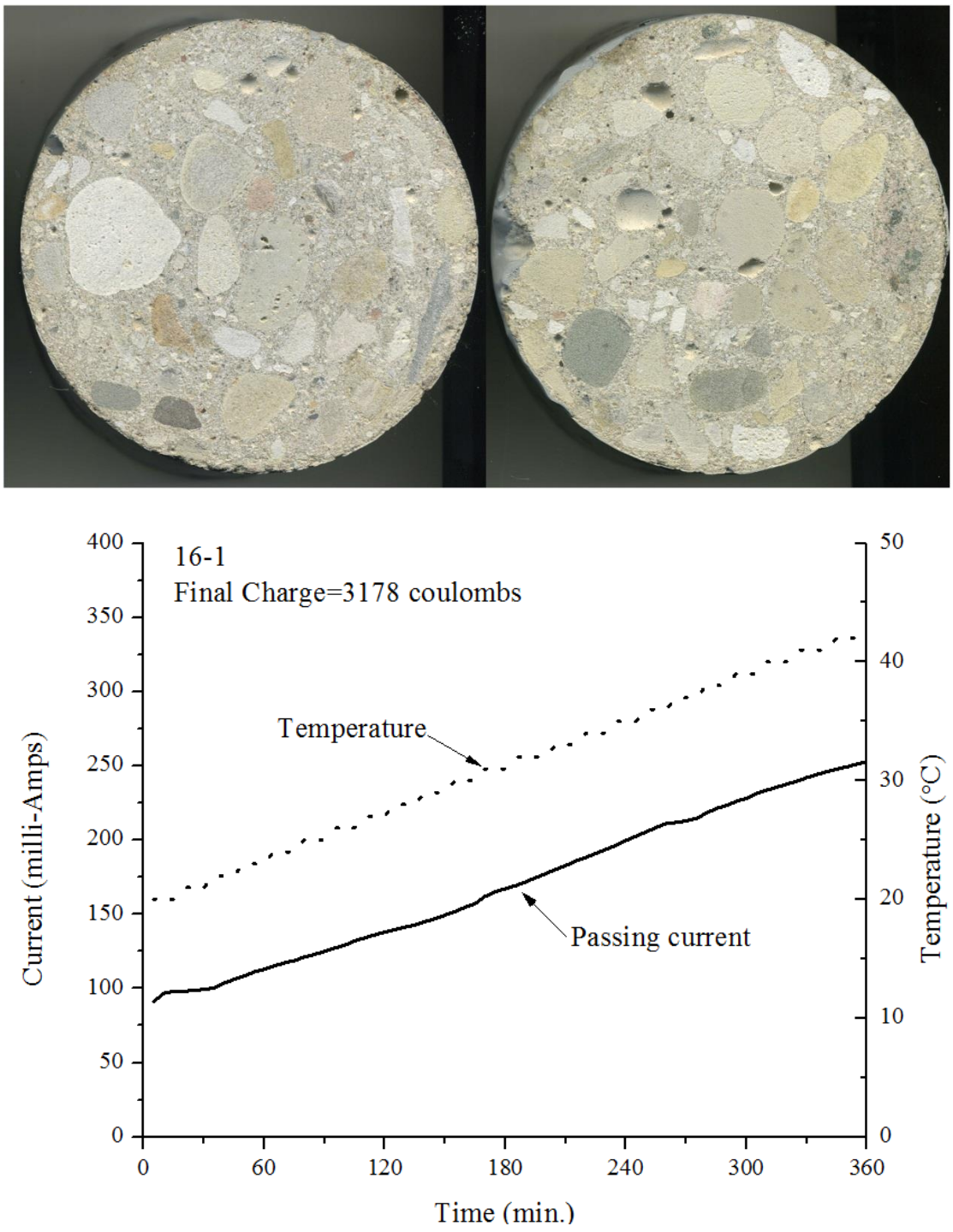

Figure A.17: The picture and graph of passing current/temperature vs. time for sample16-1.

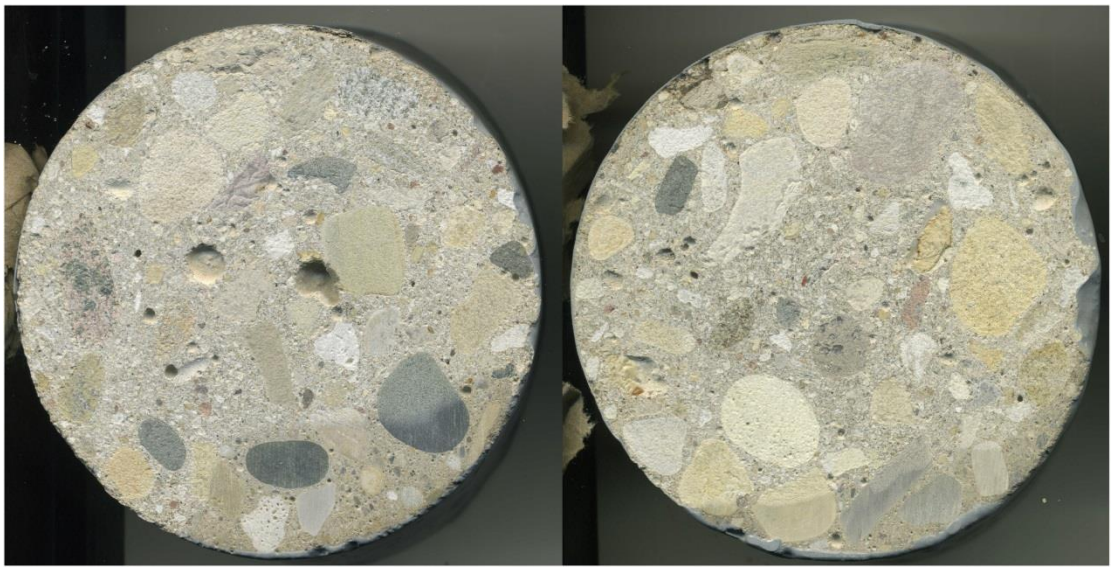

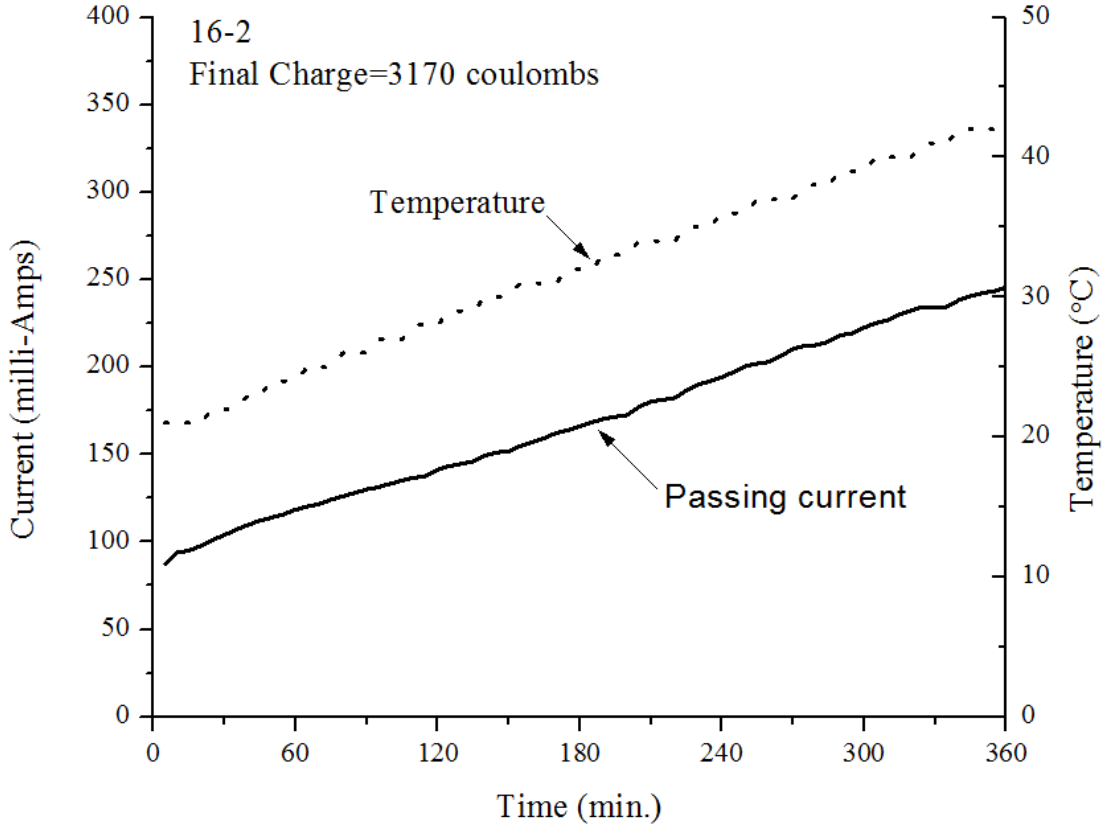

Figure A.18: The picture and graph of passing current/temperature vs. time for sample16-2.

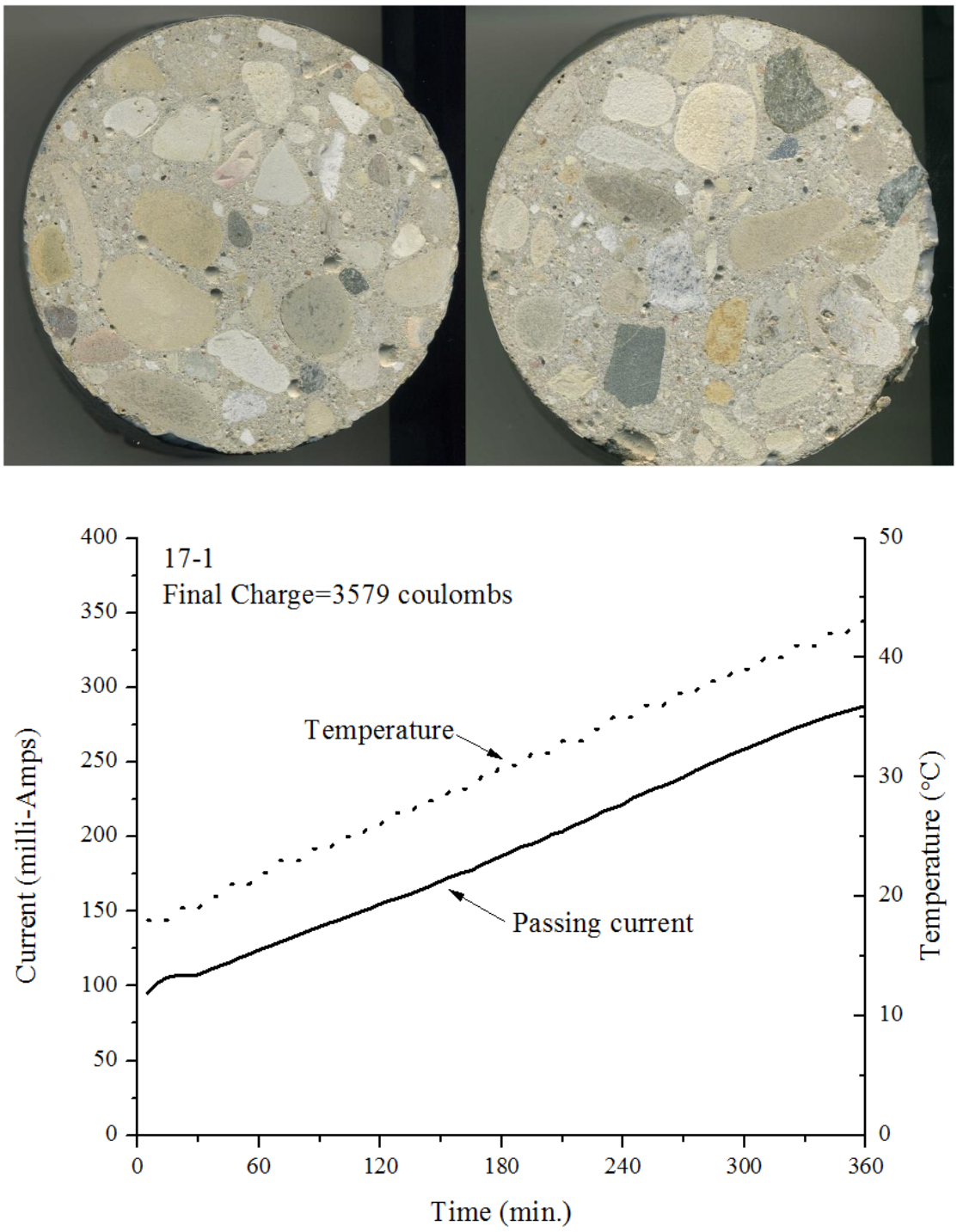

Figure A.19: The picture and graph of passing current/temperature vs. time for sample17-1.

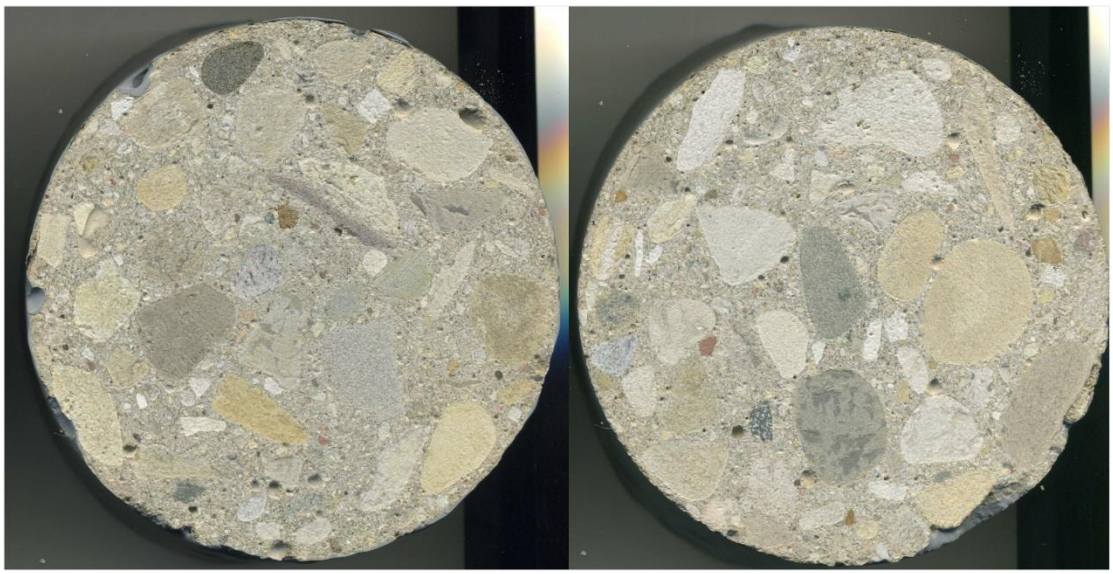

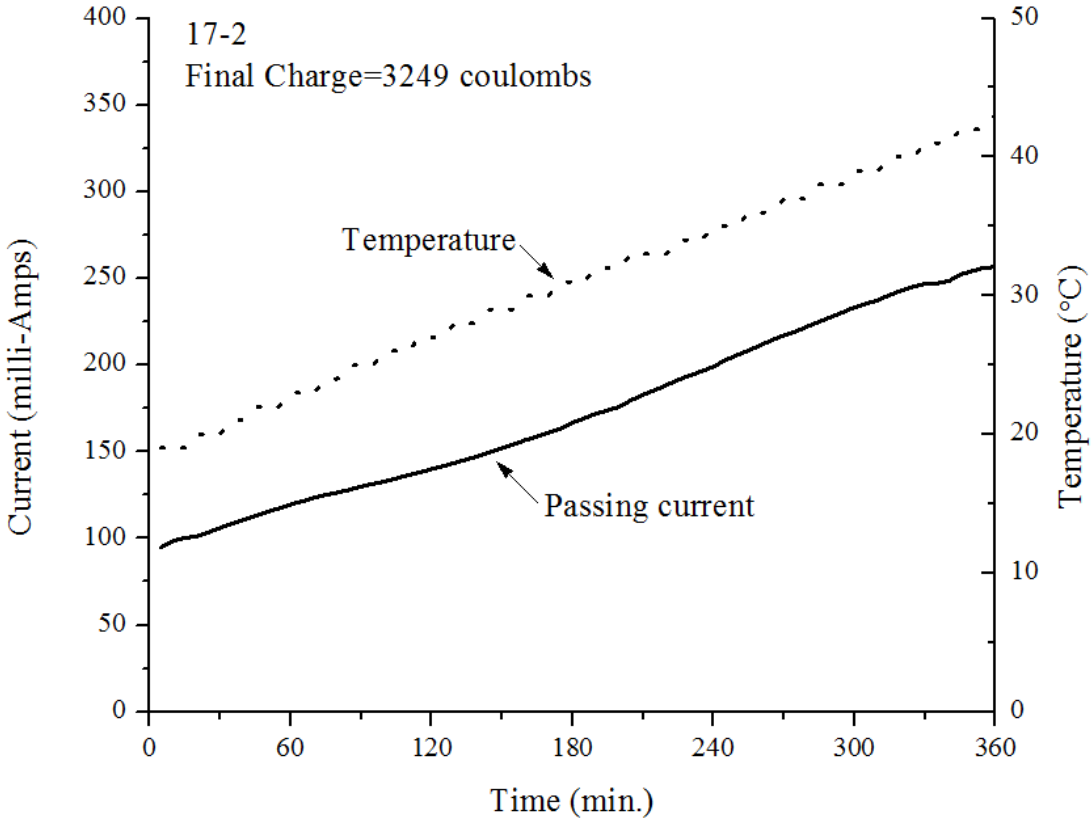

(b) Final Charge

Figure A.20: The picture and graph of passing current/temperature vs. time for sample17-2.

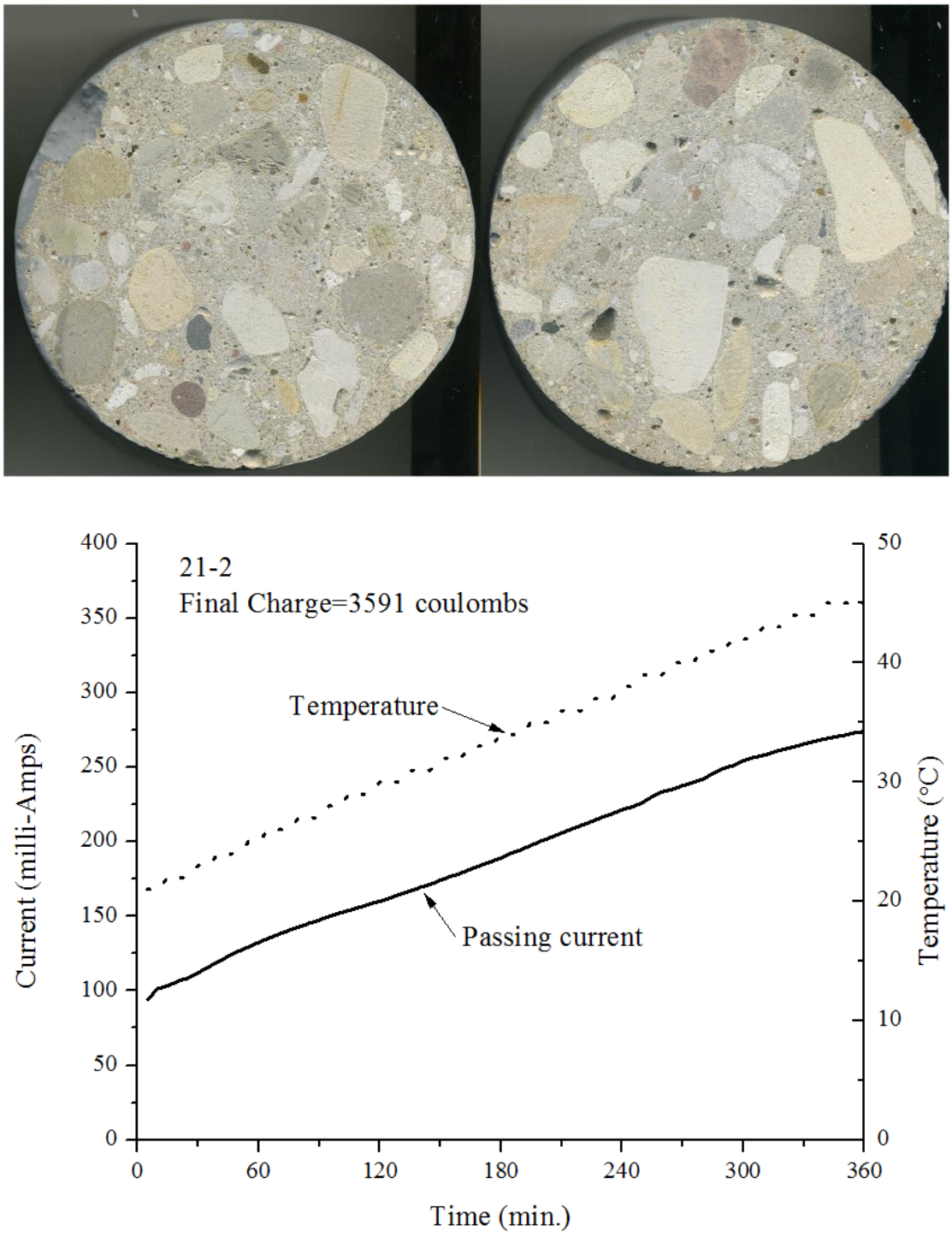

Figure A.21: The picture and graph of passing current/temperature vs. time for sample21-2.

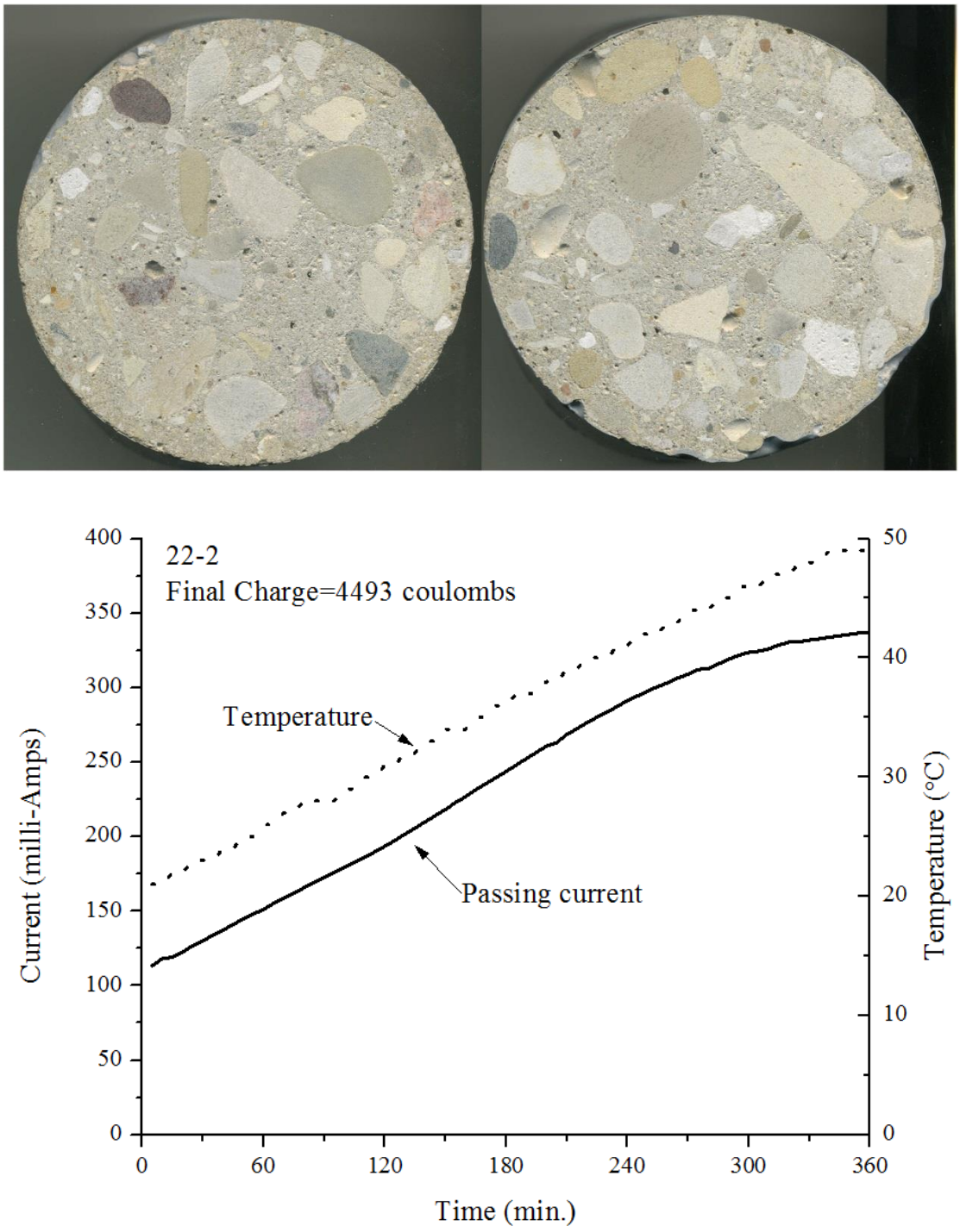

Figure A.22: The picture and graph of passing current/temperature vs. time for sample22-2.

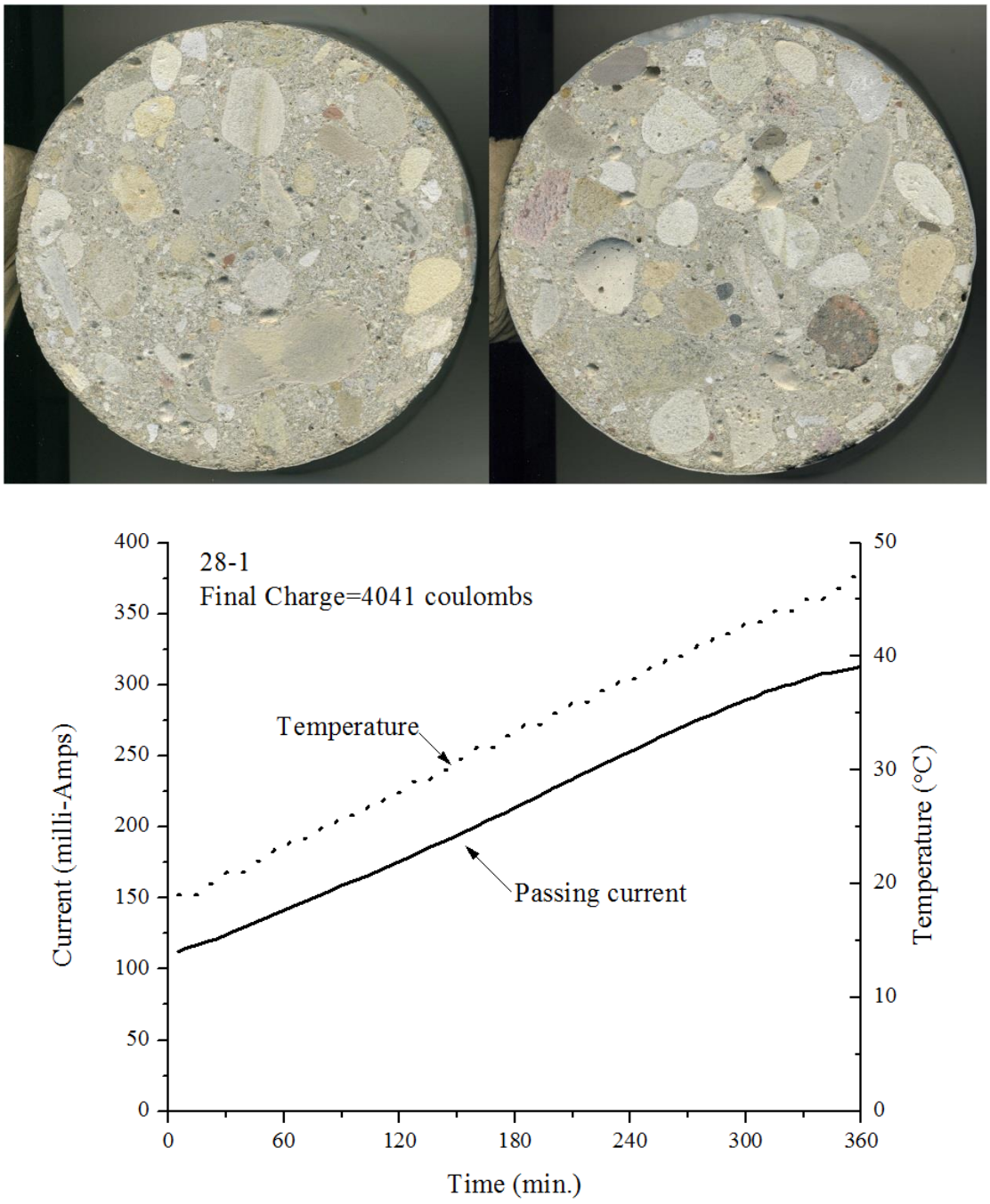

Figure A.23: The picture and graph of passing current/temperature vs. time for sample28-1.

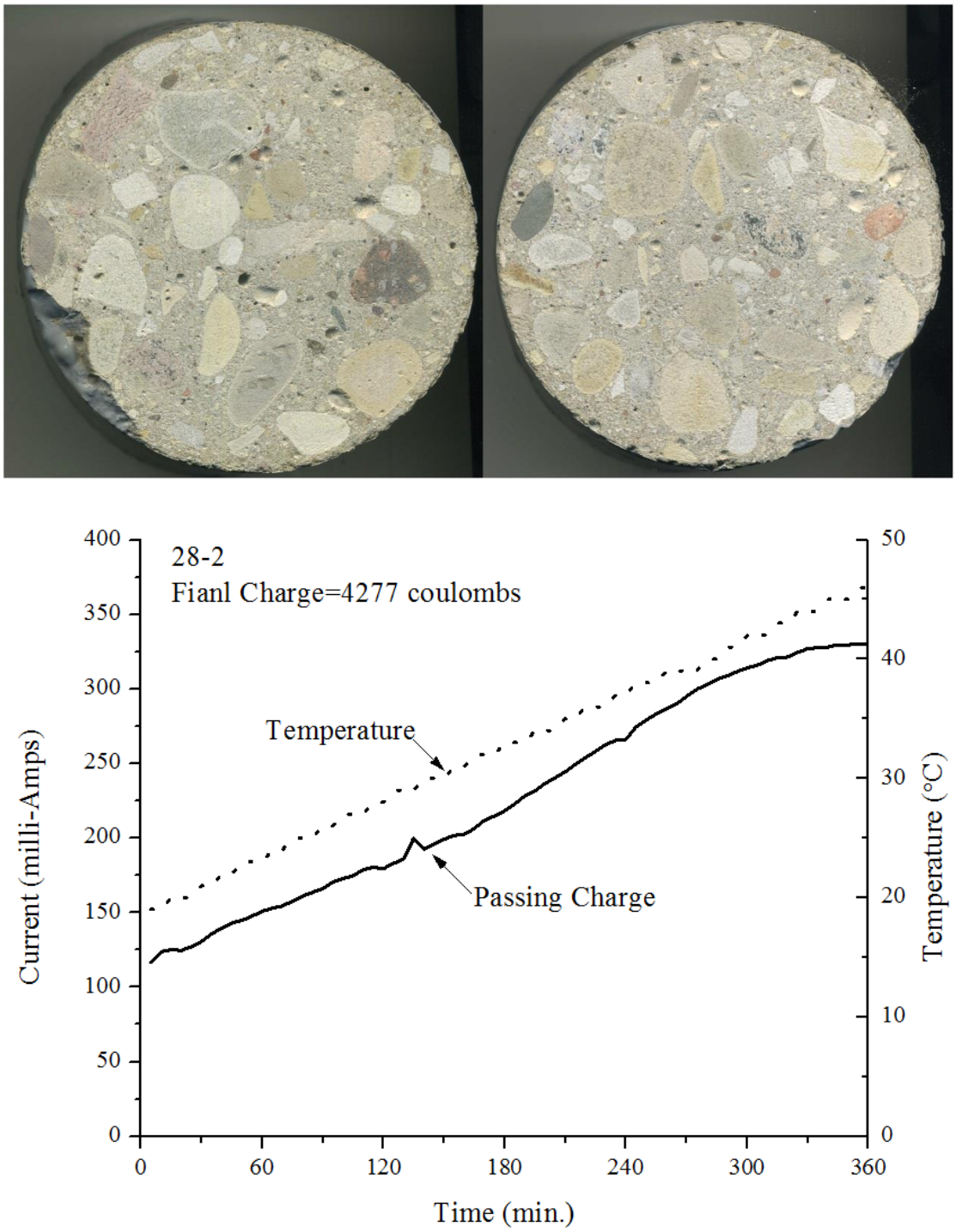

Figure A.24: The picture and graph of passing current/temperature vs. time for sample28-2.

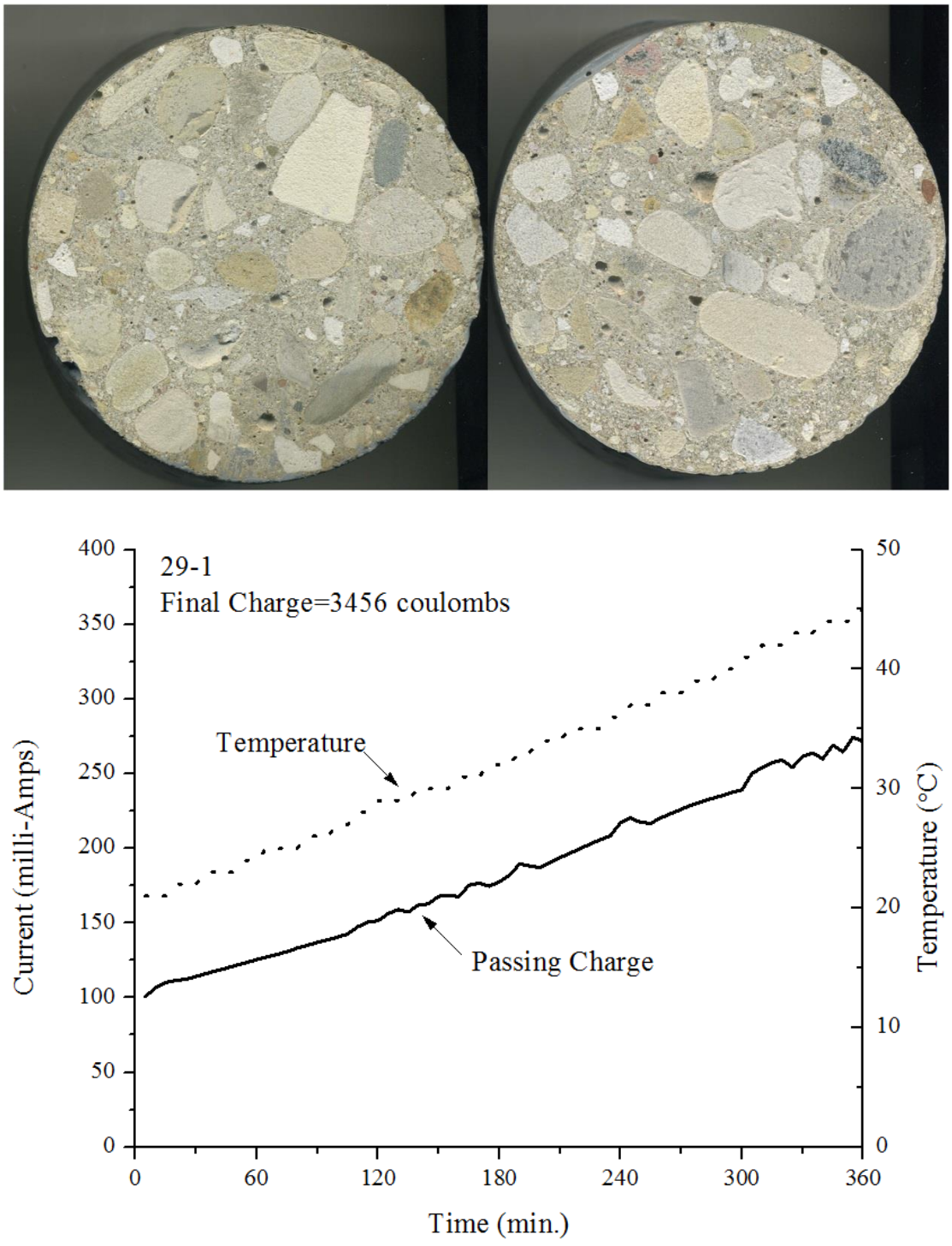

Figure A.25: The picture and graph of passing current/temperature vs. time for sample29-1.

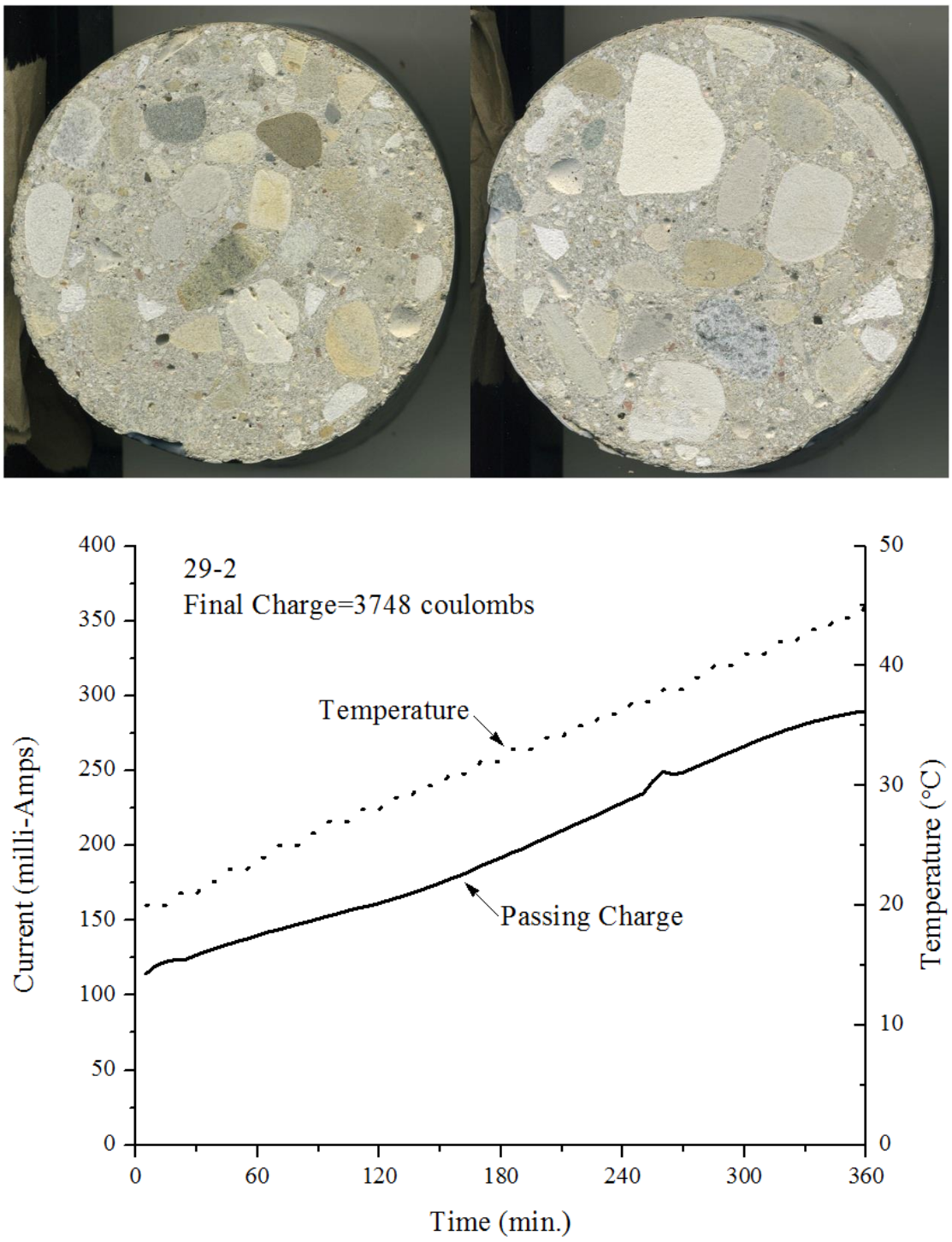

Figure A.26: The picture and graph of passing current/temperature vs. time for sample29-2.

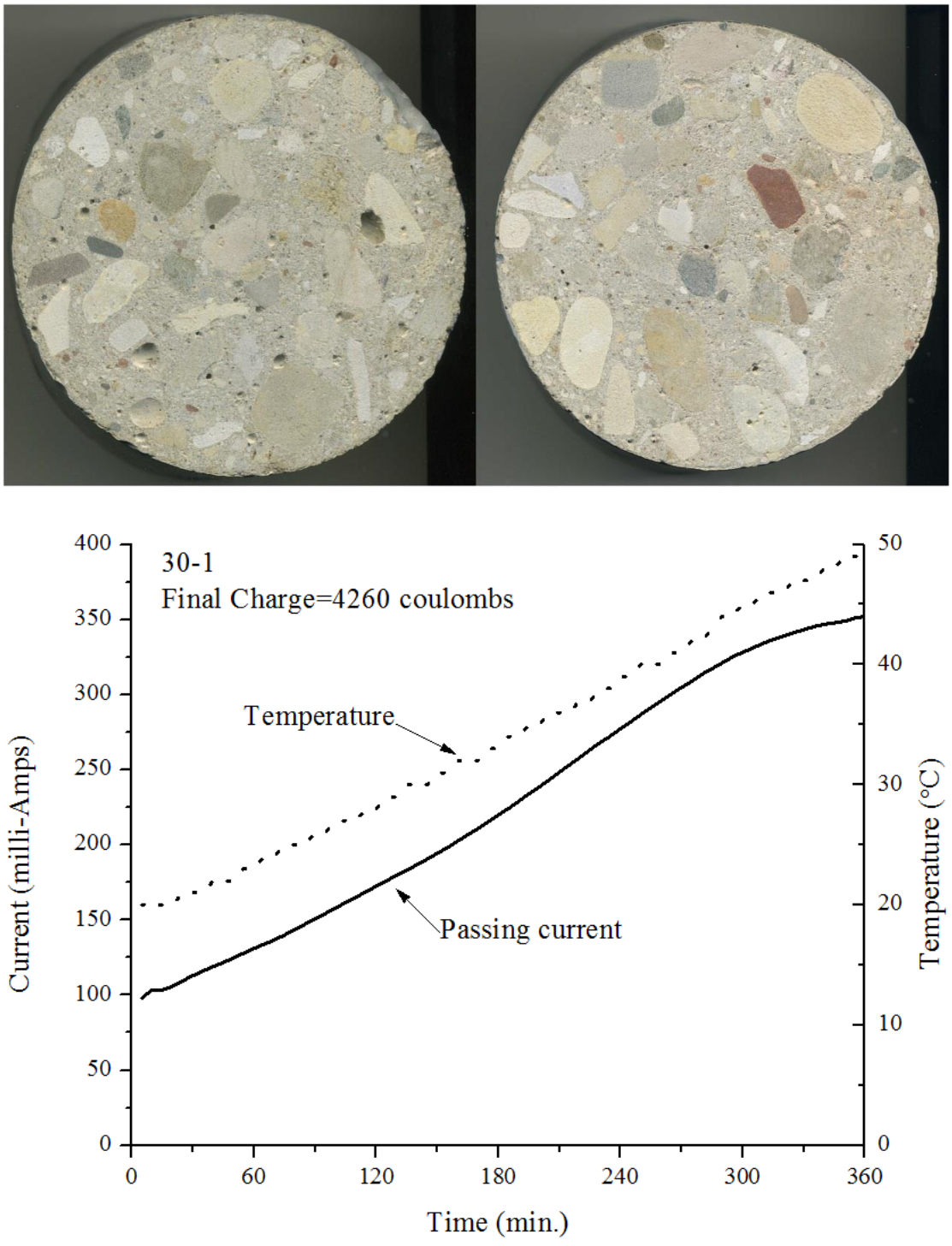

Figure A.27: The picture and graph of passing current/temperature vs. time for sample30-1.

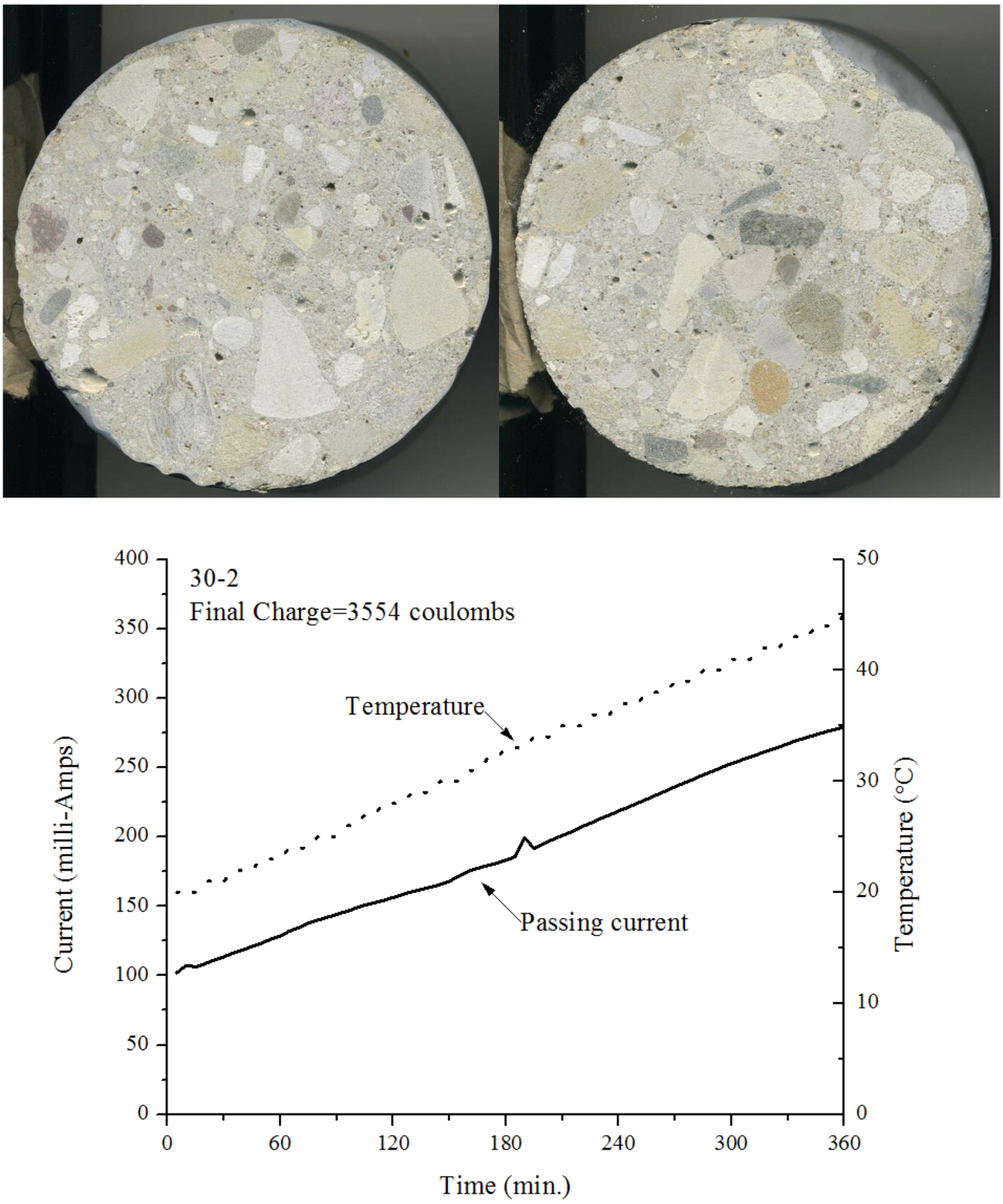

Figure A.28: The picture and graph of passing current/temperature vs. time for sample30-2.

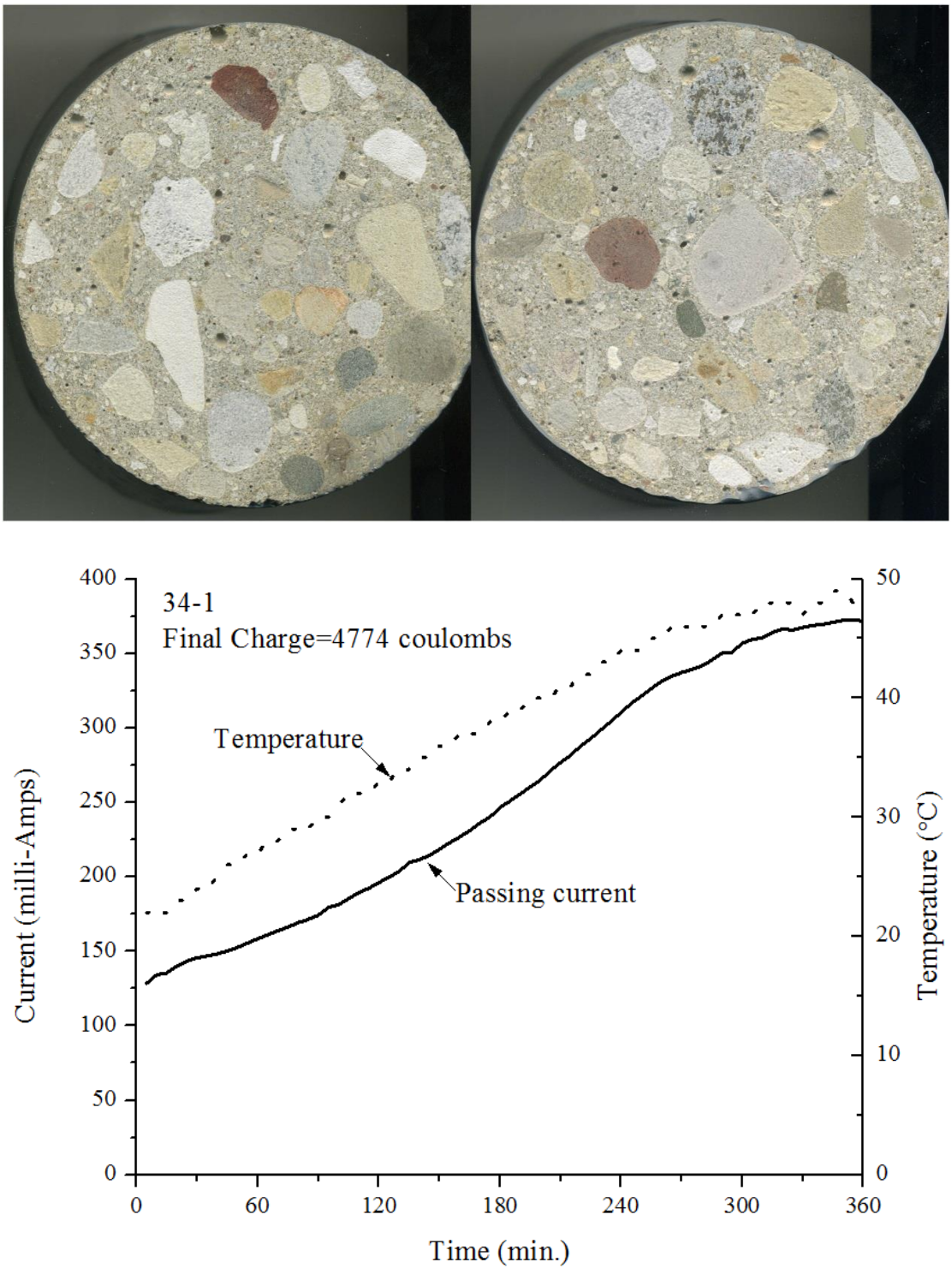

Figure A.29: The picture and graph of passing current/temperature vs. time for sample34-1.

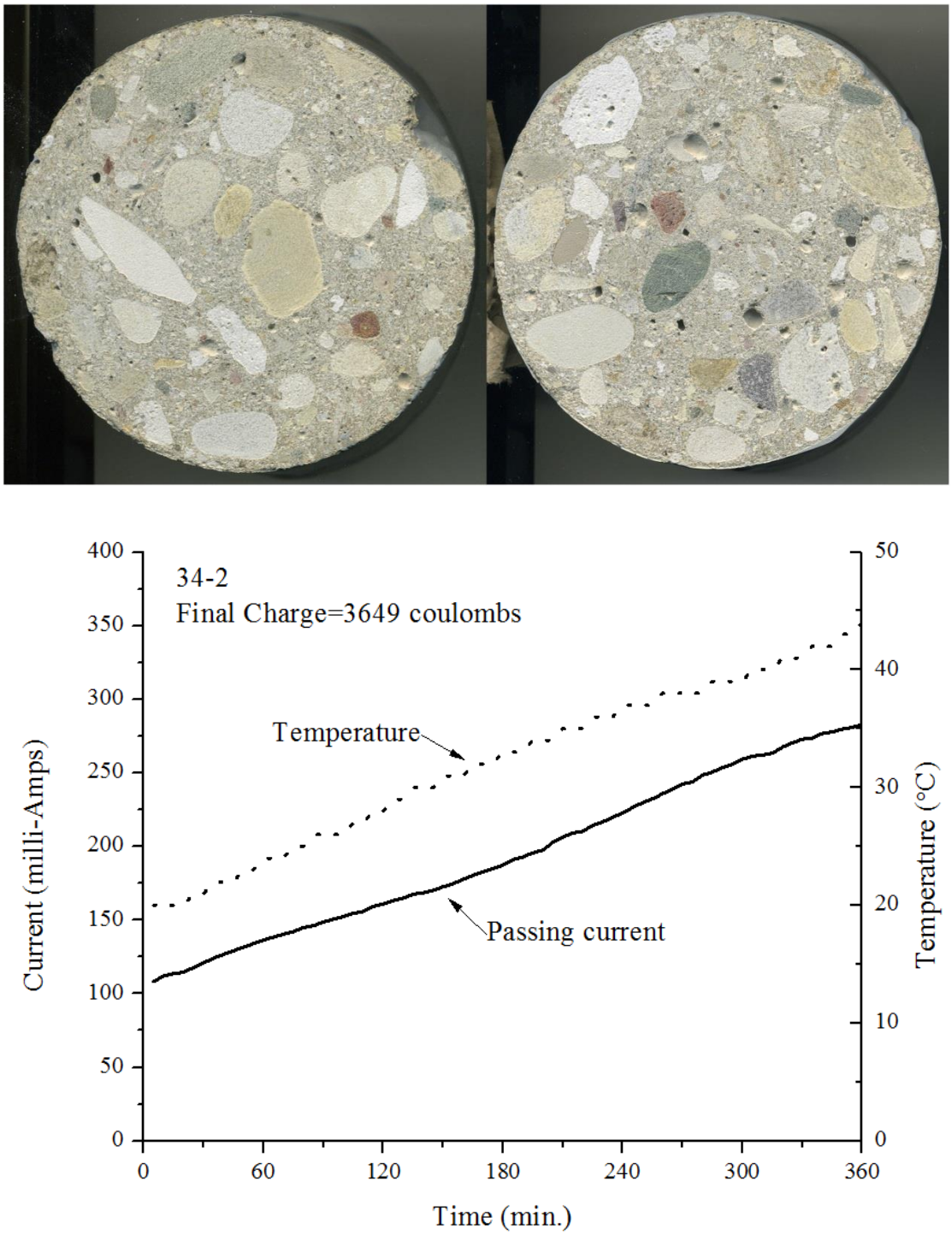

Figure A.30: The picture and graph of passing current/temperature vs. time for sample34-2.

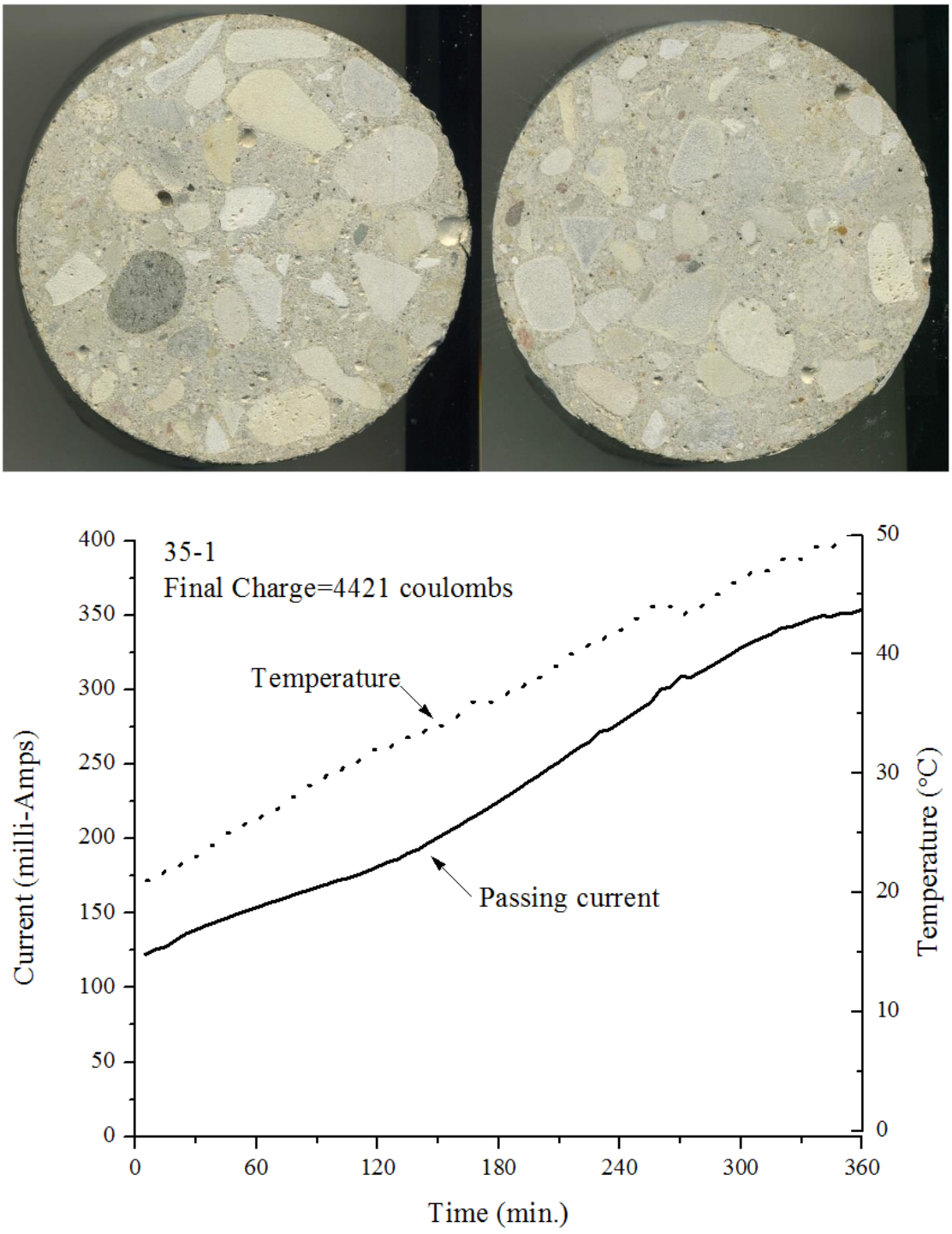

Figure A.31: The picture and graph of passing current/temperature vs. time for sample35-1.

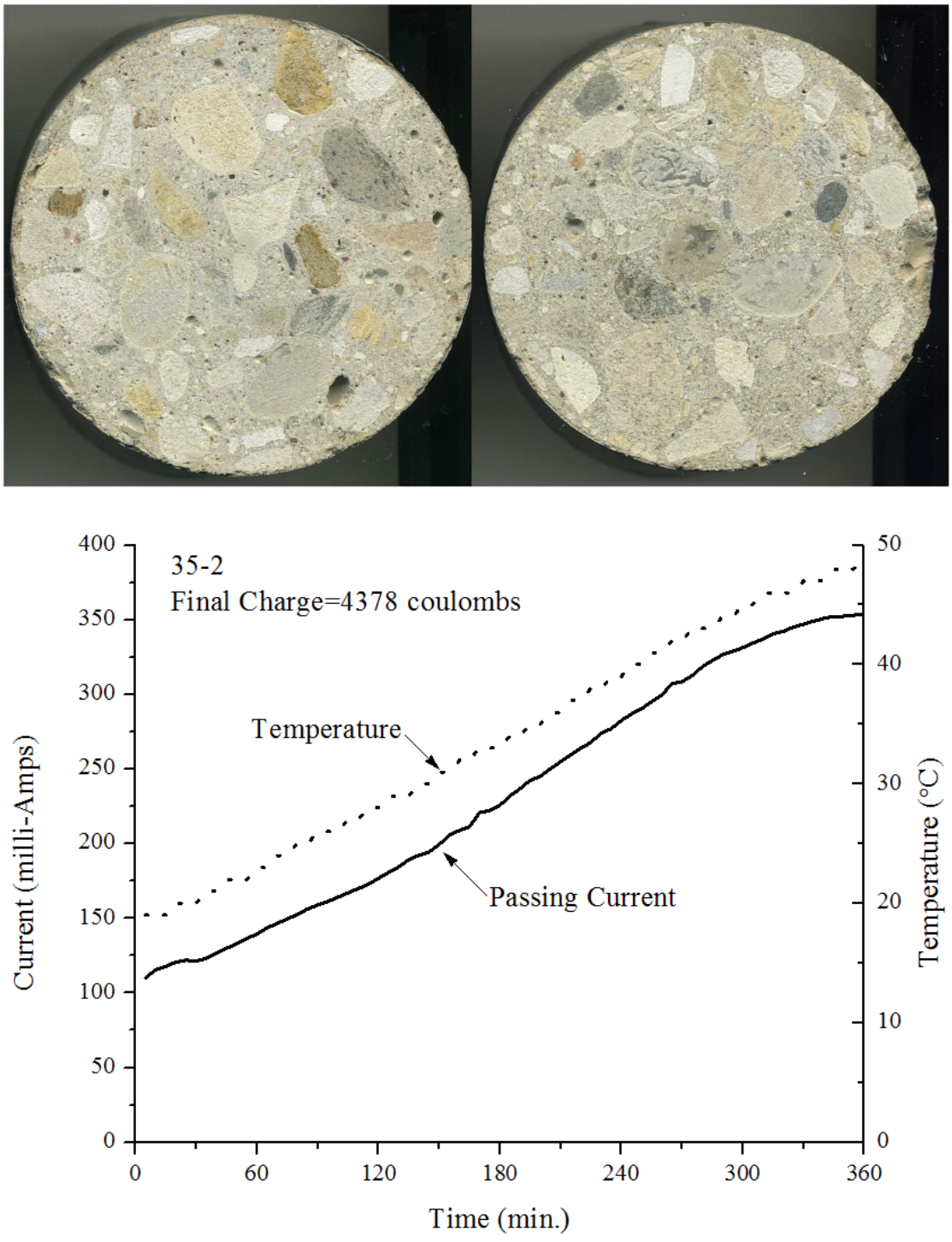

Figure A.32: The picture and graph of passing current/temperature vs. time for sample35-2.

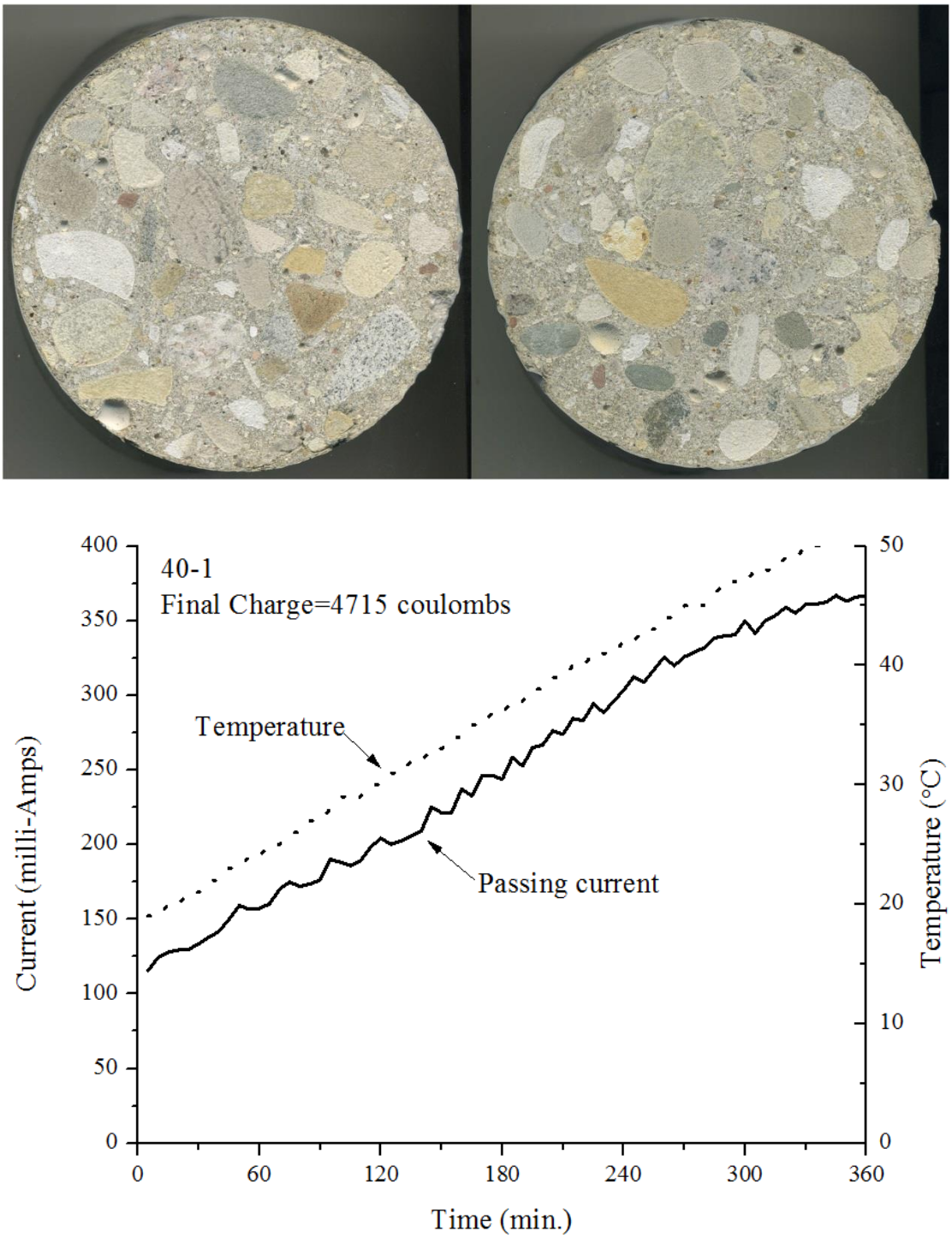

Figure A.33: The picture and graph of passing current/temperature vs. time for sample40-1.

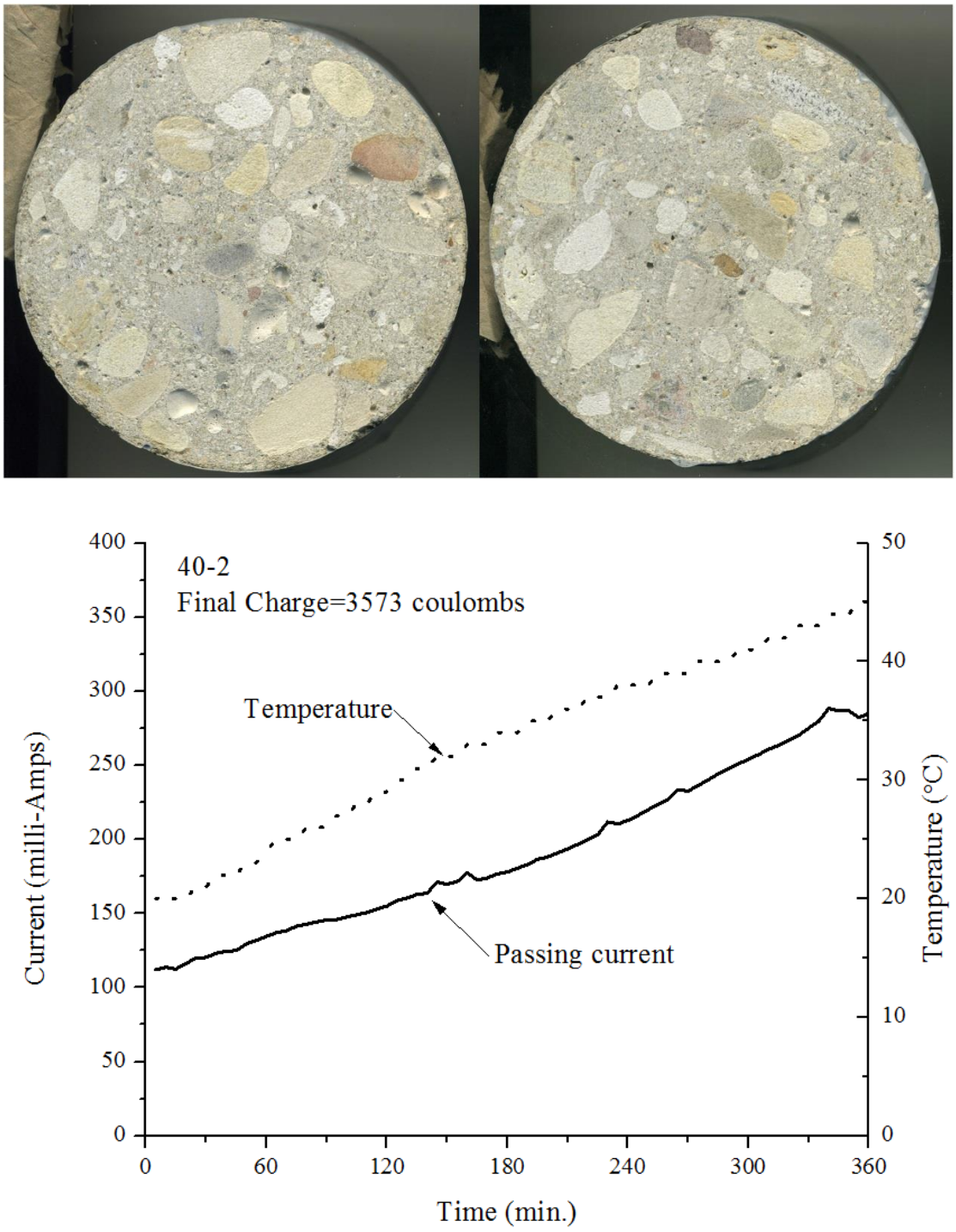

Figure A.34: The picture and graph of passing current/temperature vs. time for sample40-2.

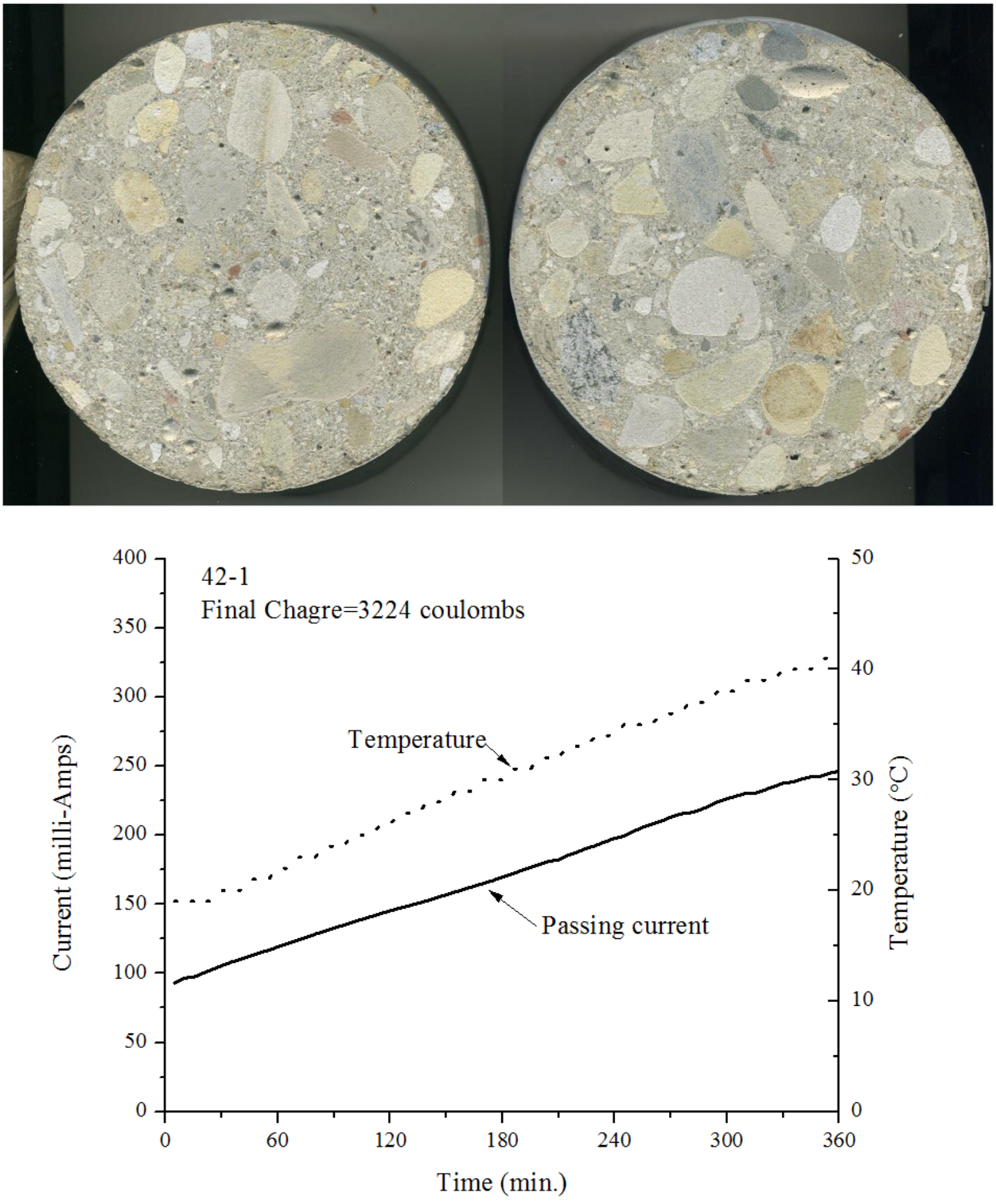

Figure A.35: The picture and graph of passing current/temperature vs. time for sample42-1.

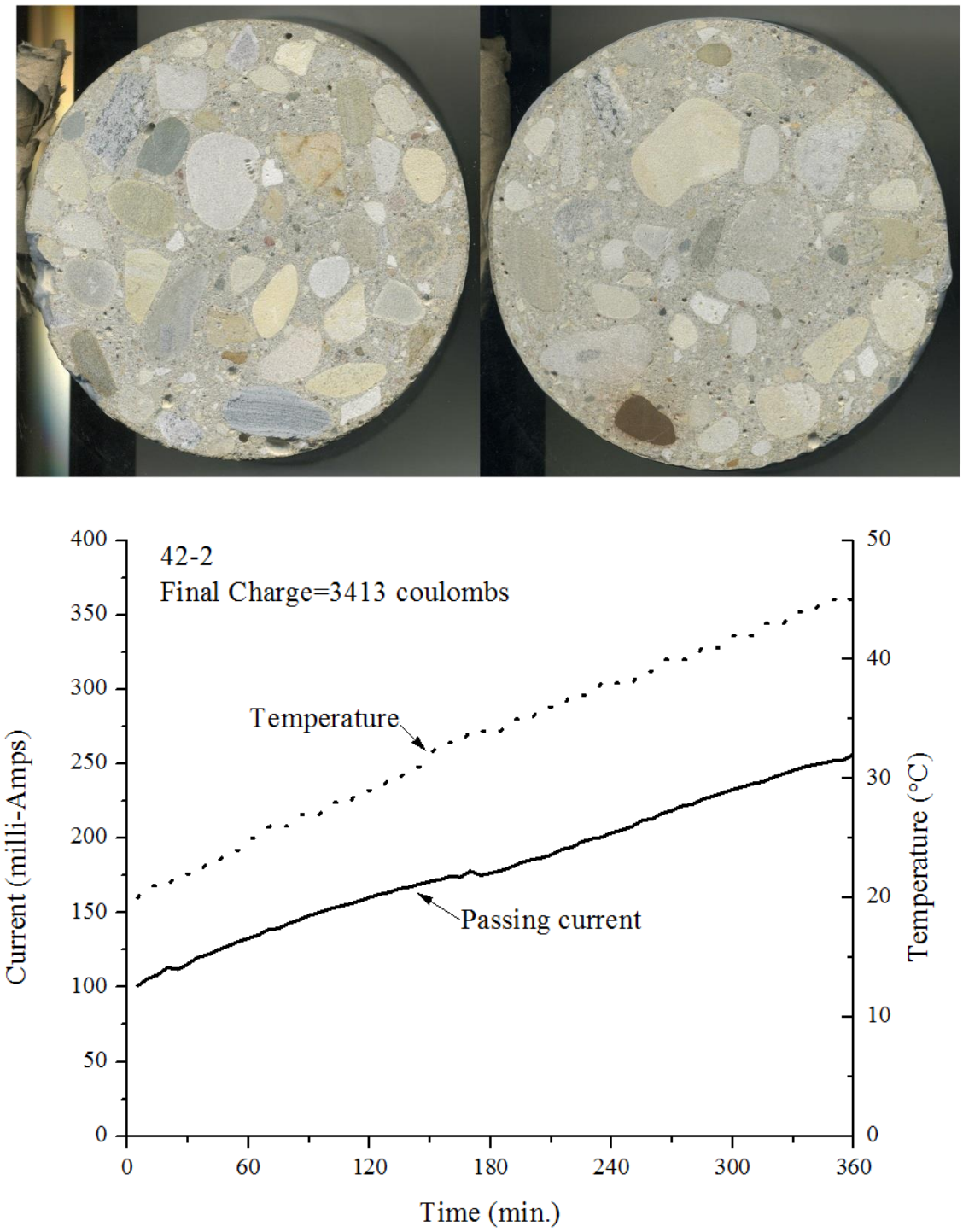

Figure A.36: The picture and graph of passing current/temperature vs. time for sample42-2.